7. SITE 805[1]

Shipboard Scientific Party[2]

HOLE 805A

Date occupied: 11 February 1990

Date departed: 11 February 1990

Time on hole: 11 hr, 30 min

Position: 1°13.68′N, 160°31.76′E

Bottom felt (rig floor; m, drill-pipe measurement): 3199.5

Distance between rig floor and sea level (m): 11.02

Water depth (drill-pipe measurement from sea level, m): 3188.5

Total depth (rig floor; m): 3250.00

Penetration (m): 50.50

Number of cores (including cores with no recovery): 6

Total length of cored section (m): 50.50

Total core recovered (m): 52.22

Core recovery (%): 103.4

Oldest sediment cored:
Depth (mbsf): 50.50
Nature: nannofossil ooze
Youngest age: Quaternary
Oldest age: late Pliocene
Measured velocity (km/s):

HOLE 805B

Date occupied: 11 February 1990

Date departed: 13 February 1990

Time on hole: 1 day, 21 hr, 45 min

Position: 1°13.68′N, 160°31.76′E

Bottom felt (rig floor; m, drill-pipe measurement): 3197.8

Distance between rig floor and sea level (m): 11.02

Water depth (drill-pipe measurement from sea level, m): 3186.8

Total depth (rig floor; m): 3671.10

Penetration (m): 473.30

Number of cores (including cores with no recovery): 50

Total length of cored section (m): 473.30 (APC, 263.2; XCB, 210.1)

Total core recovered (m): 444.89 (APC, 271.30; XCB, 173.59)

Core recovery (%): 93 (APC, 103.1; XCB, 82.6)

Oldest sediment cored:
Depth (mbsf): 473.30
Nature: nannofossil chalk
Youngest age: Quaternary
Oldest age: early Miocene
Measured velocity (km/s): 1.8

HOLE 805C

Date occupied: 13 February 1990

Date departed: 17 February 1990

Time on hole: 3 days, 18 hr, 45 min

Position: 1°13.69′N, 160°31.77′E

Bottom felt (rig floor; m, drill-pipe measurement): 3198.7

Distance between rig floor and sea level (m): 11.02

Water depth (drill-pipe measurement from sea level, m): 3187.7

Total depth (rig floor; m): 3809.70

Penetration (m): 611.00

Number of cores (including cores with no recovery): 64

Total length of cored section (m): 611.00 (APC, 235.8; XCB, 375.2)

Total core recovered (m): 495.46 (APC, 236.34; XCB, 259.12)

Core recovery (%): 81 (APC, 100.2; XCB, 69.1)

Oldest sediment cored:
Depth (mbsf): 611.00
Nature: nannofossil chalk
Youngest age: Quaternary
Oldest age: late Oligocene
Measured velocity (km/s): 1.9

Principal results: Ocean Drilling Program (ODP) Site 805 (proposed Site OJP-2) is located on the northeastern margin of the Ontong Java Plateau, close to the equator (latitude 1°13.7′N, longitude 160°31.8′E) in 3188 m of water, roughly 270 km northeast of Deep Sea Drilling Project (DSDP) Sites 289/586. The site represents the intermediate-to-deep member on a transect that was designed to detect depth-related paleoceanographic signals in Neogene sediments. It was occupied with the objective to obtain a high-resolution carbonate record in a lysoclinal setting for studies of ocean history, including biostratigraphy, chemostratigraphy, and acoustic stratigraphy.

Site 805 was positioned at the proposed location (OJP-2), within a gently sloping valley about 3.5 km wide and flanked by low ridges along either side. We used crossing *Thomas Washington* single-channel seismic (SCS) lines acquired during ROUNDABOUT Cruise 11 (2130 UTC, 24 December 1989, and 1700 UTC, 25 December). The seismic profiles showed continuous reflectors, with little or no disturbance.

Three holes were drilled using either the advanced hydraulic piston corer (APC) or the extended core barrel (XCB), with full recovery on the APC cores. Hole 805A, a dedicated hole, was cored with the APC to 50.5 mbsf into upper Pliocene sediments. Hole 805B was cored with the APC to 263.2 mbsf, where refusal occurred at the boundary between the middle and upper Miocene. The hole was continued with XCB coring to 473.3 mbsf, with 210.1 m of sediment cored and 173.6 m recovered. Coring ended about half-way through a thick section of lower Miocene sediments. Hole 805C was cored with the APC to 235.8 mbsf, at which point we began to core with the XCB. Drilling ended in upper Oligocene sediments at 611.0 mbsf, with 259.1 m cored with the XCB (69% recovery). The hole was then logged.

The entire sedimentary sequence encountered is considered as one lithologic unit (Unit I), consisting of nannofossil ooze and chalk with varying abundances of foraminifers. Radiolarians are a minor constituent throughout the section. The ooze-chalk transition is placed be-

[1] Kroenke, L. W., Berger, W. H., Janecek, T. R., et al., 1991. *Proc. ODP, Init. Repts.,* 130: College Station, TX (Ocean Drilling Program).

[2] Shipboard Scientific Party is as given in the list of participants preceding the contents.

tween 283 and 294 mbsf; it is gradational and shows alternation of layers of varying induration. The age of this interval is ca. 11 Ma. Sedimentation throughout the time interval represented seems to have been continuous at this site.

The ooze-chalk transition divides Unit I into two subunits, as follows:

Subunit IA (0–293.7 mbsf) consists of Pleistocene to middle Miocene nannofossil ooze with foraminifers, and foraminifer nannofossil ooze, with 90%–95% carbonate. The dominant color is white; the upper 30 m of the section is light gray. Bioturbation is common throughout, ranging from slight to heavy. Some well-developed burrows have concentric color rings, indicating redox gradients as the cause for color banding. Banding is common throughout the unit and is especially well expressed in the uppermost Miocene. For the most part, color bands are coarse and irregular in Subunit IA. Microfaulting was observed in Core 130-805B-18H at 166 mbsf (middle upper Miocene), and tilting is seen at the middle to upper Miocene boundary. Sediments are generally soft, but in the lowermost portion of Subunit IA (283–293 mbsf) more lithified intervals appear. A shift toward higher velocities occurs near the top of that zone, and another at the ooze-chalk transition at about 294 mbsf.

Subunit IB (293.7–611 mbsf) consists of middle Miocene to upper Oligocene nannofossil chalk, nannofossil chalk with foraminifers, and foraminifer nannofossil chalk. Foraminifer content is high down to about 380 mbsf (boundary of middle to lower Miocene) and decreases below that level, reaching a minimum in the lower Miocene. Radiolarian content is low; a moderate peak occurs near 400 mbsf, in the uppermost lower Miocene. The color is dominantly white. Color banding occurs throughout but becomes rare below 504 mbsf in the lowermost Miocene. It includes bundles of pseudo-laminae, that is, fine-scale banding showing sharp individual boundaries. Microfaulting is generally absent, except near 310 mbsf (ca. 12 Ma).

The sediments in the chalk section posed no problem for coring with the XCB down to the upper Oligocene, at which point recovery became low. Even where recovery is very good, core contents are largely disjointed chunks and chips, with evidence for grinding of chalk on chalk. This type of recovery is typical for the material below 370 mbsf. The Oligocene/Miocene boundary is located near 525 mbsf, apparently without any evidence of a hiatus (although recovery is poor at this level). Sedimentation rates for the deep chalk section are between 10 and 20 m/m.y., with the higher rates occurring in the Oligocene and the lower ones in the middle Miocene.

The middle Miocene is characterized by rather high foraminifer abundances, with a broad maximum near 12 Ma. Sedimentation rates are between 10 and 15 m/m.y. Carbonate values are quite variable, fluctuating between 85% and 95%. At the transition to the upper Miocene, there is a carbonate minimum, which also is a minimum in foraminifer content. This feature correlates with a zone of increased dissolution in the eastern equatorial Pacific (Barron et al., 1985). Carbonate values reach a maximum (near 95%) in the middle portion of the upper Miocene and tend to decrease to the present, with increasing variability reflecting increasing fluctuations in the carbon chemistry of the ocean. Sedimentation rates in the upper Miocene are very high (35– 40 m/m.y.) and drop in the Pliocene (25–30 m/m.y.). They decrease again within the Pleistocene (to below 20 m/m.y.).

Paleomagnetic stratigraphies were produced for the uppermost section of the two holes. Only the Brunhes and part of the Matuyama chrons could be identified. The sedimentation rate since 1.7 Ma was determined to be 17.1 m/m.y.

Chemical gradients in interstitial waters at this site are generally similar to those at Sites 803 and 804, reflecting the calcareous/siliceous nature of the sediments and the paucity of organic material. A somewhat higher supply of organic matter at this shallower site, close to the equator, tends to produce slightly stronger gradients. Calcium and magnesium gradients are influenced by basalt alteration reactions at depth and show the usual negative correlation. Strontium concentrations reflect recrystallization processes, which take place in younger sediments at this site than at the other two as a result of the higher sedimentation rates. Dissolved silica shows a steady increase with depth, except for a minor reversal of this trend just above the ooze-chalk transition.

Excellent logs were obtained for sound velocity and density at Site 805. The fact that this site has continuous sedimentation makes these logs especially valuable for the interpretation of seismic profiles. The geochemical log for the bottom 200 m (lower to middle Miocene) shows cycles, apparently with frequencies in the Milankovitch spectrum.

BACKGROUND AND OBJECTIVES

Overview

Site 805, the second lysocline site of the Neogene depth transect on Ontong Java Plateau, was drilled near the target Site OJP-2 (3200 m) (Fig. 1). The site is similar in water depth to Site 803 (3410 m), but it differs in being closer to the equator and just above (rather than below) the modern lysocline. At this level, contrasts in preservational state are expected to be close to maximum. Thus, the saturation history of deep waters, and its ramifications for physical properties, would be optimally recorded in sediments accumulating at a rate of some 15 m/m.y. Rich tropical assemblages of pelagic and benthic microfossils would be recovered from these sediments for use in paleoceanographic and biostratigraphic studies, covering the entire Neogene as well as the transition into the Paleogene.

The site was planned for multiple coring in the upper portion of the section (Neogene and Quaternary): two hydraulic piston-core holes to 250 mbsf, a third hole to 50 mbsf, and coring with the XCB to 500 mbsf. The multiple coring provides for overlap between cores and for sufficient material for concurrent high-resolution studies.

Background

The general background to this site is contained in the "Introduction" chapter of this volume (also see Kroenke, 1972). The Ontong Java Plateau is a broad, shallow, mid-ocean highland in the western equatorial Pacific. Its shallowest regions lie above 2000 m, and its flanks reach depths in excess of 4500 m. With an area of 1.5 million km^2, it is the largest of the "classic" Pacific plateaus. The plateau has a crustal thickness on the order of 40 km. Apparently, it roughly maintained its present depth over much of its history, indicating isostatic equilibrium. Crustal seismic velocities are in the range of that of oceanic crust (Hussong et al., 1979).

The pelagic sediment cover of the plateau is uniquely suited for paleoceanographic studies. The maximum thickness of the sediment is typically near 1200 m and occurs below the top of the plateau, in water depths between 2000 and 2500 m. The sediment thins by roughly 100 m for every 200 m of water depth increase, below 2200 m (Berger and Johnson, 1976). At Site 805 (3188 m), the sediment is approximately 700 m thick.

Site 805 was planned as a companion site to Site 803 as part of a Neogene depth transect in the equatorial portion of Ontong Java Plateau and was designed to study paleoceanographic events of global significance. Somewhat higher sedimentation rates were expected here, nearer to the equator, and at the slightly shallower depth, compared with Site 803. Gradients for physical, chemical, and paleontological properties are especially strong at this depth level (Shackleton and Opdyke, 1976; Johnson et al., 1977; Wu and Berger, 1989). Unfortunately, problems arising from the creep of large sediment bodies are ubiquitous in this depth range because of a combination of tectonic and stratigraphic factors. The site location is close to a significant offset in basement levels between the plateau and the deep ocean floor (Fig. 2). Earthquakes are to be expected in such a setting, at least occasionally. Episodic shaking, basement relief, and increased mobility of sediments at depth (because of preconditioning by partial dissolution of carbonate in certain horizons) apparently create large-scale slumping and debris flow on the flanks of the plateau. Removal of support at greater water

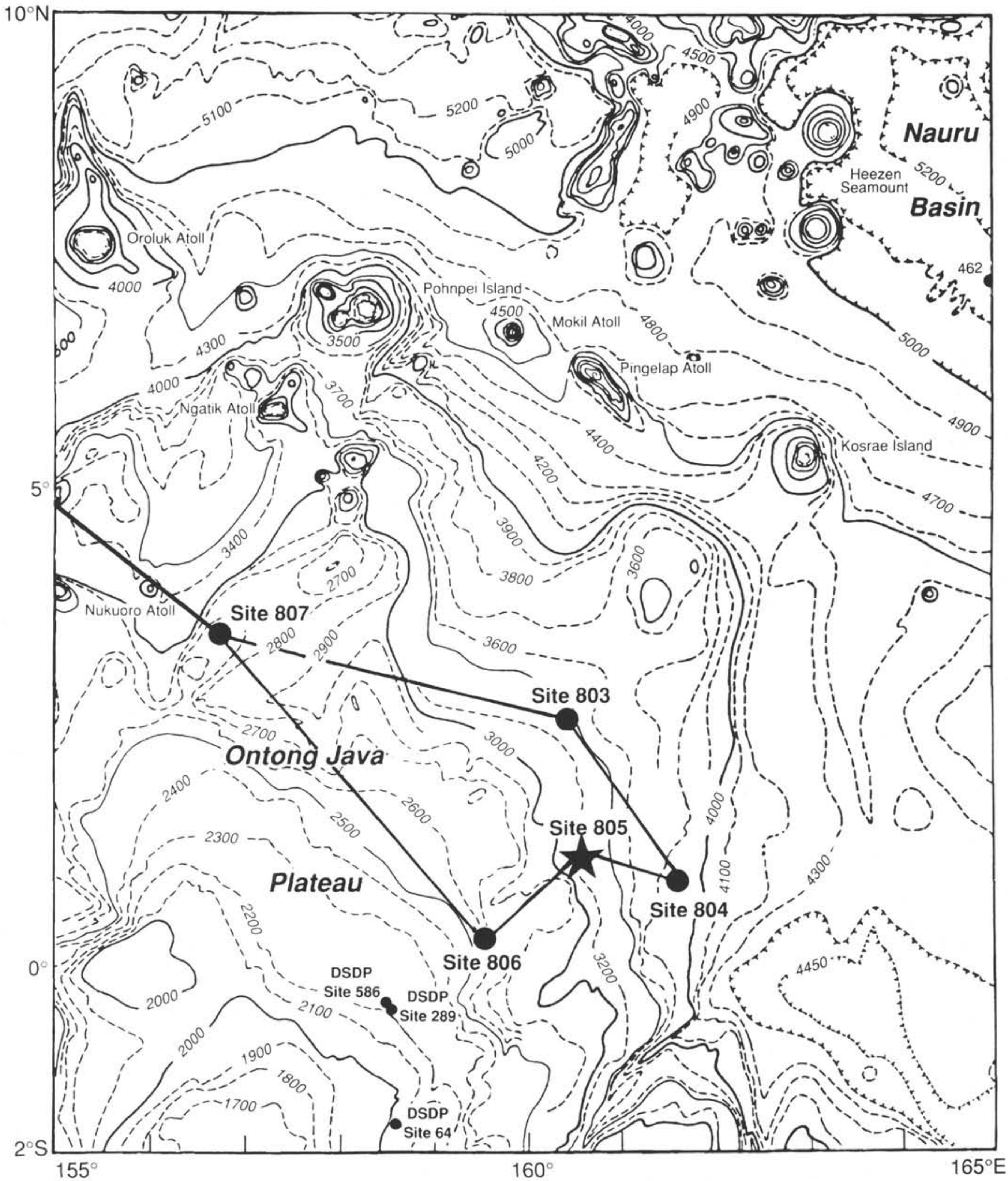

Figure 1. Bathymetry in meters of the northwestern part of the Ontong Java Plateau (after Mammerickx and Smith, 1985). The location of the Leg 130 sites together with those from DSDP Legs 7, 30, and 89 are shown for reference. Contour interval is 100 m.

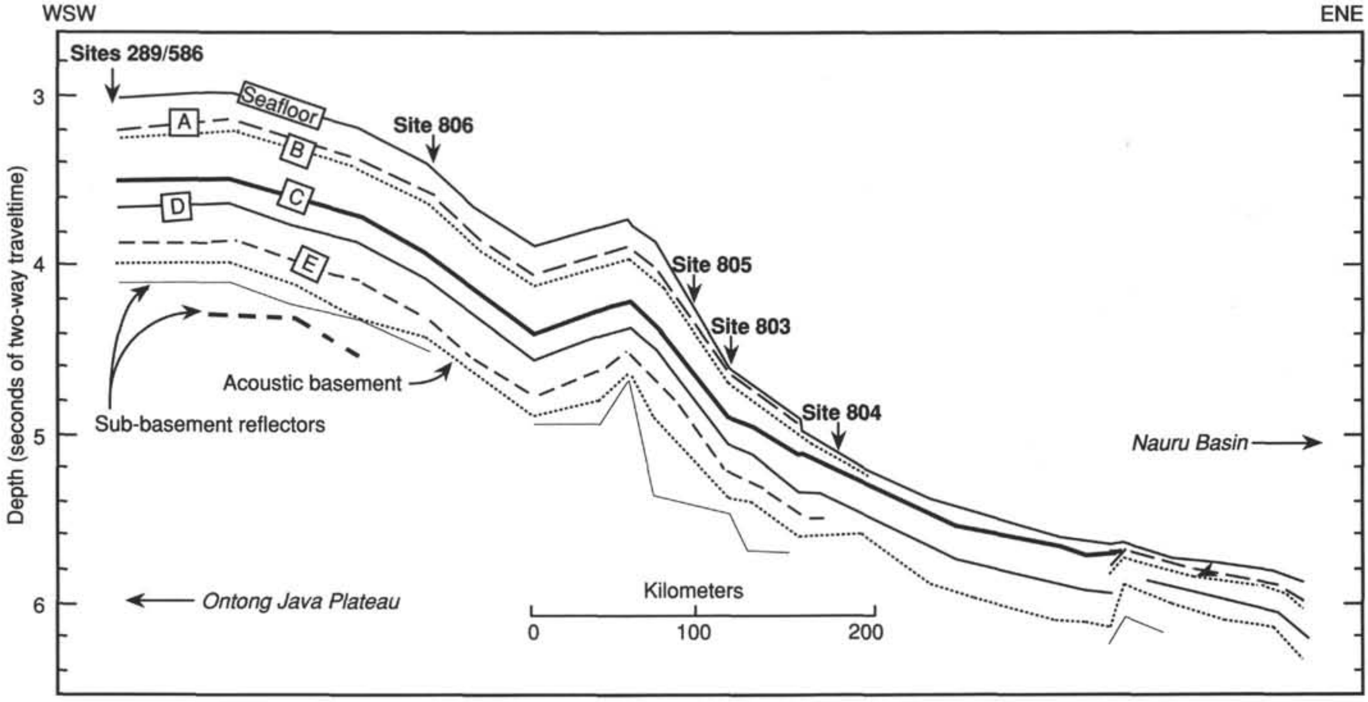

Figure 2. Simplified acoustic stratigraphy of the flank of the Ontong Java Plateau and approximate location of Sites 803–806 (the depth transect).

depths may also play a role in fostering mass movement (Berger and Johnson, 1976). Selection of a suitable site to drill a continuous record was difficult under these conditions.

The seismic profiles across Site 805 (from the ROUNDABOUT survey in December 1989) show subtle indications of mass movement within the sloping valley harboring the site. Crenulate reflectors ("crinkly horizons") are observed at several levels, as well as evidence for wedging along the basin margins (Fig. 3). Despite these indications for disturbance, a rather complete section was expected to be encountered based on these profiles, as the overall coherency of the seismic reflectors is quite good.

The plateau has long been the focus of paleoceanographic studies based on conventional coring and on seismic profiling. Leg 130 is the fourth drilling expedition to sample the sediment cover here: four DSDP sites were drilled earlier on the plateau. Leg 7 drilled Site 64 (Shipboard Scientific Party, 1971), and Leg 30 drilled Sites 288 and 289 (Shipboard Scientific Party, 1975a, 1975b). All three sites were rotary-drilled and spot-cored. The upper 969 m in Site 289 consisted of upper Eocene to Pleistocene nannofossil-foraminifer chalks and oozes. The section was found to be continuous from the lower Oligocene on, the top of which was reached at 890 mbsf. Semilithified chalk first appears near 250 mbsf (late Miocene). Site 586, drilled on Leg 89 next to Site 289, was cored with the APC to 305 mbsf, reaching upper Miocene sediments (Shipboard Scientific Party, 1986a, 1986b). It recovered well-preserved nannofossil ooze.

Objectives

Site 805, roughly 140 km northeast of DSDP Sites 289/586 on the northeastern margin of the Ontong Java Plateau, was planned as the shallower of the two lysocline sites (803 and 805) within the series of four equatorial sites that constitute a Neogene depth transect (Sites 803–806; Fig. 1). The general objective of this transect was to detect depth-related paleoceanographic signals. The sediments sampled along the transect were produced in the same surface-water conditions and thus arrived on the seafloor in the same pelagic rain, so that differences in physical, chemical, and paleontological properties can be attributed to depth-related effects.

The depth sampled at Site 805 (Fig. 1), just above the modern lysocline, is that which should show the greatest variation in dissolution-induced signals. Thus, physical properties should show maximum amplitudes here, and in turn, this imprint should be detectable in the acoustic stratigraphy (Berger and Mayer, 1978). The objective is to explore whether through such effects of dissolution a clear linkage can be established between paleoceanographic events and acoustic stratigraphy (Mayer et al., 1986). In the case of severe dissolution pulses, one would expect hiatus formation, presumably also linked to paleoceanographic events (Barron and Keller, 1982). Establishing such linkages will allow three-dimensional mapping and correlation into distant sediment sections throughout the Pacific basin.

Regarding biostratigraphic objectives at this site, we expected that changes in the preservation of calcareous fossils would provide clues to changes in the intensity of dissolution, with wide implications for the study of deep-water history and the oceanic carbon cycle. Recovery of preserved benthic foraminifers should allow reconstruction of deep-water properties directly, in their abundances and chemical composition. The effects of partial dissolution on biostratigraphic zonation (by selective removal of marker species) should be a minor problem at this depth level, but could be important during upward excursions of the carbonate compensation depth (CCD).

OPERATIONS

Site 805

Upon leaving Site 804, a 20-nmi, 2.75-hr seismic survey was run over the site at 7.3 kt. The transit from Sites 804 to 805 covered 63 nmi in 7.5 hr at an average speed of 8.4 kt. A 22-nmi, 2.75-hr, pre-site seismic survey was run over the proposed site at 8.4 kt (see "Underway Geophysics" chapter, this volume, for further details of surveys). Minimal satellite positioning was available. A beacon was dropped at 2250 hr, 10 February 1990, but the weight came off the beacon, and it floated back to the

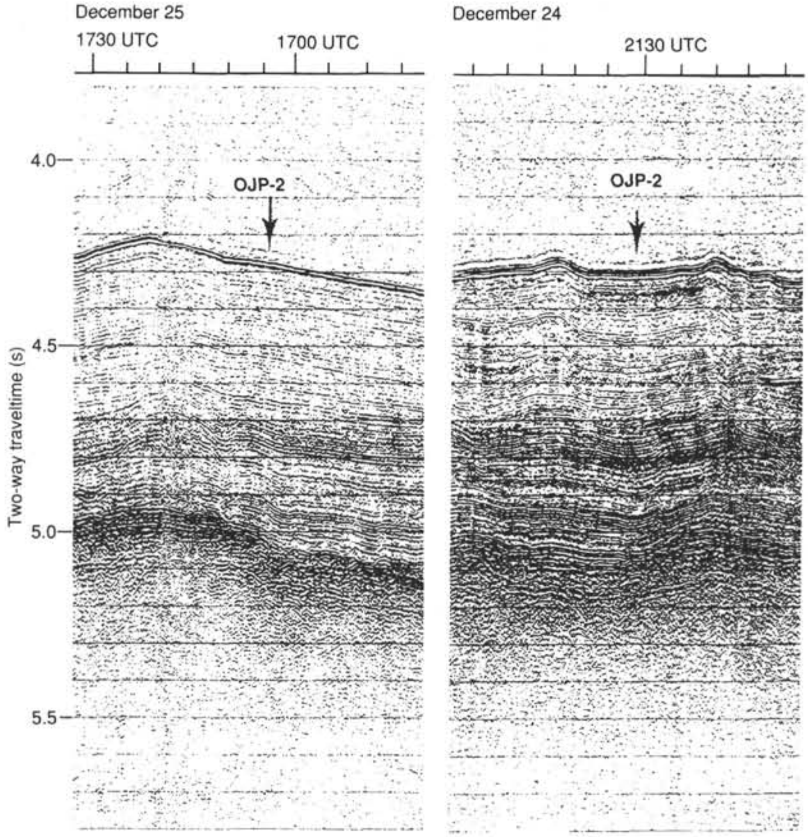

Figure 3. Seismic profiles across proposed drilling sites for Site 805, showing evidence of planar disturbance (crinkly horizons) and debris flow (wedges next to basin rim). See Mayer et al. (this volume) for details.

surface. An additional 6-nmi survey track was run, and a second beacon was dropped at 2345 hr, 10 February 1990, on the proposed site, initiating Site 805.

Hole 805A

The ship was positioned 100 m south of the beacon. Core 130-805A-1H was taken at 0700 hr, 11 February 1990, in 3188.5 m of water. Cores 130-805A-1H through -6H were taken from 0 to 50.5 mbsf, with 50.5 m of sediment cored and 52.22 m recovered (103.41% recovery; Table 1). Orientation surveys were taken during Cores 130-805A-3H through -6H. Hole 805A was terminated when we reached our depth objective of 50 mbsf. At this point, the drill pipe was pulled out of the hole and the bit cleared the seafloor at 1115 hr, 11 February 1990.

Hole 805B

The ship was positioned 100 m south and 30 m east of the beacon. Core 130-805B-1H was taken at 1155 hr, 11 February 1990, in a water depth of 3186.8. Cores 130-805C-1H through -28H were taken from 0 to 263.2 mbsf, with 263.2 m of sediment cored and 271.3 m recovered (103.08% recovery; Table 1). Orientation surveys were taken during Cores 130-805B-3H through -28H.

APC refusal was reached at Core 130-805B-28H (263.2 mbsf) when the core barrel would not pull free with 100,000 lbs of overpull. The APC core barrel was washed over for 7 m but still required 80,000 lbs of overpull to pull it free. This was another successful test of the new APC equipment, which included a stronger piston rod and washover capability. Core 130-805B-28H was recovered with 9.96 m of sediment and no damage to the core barrel.

We initiated XCB coring at this point, and Cores 130-805B-29X through -50X were taken from 263.2-473.3 mbsf, with 210.1 m of sediment cored and 173.59 m recovered (82.62% recovery). The sonic core monitor (SCM) was tested on Core 130-805B-47X. A 9.5-m section was cored but only 0.70 m of sediment was recovered. The SCM electronics performed properly but the core jammed in the cutting shoe. Hole 805B was terminated after reaching Miocene sediments.

Hole 805C

The ship was positioned 100 m south and 60 m east of the beacon. Core 130-805C-1H was taken at 1015 hr, 13 February 1990, in 3187.7 m of water. Cores 130-805C-1H through -25H were taken from 0 to 235.8 mbsf with 235.8 m of sediment cored and 236.34 m recovered (100.23% recovery; Table 1). Orientation surveys were taken during Cores 130-805C-3H through -10H.

APC coring was interrupted for 45 min after Core 130-805C-7H, when the beacon signal became intermittent at 1540 hr, 13 February 1990. A backup beacon was launched at 1552 hr, 13 February 1990.

The breakaway piston head was tested in Cores 130-805C-21H and -23H. Recovery was reduced from an average of 9.78 to 5.82 m during these test runs.

Coring with the APC ended at 235.8 m, a shallower depth than in the previous hole, to avoid getting the core barrel stuck and having to drill over the core again. Coring with the XCB began at this point, and Cores 130-805C-26X through -55X were drilled from 235.8 to 523.9 mbsf, with an average recovery of 80%. Below 523.9 mbsf, the sediment repeatedly jammed in the cutting shoe and reduced recovery in Cores 130-805C-56X

Table 1. Coring summary, Site 805.

Core no.	Date (Feb. 1990)	Time (UTC)	Depth (mbsf)	Cored (m)	Recovered (m)	Recovery (%)	Age
130-805A-							
1H	11	0700	0-3.0	3.0	2.99	99.6	NN20-NN21
2H	11	0735	3.0-12.5	9.5	9.94	104.0	NN19
3H	11	0925	12.5-22.0	9.5	9.86	104.0	NN19
4H	11	0905	22.0-31.5	9.5	9.74	102.0	NN18?
5H	11	0950	31.5-41.0	9.5	9.73	102.0	NN18
6H	11	1035	41.0-50.5	9.5	9.96	105.0	NN16
Coring totals				50.5	52.22	103.4	
130-805B-							
1H	11	1155	0-6.7	6.7	6.70	100.0	NN20
2H	11	1230	6.7-16.2	9.5	9.77	103.0	NN19
3H	11	1320	16.2-25.7	9.5	9.70	102.0	
4H	11	1400	25.7-35.2	9.5	10.05	105.8	NN18
5H	11	1455	35.2-44.7	9.5	10.00	105.2	NN16
6H	11	1600	44.7-54.2	9.5	9.96	105.0	NN16
7H	11	1655	54.2-63.7	9.5	9.65	101.0	NN16
8H	11	1745	63.7-73.2	9.5	9.83	103.0	NN16
9H	11	1850	73.2-82.7	9.5	10.10	106.3	NN15
10H	11	1940	82.7-92.2	9.5	10.12	106.5	NN15-NN14
11H	11	2040	92.2-101.7	9.5	9.90	104.0	
12H	11	2135	101.7-111.2	9.5	9.56	100.0	NN12
13H	11	2220	111.2-120.7	9.5	9.89	104.0	NN12
14H	11	2300	120.7-130.2	9.5	9.91	104.0	NN11
15H	12	0015	130.2-139.7	9.5	9.77	103.0	NN11
16H	12	0200	139.7-149.2	9.5	10.06	105.9	NN11
17H	12	0245	149.2-158.7	9.5	9.68	102.0	NN11
18H	12	0330	158.7-168.2	9.5	9.50	100.0	NN11
19H	12	0415	168.2-177.7	9.5	8.41	88.5	NN11
20H	12	0500	177.7-187.2	9.5	9.80	103.0	NN11
21H	12	0535	187.2-196.7	9.5	9.59	101.0	NN11
22H	12	0615	196.7-206.2	9.5	9.79	103.0	
23H	12	0700	206.2-215.7	9.5	9.79	103.0	NN11
24H	12	0745	215.7-225.2	9.5	9.83	103.0	NN10
25H	12	0815	225.2-234.7	9.5	9.81	103.0	NN10
26H	12	0845	234.7-244.2	9.5	9.99	105.0	NN10
27H	12	0940	244.2-253.7	9.5	10.18	107.1	
28H	12	1135	253.7-263.2	9.5	9.96	105.0	
29X	12	1230	263.2-272.9	9.7	8.41	86.7	NN9
30X	12	1315	272.9-282.5	9.6	9.13	95.1	NN9
31X	12	1400	282.5-292.2	9.7	9.02	93.0	NN9?
32X	12	1445	292.2-301.4	9.2	7.24	78.7	NN7-NN6
33X	12	1530	301.4-311.0	9.6	8.97	93.4	NN6
34X	12	1620	311.0-320.5	9.5	7.78	81.9	NN6
35X	12	1705	320.5-330.0	9.5	7.81	82.2	
36X	12	1750	330.0-339.7	9.7	7.90	81.4	NN5
37X	12	1835	339.7-349.4	9.7	8.41	86.7	NN5
38X	12	1930	349.4-359.0	9.6	7.51	78.2	NN5
39X	12	2030	359.0-368.7	9.7	8.99	92.7	NN5
40X	12	2140	368.7-378.3	9.6	8.33	86.8	NN5
41X	12	2245	378.3-388.0	9.7	7.47	77.0	NN5-NN4
42X	13	0045	388.0-397.7	9.7	8.06	83.1	NN2
43X	13	0130	397.7-407.3	9.6	9.13	95.1	NN2
44X	13	0215	407.3-417.0	9.7	9.22	95.0	NN2
45X	13	0320	417.0-426.5	9.5	8.44	88.8	NN2
46X	13	0430	426.5-436.0	9.5	8.36	88.0	NN1
47X	13	0520	436.0-445.5	9.5	0.70	7.4	NN1?
48X	13	0600	445.5-455.1	9.6	6.92	72.1	NN1?
49X	13	0645	455.1-464.8	9.7	8.42	86.8	NN1?
50X	13	0740	464.8-473.3	8.5	7.37	86.7	NN1?
Coring totals				473.3	444.89	94.0	
130-805C-							
1H	13	1015	0-7.8	7.8	7.80	100.0	NN19
2H	13	1050	7.8-17.3	9.5	9.88	104.0	
3H	13	1145	17.3-26.8	9.5	9.40	98.9	NN19
4H	13	1230	26.8-36.3	9.5	9.96	105.0	
5H	13	1320	36.3-45.8	9.5	9.67	102.0	NN17
6H	13	1410	45.8-55.3	9.5	10.09	106.2	
7H	13	1510	55.3-64.8	9.5	9.92	104.0	NN16
8H	13	1625	64.8-74.3	9.5	9.78	103.0	NN16
9H	13	1720	74.3-83.8	9.5	9.95	105.0	NN15
10H	13	1845	83.8-93.3	9.5	9.94	104.0	NN15
11H	13	1940	93.3-102.8	9.5	9.88	104.0	NN13-NN12

Table 1 (continued).

Core no.	Date (Feb. 1990)	Time (UTC)	Depth (mbsf)	Cored (m)	Recovered (m)	Recovery (%)	Age
130-805C- (Cont)							
12H	13	2040	102.8–112.3	9.5	9.71	102.0	NN12
13H	13	2115	112.3–121.8	9.5	9.98	105.0	NN12
14H	13	2245	121.8–131.3	9.5	9.93	104.0	NN11
15H	14	0000	131.3–140.8	9.5	9.77	103.0	NN11
16H	14	0055	140.8–150.3	9.5	10.01	105.3	NN11
17H	14	0110	150.3–159.8	9.5	9.78	103.0	NN11
18H	14	0250	159.8–169.3	9.5	9.83	103.0	NN11
19H	14	0335	169.3–178.8	9.5	9.83	103.0	NN11
20H	14	0415	178.8–188.3	9.5	9.73	102.0	NN11
21H	14	0450	188.3–197.8	9.5	9.56	100.0	NN11
22H	14	0530	197.8–207.3	9.5	9.93	104.0	NN11
23H	14	0620	207.3–216.8	9.5	2.07	21.8	NN11
24H	14	0650	216.8–226.3	9.5	9.87	104.0	NN10?
25H	14	0740	226.3–235.8	9.5	10.07	106.0	NN10
26X	14	0825	235.8–245.4	9.6	9.34	97.3	NN10
27X	14	0910	245.4–255.1	9.7	1.54	15.9	NN10
28X	14	0955	255.1–264.7	9.6	8.70	90.6	NN10?
29X	14	1045	264.7–274.4	9.7	8.97	92.5	NN9
30X	14	1145	274.4–284.0	9.6	8.07	84.0	NN8
31X	14	1220	284.0–293.7	9.7	9.10	93.8	NN6–NN7
32X	14	1300	293.7–302.9	9.2	9.18	99.8	NN6–NN7
33X	14	1345	302.9–312.6	9.7	9.08	93.6	NN6–NN7
34X	14	1435	312.6–322.3	9.7	8.64	89.1	NN6
35X	14	1525	322.3–331.8	9.5	8.02	84.4	NN5
36X	14	1620	331.8–341.5	9.7	8.80	90.7	NN5
37X	14	1710	341.5–351.2	9.7	7.27	74.9	NN5
38X	14	1805	351.2–360.9	9.7	9.38	96.7	NN5–NN4
39X	14	1900	360.9–370.6	9.7	9.19	94.7	NN5–NN4
40X	14	1950	370.6–380.3	9.7	8.67	89.4	NN5–NN4
41X	14	2050	380.3–389.9	9.6	6.33	65.9	NN5–NN4
42X	14	2145	389.9–399.5	9.6	6.86	71.4	NN3–NN2
43X	14	2230	399.5–409.1	9.6	8.62	89.8	NN2
44X	14	2310	409.1–418.7	9.6	9.51	99.0	NN2
45X	15	0000	418.7–428.4	9.7	8.90	91.7	NN2
46X	15	0050	428.4–438.1	9.7	8.70	89.7	NN2–NN1
47X	15	0140	438.1–447.7	9.6	9.44	98.3	NN2–NN1
48X	15	0220	447.7–457.4	9.7	7.25	74.7	NN2
49X	15	0310	457.4–467.0	9.6	5.02	52.3	NN1–NN2
50X	15	0400	467.0–475.5	8.5	6.92	81.4	NN1–NN2
51X	15	0445	475.5–485.2	9.7	7.23	74.5	NN1–NN2
52X	15	0545	485.2–494.9	9.7	5.83	60.1	NN2
53X	15	0640	494.9–504.6	9.7	7.19	74.1	NN1–NN2
54X	15	0740	504.6–514.2	9.6	6.51	67.8	NN1–NN2
55X	15	0840	514.2–523.9	9.7	4.14	42.7	NN1–NN2
56X	15	0940	523.9–533.5	9.6	0.80	8.3	NN1–NN2
57X	15	1035	533.5–543.2	9.7	2.93	30.2	NN1–NN2
58X	15	1210	543.2–552.9	9.7	0.92	9.5	NN2–NN1
59X	15	1340	552.9–562.6	9.7	2.22	22.9	NP25
60X	15	1520	562.6–572.3	9.7	0.99	10.2	NP25
61X	15	1700	572.3–582.0	9.7	9.61	99.1	NP24–NP23
62X	15	1900	582.0–591.7	9.7	5.11	52.7	NP23
63X	15	2050	591.7–601.3	9.6	2.68	27.9	NP23
64X	15	2300	601.3–611.0	9.7	1.46	15.0	
Coring totals				611.0	495.46	81.1	

through -64X to 16%. The Polypak seal in the bit seal (ring) was later found to be completely eroded away, explaining why the XCB bit nozzles were plugging and the core was jamming in the bit throat. Hole 805C was terminated after penetrating into Oligocene sediments.

A short pipe trip to 100 mbsf was made to condition the hole (no fill or drag was encountered), and a mud sweep was made to clean the hole. The bit was pulled up to 116.3 mbsf and logging began. Logs were run as follows:

Run No. 1: NGT/DIT/LSS. The first pass was run successfully at 900 ft/hr from 609.9 mbsf (1.2 m off the bottom) to 100.3 mbsf. A second, successful run was made at 900 ft/hr from 199.9 to 100.3 mbsf.

Run No. 2: NGT/ACT/HLDT/GST. The tool was run into the hole but was pulled out when it was discovered that a bullnose, used to open the lockable flapper valve, had not been run. The tool then was lowered to a depth of 609.3 mbsf, and the logging run was started. This run was aborted at 331.6 mbsf as the GST was not operating properly. The tool was lowered to 443.8 mbsf (the depth where the GST began to malfunction) and a repeat log was run. The GST did not produce neutrons properly during this repeat run. The tool was lowered to 199.9 mbsf to determine if the formation had been activated. There was no sign of neutron activation, so the string was pulled out of the hole.

Upon completion of the logging program, the pipe was pulled to the surface, and the bottom hole assembly (BHA) cleared the rotary table at 0345 hr, 17 February 1990, ending Hole 805C.

LITHOSTRATIGRAPHY

Introduction

Site 805 is located at a water depth of 3188 m, a shallower water depth than Sites 803 and 804. It was intended to occupy an intermediate position on the Neogene depth transect on the flank of the Ontong Java Plateau. Three holes were drilled at Site 805. Hole 805A was drilled with the APC to 50.5 mbsf with greater than 100% recovery. Cores from Hole 805A were stored unopened. Hole 805B was drilled to 473.3 mbsf. The upper 263.2 m were drilled with the APC and the remaining portion was drilled with the XCB. Recovery in the APC section was generally 100% or more, except for Core 130-805B-19H, and recovery in the XCB section averaged 83%. Hole 805C covered the same section as Hole 805B and was further extended to 611 mbsf. It was cored with the APC to 235.8 mbsf and with the XCB throughout the rest of the section. Recovery was 100% in the section cored with the APC, except for Core 130-805C-23H, which only recovered 2 m of sediment. Flow-in was observed in the upper five sections of Core 130-805C-7H and in all of Core 130-805C-8H. Shorter intervals of Cores 130-805C-10H, -11H, -14H, -16H, and -17H also exhibit flow-in structures and sediment distortion. This reduces the quality of the recovered material in this hole. Recovery in the part of Hole 805C drilled with the XCB was generally above 70% through Core 130-805C-54X (514.2 mbsf). Below this level, recovery was drastically reduced but variable, ranging from 8% (Core 130-805C-56X) to 99% (Core 130-805C-61X).

Nannofossil ooze and chalk are the predominant sediment types recovered at Site 805. Intervals of foraminifer nannofossil ooze and chalk are also present. Radiolarians are the most significant minor constituent of the sediments. Site 805 differs from Sites 803 and 804 in having a higher foraminifer content and in lacking intervals with high radiolarian abundances. The sedimentary section at Site 805 is stratigraphically complete, covering the Pleistocene to the upper Oligocene (see "Biostratigraphy" section, this chapter).

The sediments at Site 805 were grouped into one lithologic unit (Unit I) (Table 2 and Fig. 4). This unit is composed of upper Oligocene to Pleistocene nannofossil chalk and ooze and foraminifer nannofossil chalk and ooze. The unit was divided into two subunits (IA and IB) based on the degree of consolidation. Subunit IA is composed of ooze, whereas Subunit IB is composed of chalk. The Subunit IA/IB boundary is located at 282.5 mbsf in Hole 805B (base of Core 130-805B-30X), and at 293.7 mbsf (base of Core 130-805C-31X) in Hole 805C, and is gradational within each hole. Semi-indurated layers and stiffer portions are embedded in the softer ooze in the lower cores of Subunit IA, and the uppermost cores of Subunit IB include intervals of ooze.

Description of Units

Unit I

Intervals: Hole 805B, Cores 130-805B-1H to -50X, and Hole 805C, Cores 130-805C-1H to -64X
Age: Pleistocene-late Oligocene
Depth: 0-611 mbsf

Unit I is composed of nannofossil ooze and chalk to foraminifer nannofossil ooze and chalk and has been divided into two subunits. Subunit IA (0-293.7 mbsf) consists of nannofossil ooze and foraminifer nannofossil ooze, whereas Subunit IB (293.7-611 mbsf) contains nannofossil chalk and foraminifer nannofossil chalk.

Subunit IA

Intervals: Hole 805B, Cores 130-805B-1H to -30X, and Hole 805C, Cores 130-805C-1H to -31X
Age: Pleistocene-middle Miocene
Depth: 0-293.7 mbsf

Subunit IA is composed of 293.7 m of nannofossil ooze, nannofossil ooze with foraminifers, and foraminifer nannofossil ooze. The average foraminifer content is noticeably higher than at Sites 803 and 804. Foraminifer abundance is variable, with foraminifer-rich intervals in the Pleistocene and the Pliocene sections. Foraminifer abundances are low in parts of the upper Miocene section (Cores 130-805B-19H to -22H and 130-805C-19H to -22H) between 169 and 207 mbsf (Fig. 5), and increase again below this interval (Cores 130-805B-25H to -27H and Cores 130-805C-24H to -27H; 225-254 mbsf), and in parts of Core 130-805B-29X (263.2-272.9 mbsf), close to the ooze-chalk transition. Foraminifer abundances are variable at the middle/upper Miocene boundary, as seen in the alternations between nannofossil ooze and foraminifer nannofossil ooze in Figure 4. There is no clear relationship between the shipboard estimates of carbonate content and foraminifer content; carbonate content is low (82%-94%) and foraminifer content is high in the upper 150 m of the section (Fig. 6) (last 5-6 m.y.), whereas high foraminifer and high carbonate contents coincide in other portions of the section. Radiolarians are commonly present as a minor constituent in Subunit IA, but at concentrations too low to estimate abundance changes from smear slide analyses (Fig. 5).

The dominant color of the sediments of Subunit IA is white (2.5Y 8/0, 5Y 8/1), although the upper 30 m are light gray (5Y 7/1, 2.5Y 7/1). Bioturbation, ranging from slight to heavy, is common throughout the subunit, as evidenced by burrow mottling, pyritized burrow fills and specks, and numerous trace fossils that range in size from several millimeters to almost 10 cm in length (Fig. 7). As at Sites 803 and 804, the sediments through-

Table 2. Lithologic summary, Site 805.

Lithologic unit	Cores	Depth (mbsf)	Age	Lithology
IA	805B-1H to -30X 805C-1H to -31X	0-293.7	Pleistocene to middle Miocene	Nannofossil ooze to foraminifer nannofossil ooze
IB	805B-31X to -50X 805C-32X to -64X	293.7-611.0	middle Miocene to late Oligocene	Nannofossil chalk to foraminifer nannofossil chalk

out Subunit IA display numerous faint to sharp color bands that are light gray (5Y 7/2), pale blue (5PB 7/2), pale purple (5P 6/2), grayish blue (5PB 5/2), and light greenish gray (5G 7/1). The color bands are normally horizontal, but a few steeply inclined bands were also observed. In some instances, these bands clearly spread as concentric rings from well-developed burrows. The vertical bands were observed to cut through horizontal bands in some cases, apparently changing or diminishing the color of the horizontal band in the process. An example of this relationship is shown in Figure 8. This style of banding indicates that either the vertical or both the vertical and horizontal bands were formed diagenetically along diffusion gradients. The sediments at Site 805 appear to be much less influenced by microfaulting and distorted bedding than those at Sites 803 and 804. Only a few microfaults were observed, particularly in Section 130-805B-18H-5 (Fig. 9).

A thin, bioturbated ash-layer was observed at 260.29 mbsf in Hole 805C (Core 130-805C-28X-4, 69 cm) (see also Fig. 5). This ash was not found in Hole 805B either because of the disseminated nature of the ash or the loss at a core break.

The dominance of carbonate in the sediments of Subunit IA is clearly reflected by X-ray diffraction (XRD) scans and calcium carbonate contents (Fig. 6). Relative peak intensities from the XRD analyses agree with the general trends of the shipboard carbonate measurements and indicate somewhat lower calcite content in Cores 130-805B-15H to -21H, which generally coincides with the interval of low foraminifer content. Clays, quartz, and feldspars are the important nonbiogenic constituents of Subunit IA.

The predominance of nannofossils in the sediments of Subunit IA produces a silty texture. This observation is supported by shipboard grain-size analyses (Table 3). Figure 10 shows that mean grain size varies within the fine to medium silt-size range (10–30 μm) as a series of high-frequency, grain-size fluctuations throughout the upper 300 m of sediment, superimposed on longer intervals of variation. The most noticeable of these longer term changes is a trend toward coarser mean values below 200 mbsf. This trend is probably the result of increased foraminifer abundances (see Fig. 5 for comparison).

In the lower portion of Subunit IA (283–293.7 mbsf), the sediment gradually becomes stiffer, as seen by the development of interbedded semi-indurated layers and more lithified, nodule-like intervals. The downhole velocity log (see "Logging" section, this chapter) documents a marked shift toward higher velocities at 250 mbsf, which probably reflects the onset of such interbedding. Spikes in the velocity log between 250 and 300 mbsf may reflect the variable degree of lithification in lower Subunit IA. The ooze-chalk transition at about 294 mbsf is also reflected by a steplike increase in sonic velocity in the downhole log.

Subunit IB

Intervals: Hole 805B, Cores 130-805B-31X to -50X, and Hole 805C, Cores 130-805C-32X to -64X
Age: middle Miocene–late Oligocene
Depth: 293.7–611 mbsf

Subunit IB is composed of 317.3 m of nannofossil chalk, nannofossil chalk with foraminifers, and foraminifer nannofossil chalk. The average foraminifer content is high throughout the upper 90 m of Subunit IB (to Core 130-805C-41X), an interval composed of alternations of foraminifer nannofossil chalk and nannofossil chalk with foraminifers. The foraminifer content decreases below this level, and nannofossil chalk forms the remainder of the section (Figs. 4 and 5). Radiolarians are present in minor quantities in Subunit IB except for Core 130-805B-43X, in which radiolarian abundances as high as 10% were observed in smear slides.

The dominant color of Subunit IB sediment is white (2.5Y 8/0). As in Subunit IA, the sediments of Subunit IB display numerous faint to sharp color bands, which are light gray (5Y 7/2), pale blue (5PB 7/2), pale purple (5P 6/2), grayish blue (5PB 7/2), and light greenish gray (5G 7/1) in color. The color bands of this subunit are commonly sharply defined and concentrated in groups of millimeter-scale thin bands (Fig. 11). Color bands are not common below 504 mbsf (below Core 130-805C-54X), where the sediments are fairly homogeneous. The lack of color banding in this interval could also be the result of reduced recovery in the lower part of the hole. Concentric color rings that form "haloes" around burrows are common (Fig. 12). Bioturbation ranges from slight to heavy throughout the section. This is documented by the presence of numerous burrows, which range in size from several millimeters to almost 10 cm, and by burrow mottles, pyritized burrow fills, and disseminated pyrite that locally color the sediment pale blue (5PB 7/2) to pale purple (5P 6/2). The effects of heavy bioturbation are generally most visible in the darker layers, as shown in Figure 13.

Microfaulting and contortion of color bands generally were not observed in Subunit IB. The only noticeable exception is in Core 130-805C-33X (309.2–312.6 mbsf), which contains wispy laminations and smeared banding (Fig. 14). It is unclear whether these structures were the result of drilling disturbance or if they record sediment destabilization that occurred before drilling began.

Small nodules of chert, each a few centimeters thick, were recorded at 344.35 (Interval 130-805C-37X-2, 135–137 cm) and 370.6 mbsf (Interval 130-805C-40X-1, 0–10 cm). The absence of cherts at these levels in Hole 805B suggests that the cherts are nodular and do not form continuous layers. Shipboard pore-water measurements indicate that the dissolved silica content is high and close to saturation throughout Subunit IB, making the precipitation of chert likely. The levels that contain chert, however, are not accompanied by any noticeable change in pore-water silica concentrations (see "Inorganic Geochemistry" section, this chapter), suggesting that only a minor amount of chert precipitation has occurred. High pore-water silica is probably caused by dissolution of sedimentary silica, but no silica-enriched sediments were recovered at this site; for that reason, the silica source is interpreted to lie below the bottom of Hole 805C.

A thin ash layer was observed at 295.96 mbsf (Section 130-805C-32X-2, 76 cm). With the exception of the chert nodules and the ash layer, Subunit IB is composed almost entirely of calcareous sediments, although the poor recovery in the lower portion of the hole may indicate the presence of cherts in that interval.

The compositional predominance of carbonate is evident in the XRD scans and the shipboard carbonate measurements (Fig. 6). Calcite peak intensities are especially large in diffractograms of samples from the uppermost cores of Subunit IB, in accordance with their high foraminifer content. Nonbiogenic components, which include clays, quartz, and feldspar, are minor constituents in Subunit IB.

The uppermost 2–3 cores of Subunit IB exhibit variable degrees of lithification and contain interbeds of chalk and ooze. Below this interval, the section is composed of more uniformly firm chalk, which becomes increasingly stiff downhole. This transitional interval from ooze to chalk is expressed as a zone of fluctuations in the sonic velocity and density logs (see "Logging" section, this chapter). Much of the remaining variation in the apparent hardness of the sediments can be attributed to the extent of drilling disturbance.

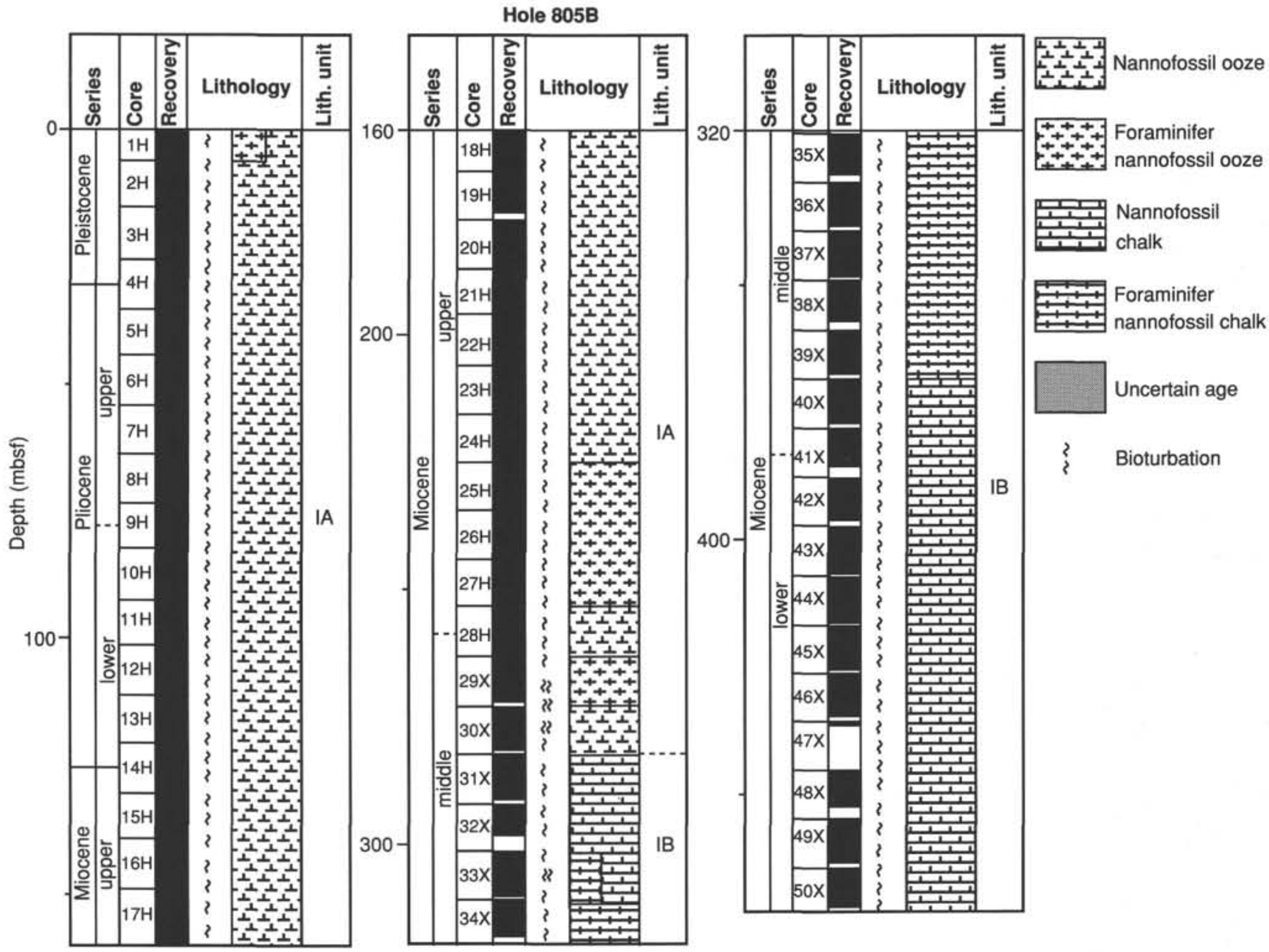

Figure 4. Lithologic summary, Holes 805B and 805C.

Discussion

Site 805 has been characterized by continuous biogenic, pelagic deposition above the CCD since the late Oligocene. This history is documented by the stratigraphic continuity of the recovered pelagic sediments, their generally high sedimentation rates, and the predominance of biogenic carbonate in the sediments. Intervals of reduced sedimentation rate, probably caused by increased dissolution and closer proximity to the CCD, occurred at approximately 10 and 20 Ma (see "Biostratigraphy" section, this chapter).

The most noticeable variation in the sediments of Site 805 is the change in foraminifer content. Foraminifer abundance is generally low in the Oligocene and lower Miocene sections of the record, and it increases in the upper parts of the middle Miocene, in parts of the upper Miocene, and in intervals of the Pleistocene. The changes in foraminifer content may have been caused by variations in the relative production of the different fossil groups, by preservational effects, or by variations in winnowing. Enhanced dissolution can reduce the relative importance of foraminifers in the sediments (Berger, 1976; Berger et al., 1977), because foraminifer preservation is more sensitive than calcareous nannofossil preservation to the position of the calcite lysocline. Changes in the depth of the lysocline and the thickness of the interval from the lysocline to the CCD, therefore, will affect the dissolution of nannofossils and foraminifers differently (Berger et al., 1977). As a result, the foraminifer-rich intervals may indicate times of better foraminifer preservation caused by reduced dissolution. Long-term trends in the relative abundances of the various microfossil groups may be linked to movement of the Ontong Java Plateau into the equatorial zone.

The ooze-chalk transition is located deeper in the sediment column at Site 805 than at Sites 803 and 804, suggesting that this boundary depends on sediment age as well as depth of burial. The depth of the ooze-chalk transition may also be related to the original sediment composition, such as the extent of dissolution experienced before burial (Schlanger and Douglas, 1974). The transition from ooze to chalk is gradational and occurs through a change in the relative abundances of interbedded soft and indurated layers. It is noted that intensively burrowed intervals are often the first to become indurated.

BIOSTRATIGRAPHY

Introduction

Site 805, in 3200 m water depth, is intermediate in position on the Ontong Java Plateau depth transect. A 611 m sedimentary section was drilled and an apparently continuous stratigraphic section of calcareous ooze and chalk of Holocene to late Oligocene age was recovered (Fig. 15). The strata contain a mixture of calcareous and siliceous microfossils suitable for correlation between zonal schemes of the various groups. These microfossil assemblages have various states of preservation pertinent to the interpretation of paleoceanography and/or diagen-

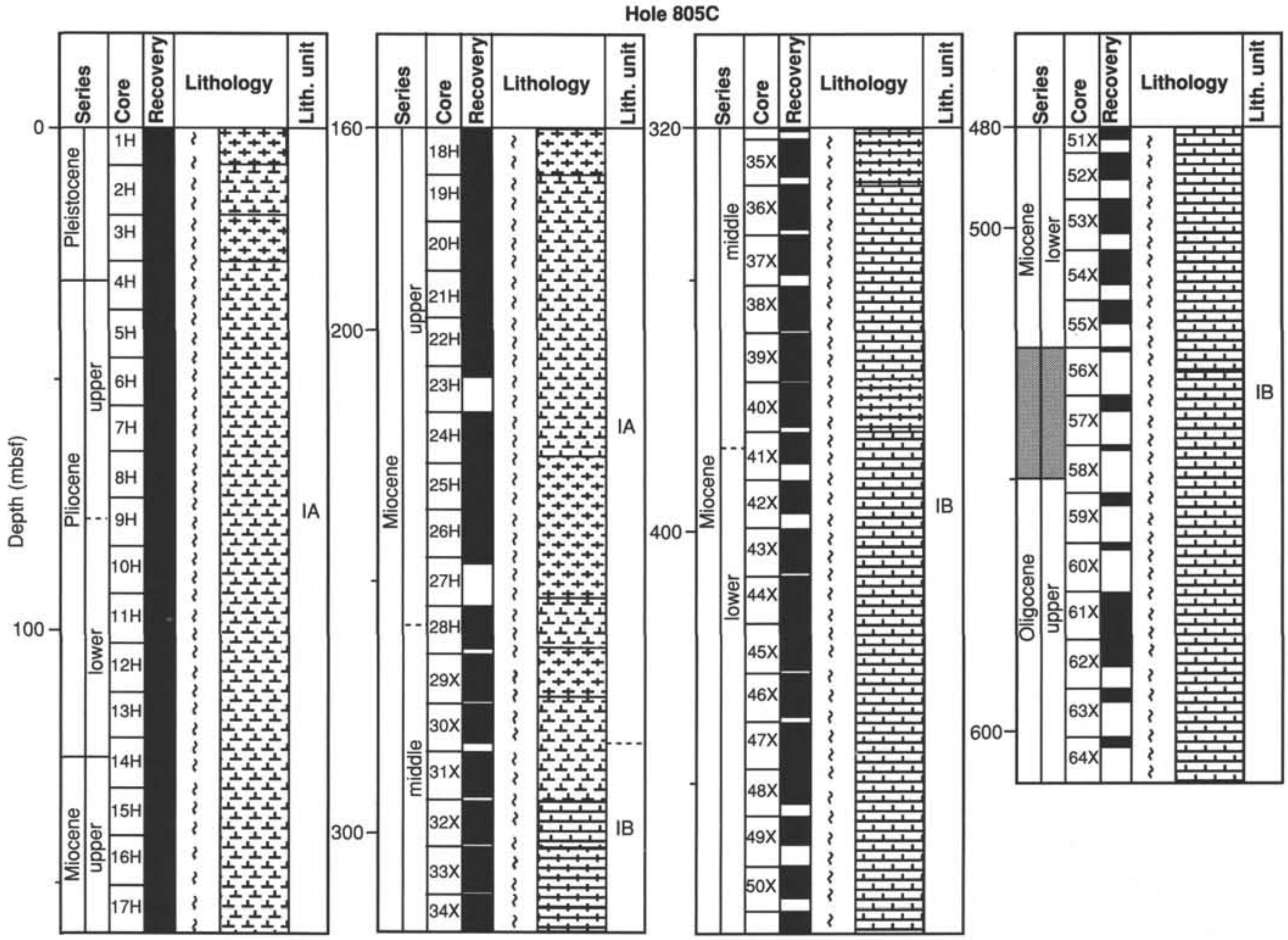

Figure 4 (continued).

esis at intermediate depths on the flanks of the Ontong Java Plateau. The 135-m lower Miocene section is unusually thick, only about 15 m less than that recovered on the upper surface of the Ontong Java Plateau at DSDP Site 289.

Evidence for a significant amount of reworked microfossils was found only among the Quaternary radiolarian assemblages. Problems encountered among all the microfossil groups are the occasional absence of index fossils to differentiate zones and some intervals of poor preservation. These problems are limited and probably can be resolved through examination of sectional samples. Detailed discussion of the stratigraphy as well as the condition of the samples examined follows.

Calcareous Nannofossils

Hole 805A

Pleistocene

The uppermost sample of this hole (Sample 130-805A-1H-CC) contains a Pleistocene to Holocene coccolith assemblage without *Pseudoemiliania lacunosa.* This sample is placed in the NN21/NN20 zonal interval. The assemblages in the next lower two samples (Samples 130-805A-2H-CC and -3H-CC) are characterized by the presence of abundant *Pseudoemiliania lacunosa* and the absence of discoasters. These two samples are placed in Zone NN19. The last occurrence (LO) of *Helicosphaera sellii* was observed in Core 130-805A-3H.

Pliocene

Sample 130-805A-4H-CC contains *Calcidiscus macintyrei, Discoaster brouweri,* and *D. triradiatus,* implying that the Pliocene/Pleistocene boundary falls in Core 130-805A-4H. Sample 130-805A-5H-CC lies below the acme interval of *D. triradiatus* but still belongs to Zone NN18. The bottom of this hole (Sample 130-805A-6H-CC) is late Pliocene in age (the upper part of Zone NN16), based on the occurrences of *Discoaster brouweri, D. pentaradiatus, D. surculus,* and *D. asymmetricus* and the absence of *D. tamalis* and *Reticulofenestra pseudoumbilica.*

Hole 805B

The nannofossil assemblages in the uppermost six cores in this hole are similar to those observed in Hole 803A, and this description of the nannofossil biostratigraphy begins in the upper Pliocene where the NN17/NN18 zonal boundary was observed between Samples 130-805B-5H-6, 70 cm, and -5H-7, 70 cm. The NN16/NN17 boundary falls between the latter sample and Sample 130-805B-5H-CC.

Although the relative abundances of *Discoaster tamalis* and *Discoaster asymmetricus* have not been investigated systematically at closely spaced sample intervals in the upper Pliocene sediments of Leg 130, it is nevertheless obvious that these morphotypes did not thrive in this region because they are notoriously rare. *Discoaster tamalis* is found only in Sample 130-805B-6H-CC.

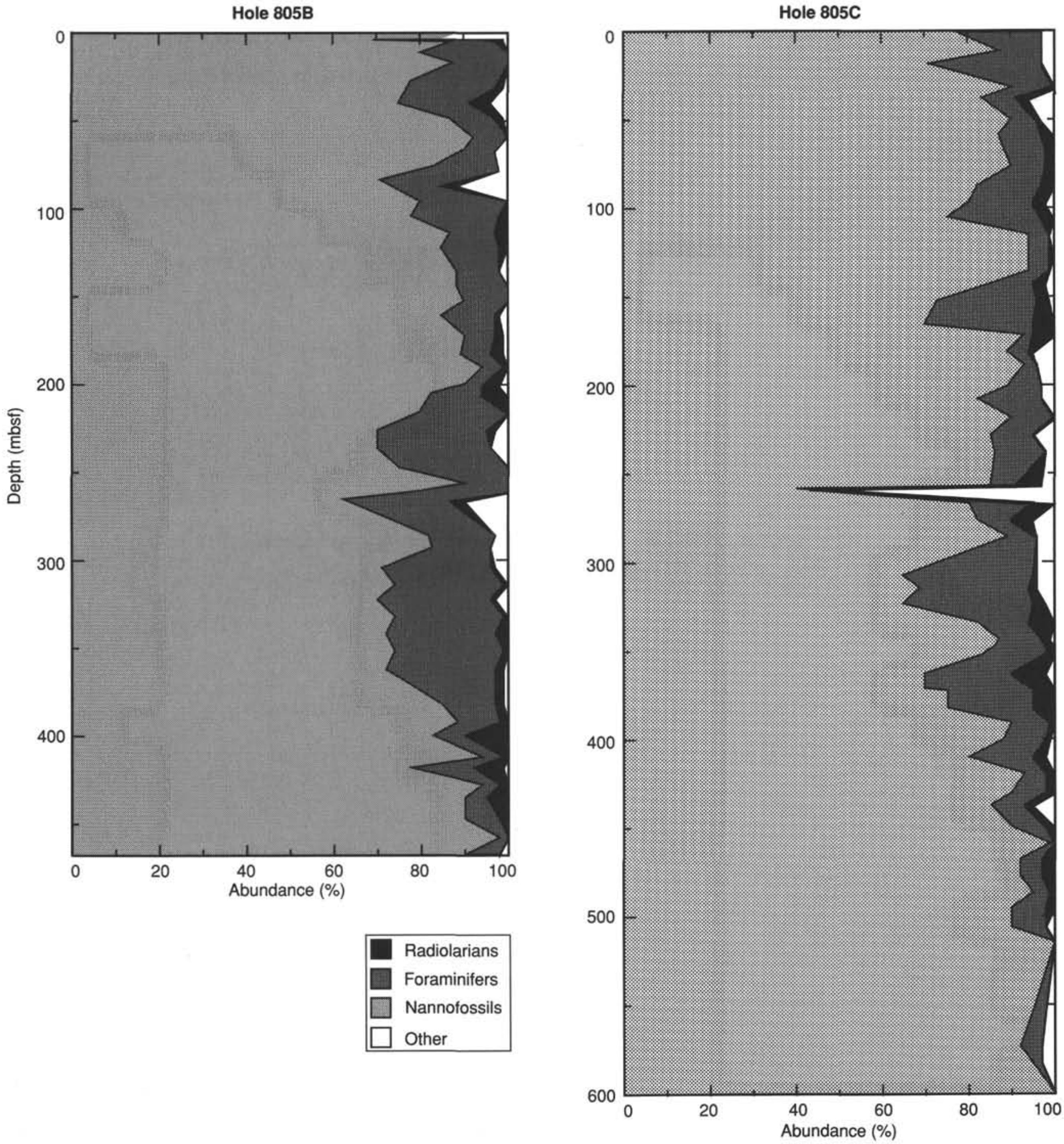

Figure 5. Abundances of major sediment components at Site 805, as determined by smear slide analysis.

Reticulofenestra pseudoumbilica occurs within and below Sample 130-805B-9H-CC. This sample and the next lower sample (130-805B-10H-CC) contain *Discoaster asymmetricus*. The NN15/NN14 boundary cannot be distinguished because *Amaurolithus* is very rare or absent. Therefore, these two samples are tentatively placed in the NN15/NN14 zonal interval. The assemblage in the next deeper sample (Sample 130-805B-11H-CC) is characterized by the presence of *Reticulofenestra pseudoumbilica, Ceratolithus acutus,* and a specimen similar to *Discoaster asymmetricus*. Moreover, this sample lacks *Ceratolithus rugosus* and *Discoaster quinqueramus*. Taken together, this assemblage clearly indicates Zone NN12 of the lowermost Pliocene. The two next deeper samples (Samples 130-805B-12H-CC and -13H-CC) are also considered to belong to Zone NN12 because of the absence of *Ceratolithus rugosus* and *Discoaster quinqueramus*. In Samples 130-805B-11H-CC, -12H-CC, and -13H-CC, peculiar subcircular *Reticulofenestra* specimens are fairly abundant; for example, they occupy nearly 50% of the total assemblage in the former two samples.

Miocene

The section ranging from Samples 130-805B-14H-CC through -23H-CC is referred to Zone NN11 based on the continuous occurrence of *D. quinqueramus*. As mentioned previously, the top

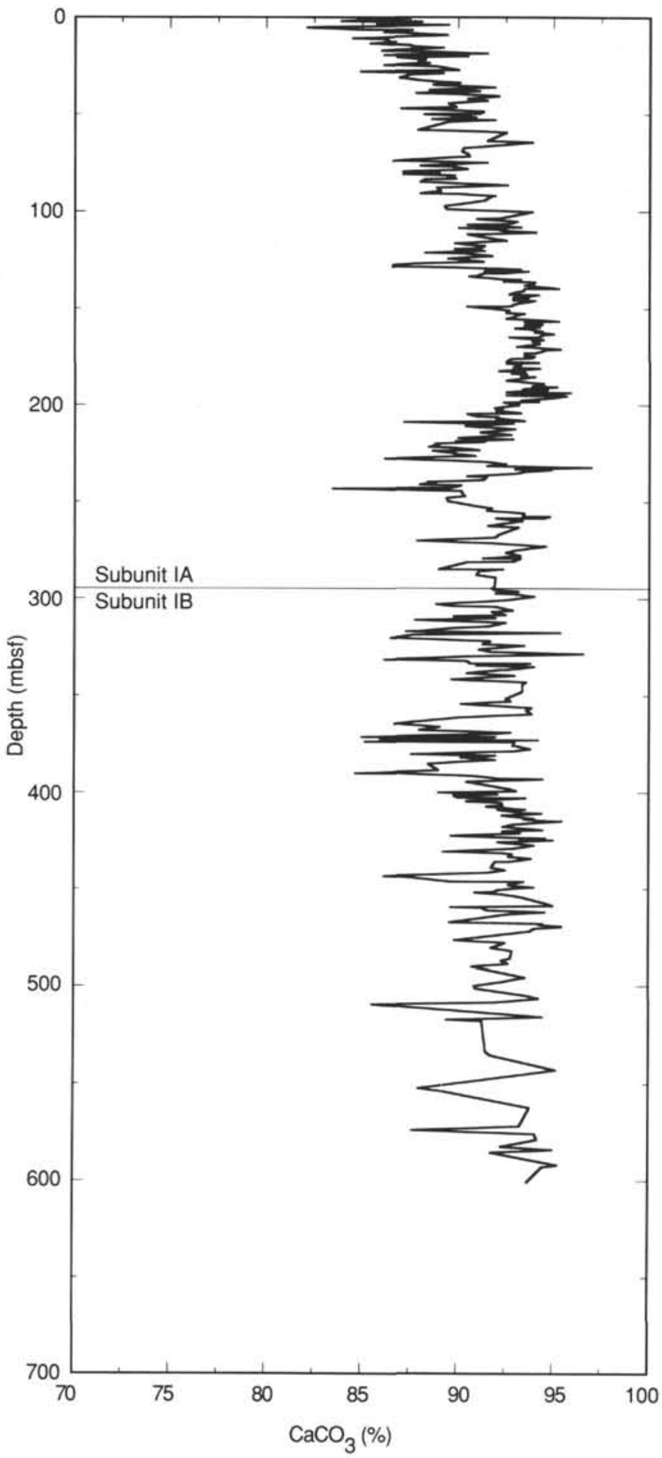

Figure 6. Calcium carbonate content, Hole 805B, based on shipboard measurements.

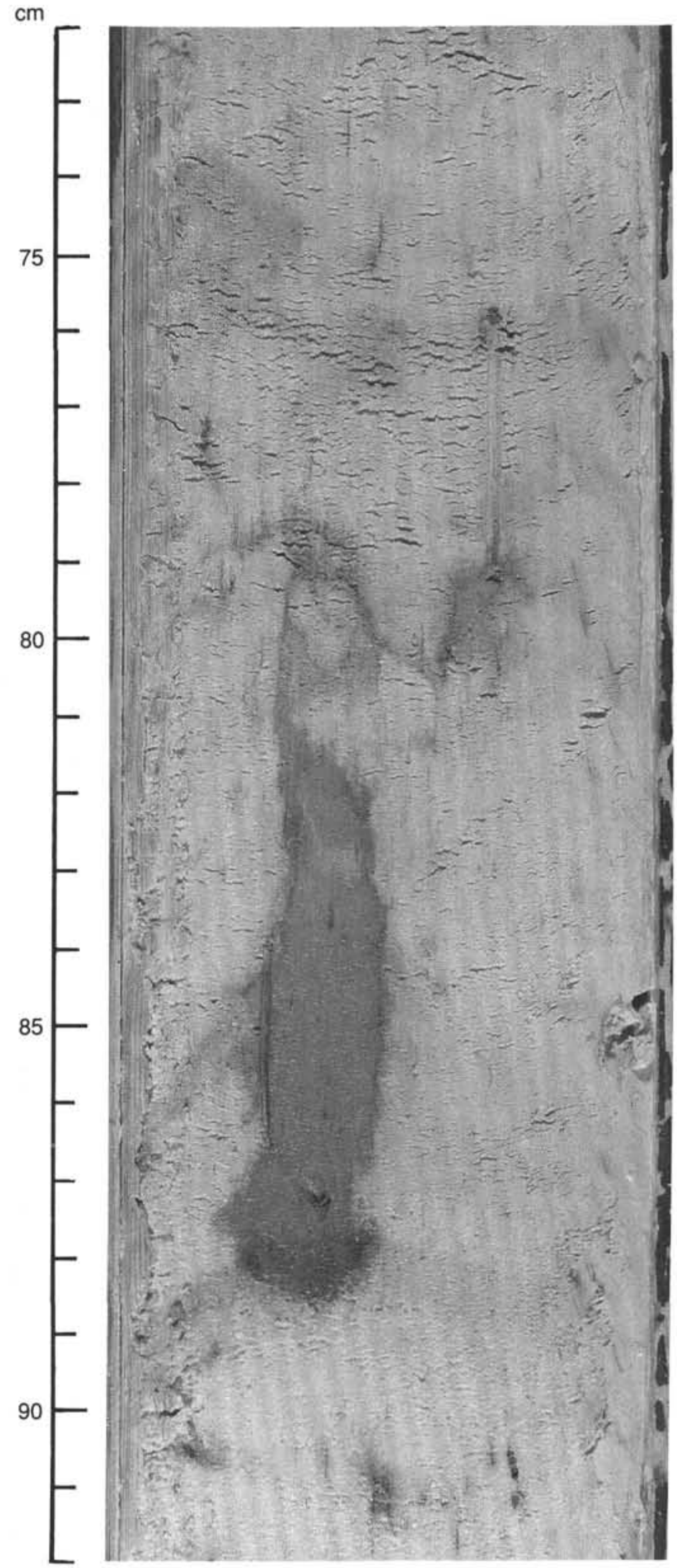

Figure 7. Photograph of large burrow in Subunit IA (Section 130-805B-21H-3, 72–92 cm).

of this zone approximately indicates the position of the Miocene/Pliocene boundary. Specimens belonging to *Amaurolithus* are rare and poorly preserved; their first occurrence (FO) was observed in the interval between Cores 130-806B-22H to -23H. The latter core contains the LO of *Discoaster neohamatus*. The underlying Zone NN10 is represented by the stratigraphic interval ranging from Samples 130-805B-24H-CC through -28H-CC because of the absence of *Discoaster quinqueramus* and *D. hamatus*. The lower part of Zone NN11 and the upper part of Zone NN10 (Samples 130-805B-22H-CC down to -25H-CC) is characterized by a bloomlike abundance of small sphenolith species, such as *Sphenolithus abies* and *S. neoabies*.

The first downhole observation of *Discoaster hamatus* was made in Sample 130-805B-29X-CC, marking the top of Zone NN9. *Catinaster coalitus*, *Catinaster calyculus*, and *Discoaster*

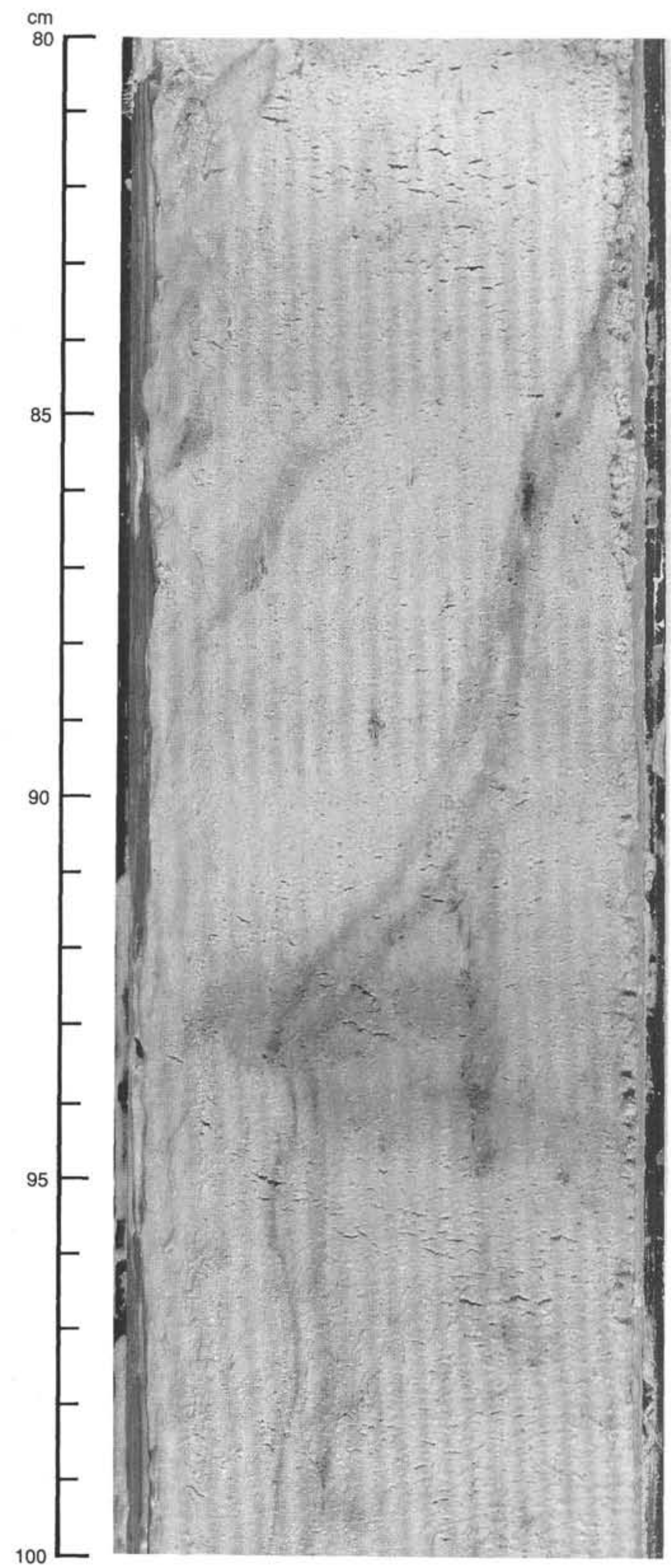

Figure 8. Photograph of a vertical color band in Subunit IA (Section 130-805B-20H-1, 80–100 cm). Formation of the vertical band appears to have changed the color of the horizontal band across the width of the core.

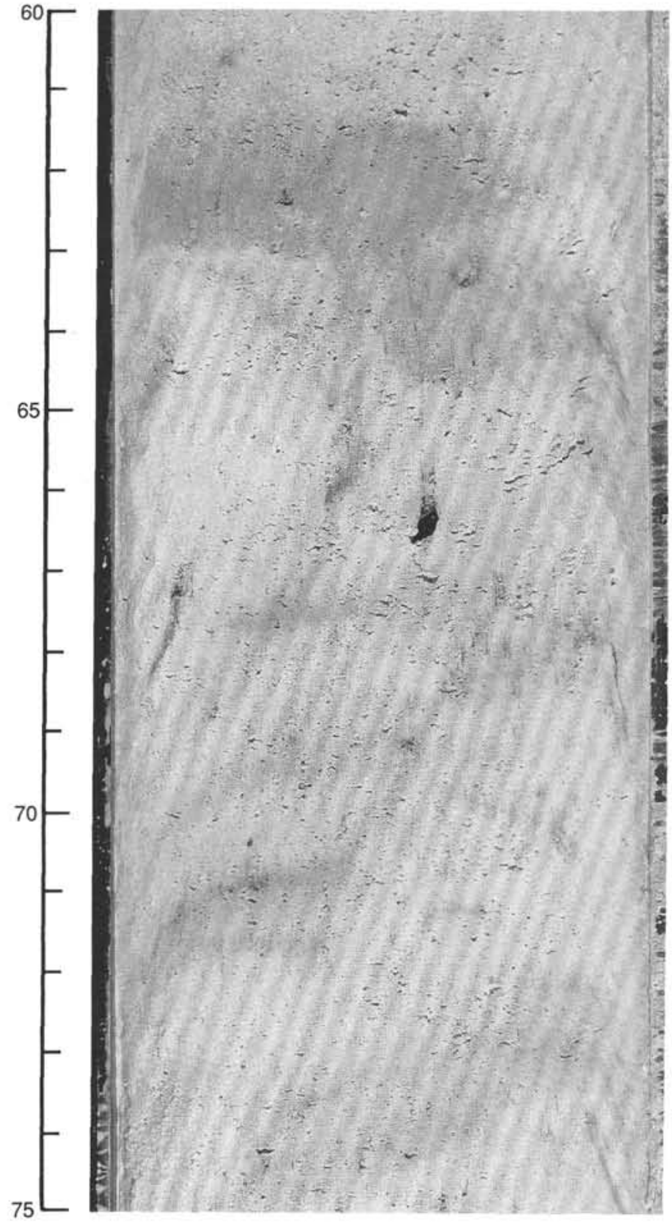

Figure 9. Microfaulting (Section 130-805B-18H-5, 60–75 cm).

neohamatus were also observed in Sample 130-805B-29H-CC. The next lower sample (Sample 130-805-30X-CC) also contains *D. hamatus*. Sample 130-805B-31X-CC contains neither *Discoaster hamatus* nor *Catinaster coalitus*. As at the previous sites, secondary calcite overgrowth on discoasters prevents accurate identification of *Discoaster kugleri*. In addition, this species is a warm-water form (Wise, 1973) but it is generally rare in oceanic sediments (Hay, 1970). Therefore, we were unable to recognize the NN6/NN7 boundary in this hole.

Sample 130-805B-32X-CC is rich in typical *Reticulofenestra pseudoumbilica* and *Dictyococcites perplexus*, as well as typical middle Miocene discoasters that predominantly belong to the *Discoaster variabilis* complex. Having passed through Zone NN8 and not yet reached Zone NN5, and not relying on *Discoaster kugleri* as a marker species, Core 130-806B-32X was placed in the NN6/NN7 zonal interval. Samples 130-805B-33X-CC and -34X-CC lie between the LOs of *Coronocyclus nitescens* and *Cyclicargolithus floridanus*, and between the LOs of *Cyclicargo-*

Table 3. Mean grain size of sediments, Subunit IA.

Core, section, interval (cm)	Depth (mbsf)	Mean grain size (μm)
130-805B-		
1H-1, 10	0.10	31.30
1H-3, 10	3.10	12.50
1H-4, 10	4.60	15.90
1H-5, 11	6.11	16.20
2H-1, 10	6.80	14.60
2H-2, 10	8.30	15.30
2H-3, 118	10.88	12.90
2H-4, 111	12.31	18.60
2H-5, 111	13.81	12.00
2H-6, 111	15.31	8.70
3H-1, 70	16.90	12.50
3H-2, 70	18.40	15.60
3H-3, 70	19.90	31.60
3H-4, 70	21.40	18.30
3H-5, 70	22.90	17.30
3H-6, 70	24.40	17.70
3H-7, 70	25.40	15.80
4H-1, 145	27.15	25.60
4H-2, 145	28.65	23.30
4H-3, 145	30.15	17.30
4H-4, 145	31.65	22.40
4H-5, 145	33.15	16.30
4H-6, 145	34.65	20.50
4H-7, 70	35.40	19.00
5H-1, 70	35.90	14.10
5H-2, 70	37.40	16.20
5H-3, 70	38.90	18.20
5H-4, 70	40.40	18.40
5H-5, 70	41.90	21.80
5H-6, 70	43.40	17.10
6H-1, 122	45.92	20.30
6H-2, 70	46.90	24.70
6H-2, 70	46.90	29.20
6H-3, 70	48.40	15.60
6H-4, 70	49.90	20.40
6H-4, 70	49.90	22.90
6H-5, 70	51.40	11.30
6H-5, 70	51.40	14.00
6H-6, 70	52.90	17.10
6H-6, 70	52.90	16.70
8H-2, 106	66.26	13.70
8H-3, 106	67.76	14.00
8H-4, 106	69.26	17.20
8H-5, 100	70.70	21.40
8H-6, 91	72.11	19.90
9H-1, 114	74.34	10.90
9H-2, 114	75.84	15.30
9H-3, 114	77.34	14.30
9H-4, 114	78.84	22.00
9H-5, 114	80.34	16.80
9H-6, 80	81.50	14.80
10H-1, 104	83.74	12.10
10H-2, 104	85.24	13.30
10H-3, 104	86.74	18.40
10H-4, 104	88.24	19.40
10H-5, 104	89.74	15.70
10H-6, 104	91.24	16.60
10H-7, 60	92.40	21.80
11H-1, 108	93.28	16.40
11H-2, 108	94.78	10.60
11H-3, 106	96.26	12.00
11H-4, 106	97.76	12.20
11H-5, 106	99.26	12.80
11H-6, 106	100.76	15.40
12H-1, 10	101.80	11.50
12H-2, 10	103.30	20.60
12H-3, 10	104.80	15.10
12H-4, 10	106.30	17.20
12H-5, 10	107.80	12.80
12H-6, 10	109.30	16.30
12H-7, 10	110.80	14.10
13H-1, 110	112.30	16.90
13H-2, 110	113.80	23.30
13H-3, 110	115.30	20.70

Table 3 (continued).

Core, section, interval (cm)	Depth (mbsf)	Mean grain size (μm)
130-805B- (Cont)		
13H-4, 110	116.80	14.80
13H-5, 110	118.30	13.90
13H-6, 110	119.80	14.60
13H-7, 35	120.55	18.90
14H-1, 111	121.81	12.50
14H-2, 111	123.31	15.60
14H-3, 111	124.81	17.20
14H-4, 116	126.36	22.00
14H-5, 109	127.79	13.40
14H-6, 110	129.30	16.30
14H-7, 45	130.15	17.70
15H-1, 111	131.31	17.80
15H-2, 109	132.79	19.00
15H-3, 110	134.30	18.70
15H-4, 110	135.80	19.10
15H-5, 110	137.31	17.80
15H-6, 106	138.76	26.10
15H-7, 46	139.66	27.00
16H-1, 35	140.05	29.30
16H-2, 35	141.55	21.40
16H-3, 35	143.05	28.50
16H-4, 35	144.55	10.80
16H-5, 35	146.05	10.00
16H-6, 35	147.55	15.00
16H-7, 35	149.05	16.30
17H-1, 110	150.30	12.40
17H-2, 110	151.80	16.90
17H-4, 110	154.80	16.70
17H-5, 110	156.30	14.10
17H-6, 110	157.80	15.50
18H-1, 10	158.80	15.10
18H-2, 10	160.30	19.60
18H-2, 108	161.28	16.70
18H-3, 10	161.80	16.30
18H-3, 110	162.80	17.00
18H-4, 10	163.30	17.50
18H-4, 110	164.28	14.10
18H-5, 10	164.80	17.70
18H-5, 110	165.80	15.40
18H-6, 10	166.30	12.50
18H-6, 110	167.30	11.40
18H-7, 10	167.80	21.80
18H-7, 35	168.05	14.40
19H-2, 10	169.80	24.80
19H-3, 10	171.30	25.30
19H-4, 10	172.80	21.00
19H-5, 10	174.30	23.60
19H-6, 10	175.80	20.40
20H-1, 50	178.20	16.70
20H-2, 50	179.70	12.70
20H-3, 50	181.20	13.10
20H-4, 50	182.70	14.60
20H-5, 50	184.20	14.60
20H-6, 50	185.70	10.20
20H-7, 50	186.80	14.80
21H-1, 60	187.80	17.60
21H-2, 60	189.30	22.10
21H-3, 60	190.80	17.40
21H-4, 60	192.30	19.20
21H-5, 60	193.80	26.90
21H-6, 60	195.30	21.30
22H-2, 50	198.70	14.60
22H-3, 50	200.20	27.90
22H-4, 50	201.70	25.80
22H-5, 50	203.20	23.20
22H-6, 50	204.70	23.80
23H-1, 83	207.03	19.80
23H-2, 83	208.53	24.00
23H-3, 83	210.03	22.20
23H-4, 83	211.53	25.50
23H-5, 83	213.03	27.40
23H-6, 83	214.53	24.60
24H-1, 88	216.58	18.00
24H-2, 88	218.08	24.40

Table 3 (continued).

Core, section, interval (cm)	Depth (mbsf)	Mean grain size (μm)
130-805B- (Cont)		
24H-3, 88	219.58	22.30
24H-4, 88	221.08	17.30
24H-5, 88	222.58	17.90
24H-6, 88	224.08	17.70
25H-1, 130	226.50	18.30
25H-2, 105	227.75	27.60
25H-3, 107	229.27	27.70
25H-4, 104	230.74	30.10
25H-5, 108	232.28	23.50
25H-6, 103	233.73	24.00
26H-2, 107	237.27	18.70
26H-3, 113	238.83	23.80
26H-4, 86	240.06	30.80
26H-5, 101	241.71	23.40
26H-6, 106	243.26	27.10
27H-3, 118	248.38	20.70
27H-4, 98	249.68	30.40
27H-5, 109	251.29	21.90
27H-6, 109	252.79	26.50
27H-7, 106	254.26	15.50
28H-1, 100	254.70	25.70
28H-2, 100	256.20	15.90
28H-3, 100	257.70	15.70
28H-4, 60	258.80	17.50
28H-6, 100	262.20	23.00
28H-7, 40	263.10	22.80
29H-1, 33	263.53	21.80
29H-2, 46	265.16	22.20
29H-3, 46	266.66	29.20
29H-4, 45	268.15	15.40
29H-5, 45	269.65	17.20
29H-6, 19	270.89	25.30
30H-4, 60	278.00	19.90
30H-5, 60	279.50	18.50
30H-6, 65	281.05	27.80

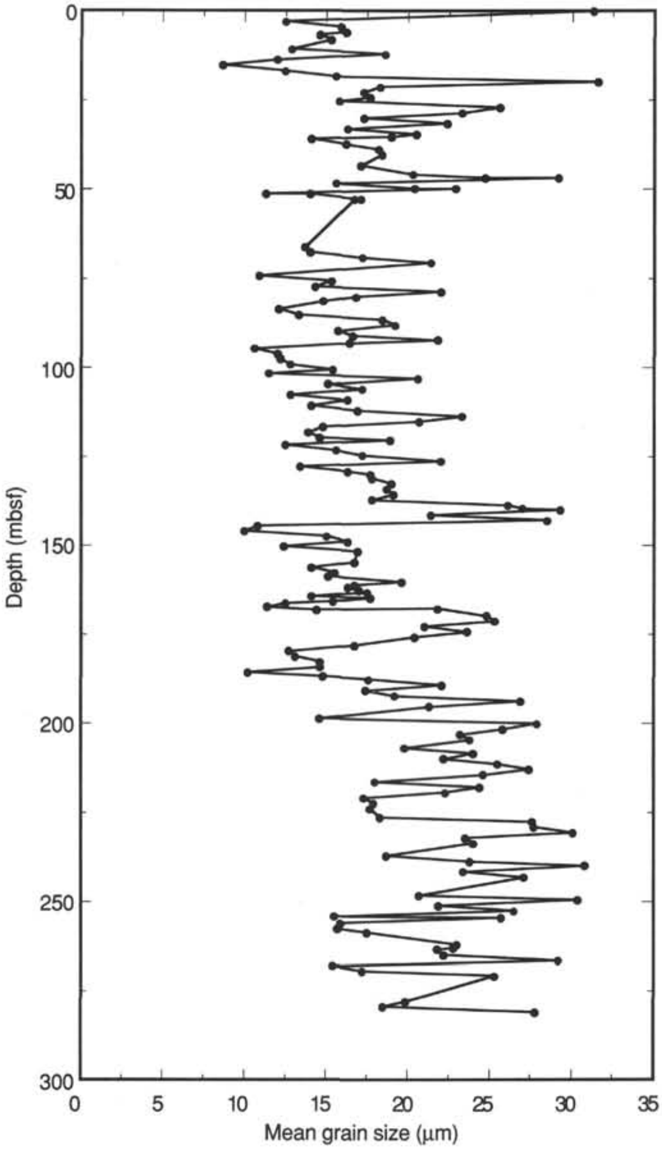

Figure 10. Mean grain size of sediments in Subunit IA (Hole 805B), based on shipboard measurements.

lithus floridanus and *Sphenolithus heteromorphus,* respectively. Therefore, these two samples are considered to belong to Zone NN6. The NN6/NN5 boundary was observed in Core 130-805B-35X. The absence of *Helicosphaera ampliaperta* prevents recognition of the NN4/NN5 boundary in this hole. The change in ratio of the *Discoaster deflandrei* group to total discoasters, however, was observed in Core 130-805B-39X.

The FO of *Sphenolithus heteromorphus* was found between Samples 130-805B-41X-CC and -42X-1, 92 cm. Therefore, the section ranging from Samples 130-805B-35X-CC through -41X-CC was referred to Zones NN5 and NN4. *Triquetrorhabdulus carinatus* was found as high as Sample 130-805B-42X-CC, although a common abundance was observed first in Core 130-805B-45X. *Sphenolithus belemnos* was observed in Core 130-805B-42X. The interval from this core down to Sample 130-805B-45X-CC was placed in the lower Miocene Zone NN2 based on the co-occurrence of *T. carinatus* and *D. druggii.* The section below this zone probably belongs to the NN1 *Triquetrorhabdulus carinatus* Zone. A single specimen of *Sphenolithus ciperoensis* in Sample 130-805B-48X-CC is considered to be reworked.

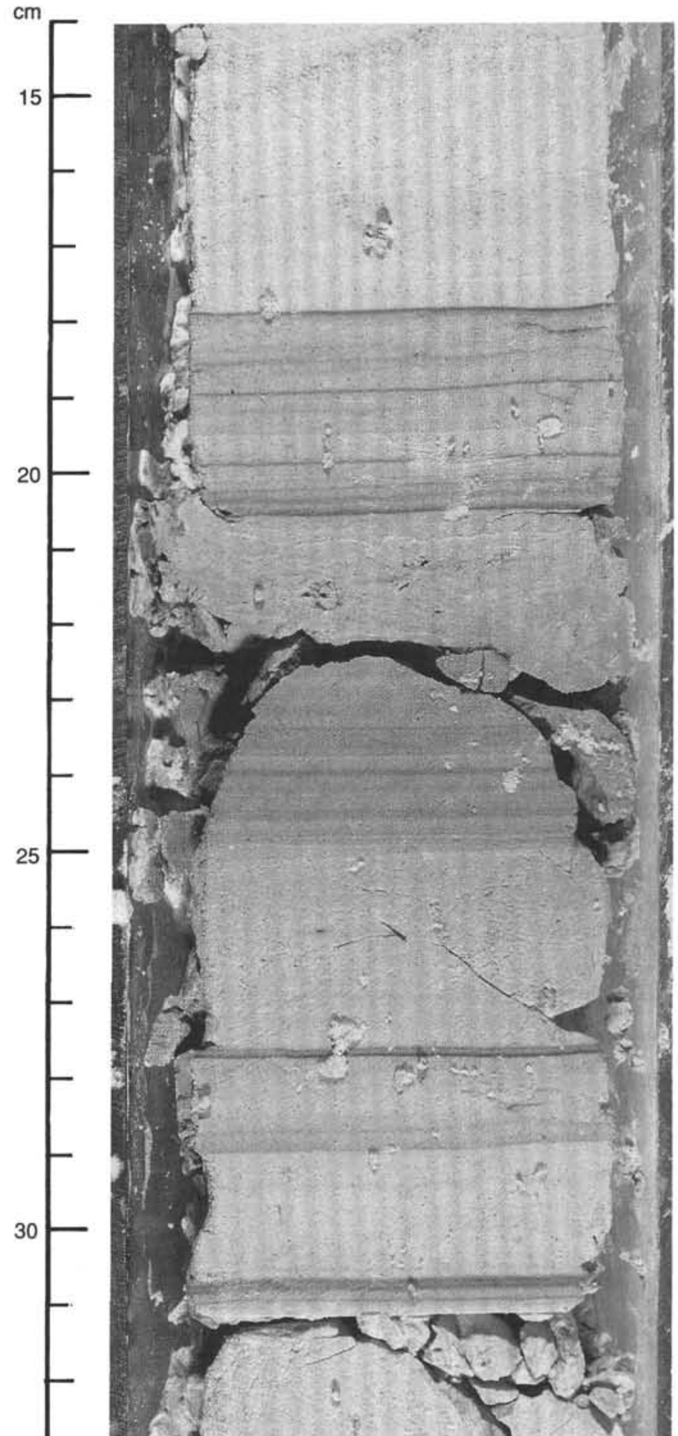

Figure 11. Concentration of well-defined, millimeter-sized color bands in Subunit IB (Section 130-805B-45X-6, 14–34 cm).

Hole 805C

Only core-catcher samples were investigated in the upper 50 cores of Hole 805C (i.e., in the Pleistocene to lower Miocene interval). The results from these core-catcher samples are quite

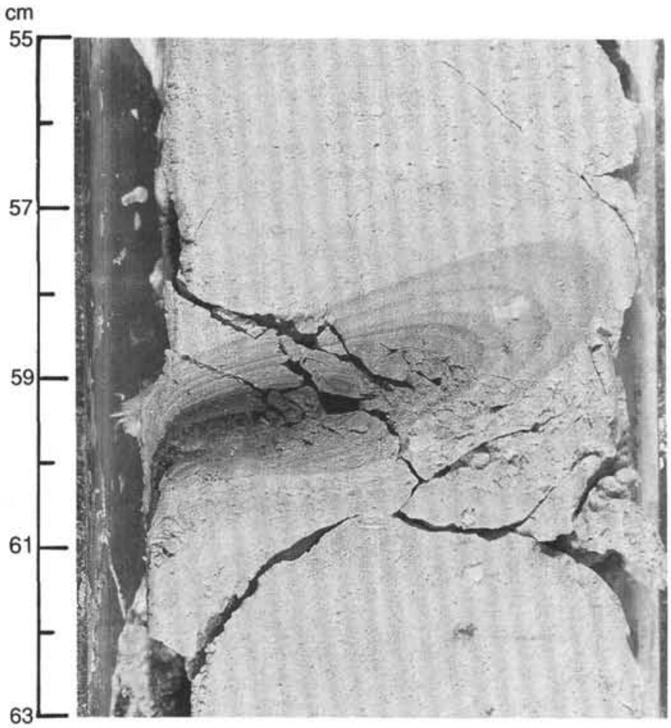

Figure 12. Concentric color bands surrounding a pyritized burrow (Section 130-805B-46X-1, 55–63 cm).

similar to the results obtained from the previous hole and are summarized in Figure 15.

The blooms of the peculiar *Reticulofenestra* morphotype and small sphenoliths again are found in this hole in Samples 130-805C-10H-CC through -12H-CC and in Samples 130-805C-24H-CC and -25H-CC, respectively.

Lower Miocene and Oligocene

Sporadic occurrences of *Discoaster druggii* were recognized in the interval ranging from Samples 130-805C-42X-CC through 130-805C-52X-CC. This interval is also characterized by the continuous occurrences of *Triquetrorhabdulus carinatus*, indicating Zone NN2. The underlying six samples (Samples 130-805C-53X-CC through -58X-CC) contain no age-diagnostic species. These samples may be assigned to the NN2/NN1 zonal interval. A few specimens of *Sphenolithus ciperoensis* were observed in Sample 130-805C-59X-CC, suggesting a late Oligocene age for this sample. Sample 130-805C-60X-CC contains *Sphenolithus ciperoensis* together with *Cyclicargolithus abisectus, C. floridanus, Discoaster deflandrei,* and *Sphenolithus moroformis.*

Neither *Helicosphaera recta,* which defines the NN1/NP25 boundary, nor *Dictyococcites bisectus* were found in the Miocene to Oligocene transitional interval. Therefore, this sample was placed in Zone NP25. The state of preservation becomes poor with abundant fragments below Sample 130-805C-61X-CC. *Sphenolithus ciperoensis* and *S. distentus* were observed in Sample 130-805C-61X-CC, which was placed in Zone NP24. The deepest three samples obtained from this hole, Samples 130-805C-62X-CC through -64X-CC contain both *S. distentus* and *S. predistentus* and are placed in early Oligocene Zone NP23.

Planktonic Foraminifers

Planktonic foraminifers were recovered from all of the core-catcher samples from Holes 805A, 805B, and 805C, but they are few in number in some of the lowermost Miocene and all of the upper Oligocene strata at the base of Hole 805C.

The section appears to be complete, but that spanning the lower/middle Miocene boundary may be condensed, or contain a hiatus, as at Sites 803 and 804. Zone N15, an interval zone,

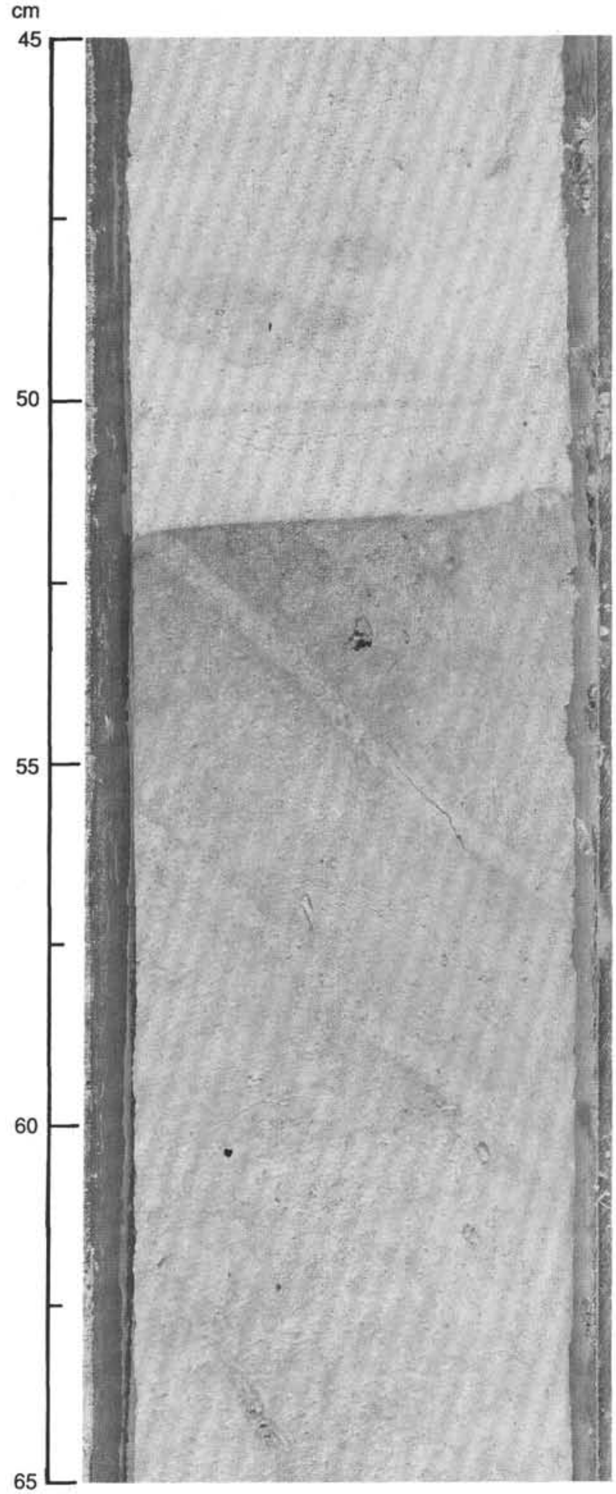

Figure 13. Example of bioturbation (*Zoophycos* trace fossils) easily observed in a darker interval (Section 130-805C-31X-1, 45–65 cm). Note the possible truncation of a burrow at the boundary between the light- and dark-colored intervals.

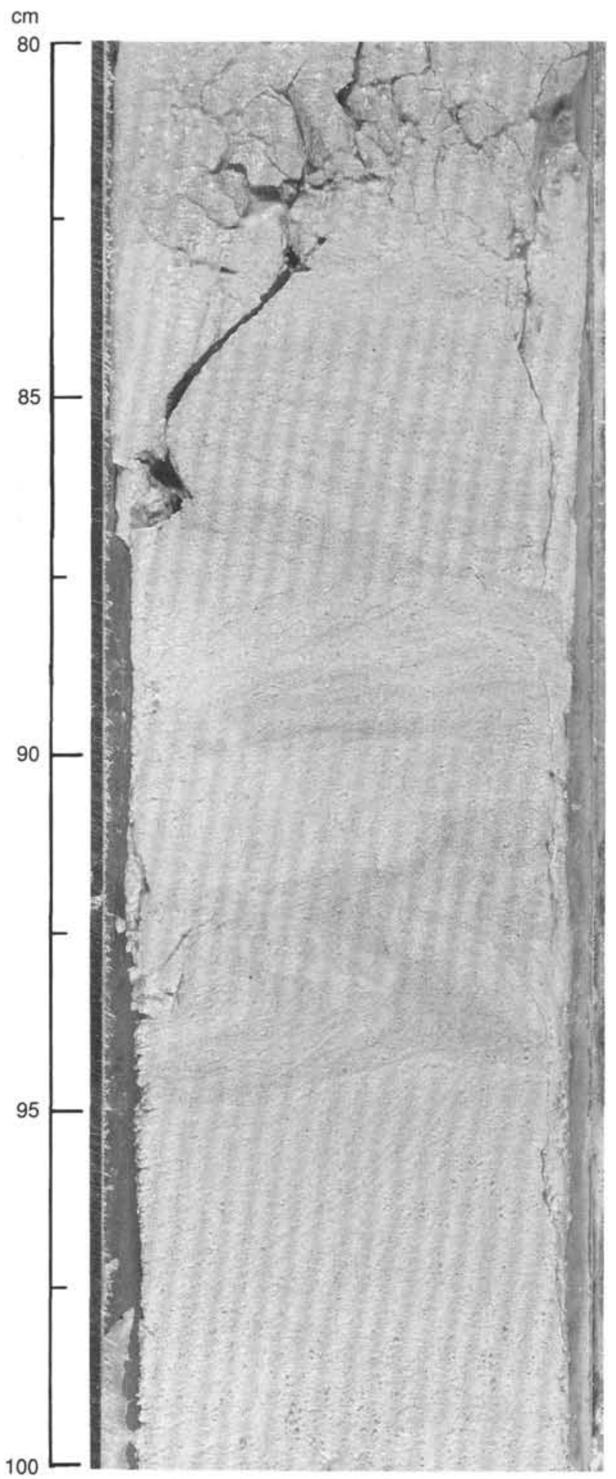

Figure 14. Wispy and contorted(?) laminations (Section 130-805C-33X-4, 80–100 cm). The origin and significance of these features are unclear.

also was not recognized at this site, but it may be represented in a part of Core 130-805B-28X. The lack of diagnostic species in the core-catcher samples examined prevents the resolution of these problems at this time.

The stratigraphy of the three holes is shown in Figure 15 and is discussed below. Remarks concerning the condition of the assemblages and the basis for zonation are also included.

Hole 805A

Planktonic foraminifers are abundant and assemblages are moderately well preserved in the Pleistocene and uppermost Pliocene strata; they are abundant but poorly preserved because of dissolution in the middle Pliocene strata at the base of the hole. The assemblages contain a diversity of tropical species, including many representatives of the genus *Globigerinoides.*

The Pliocene/Pleistocene boundary was placed between Samples 130-805A-2H-CC and -3H-CC, based on the FO of *Globorotalia truncatulinoides.* Sample 130-805A-1H-CC is without *G. tosaensis* and falls within the late part of Zone N22 or within N23. Sample 130-805A-2H-CC contains *G. tosaensis* and *G. truncatulinoides,* which are definitive for Zone N22. Samples 130-805A-3H-CC and -5H-CC contain *G. tosaensis* without *G. truncatulinoides* and are in Zone N21. Between these samples, Sample 130-805A-4H-CC does not contain *G. tosaensis,* possibly because of dissolution, as the assemblage appears more fragmented than assemblages in the adjoining core-catcher samples. The final sample of the hole, Sample 130-805A-6H-CC, is without *G. tosaensis,* but it contains *Sphaeroidinella dehiscens* and was assigned to Zones N19–N20, therefore.

Hole 805B

The first six cores in Hole 805B duplicate the section in Hole 805A. The Pliocene/Pleistocene boundary was placed between Samples 130-805B-2H-CC and -3H-CC; the Miocene/Pliocene boundary between Samples 130-805B-13H-CC and -14H-CC; the middle Miocene/upper Miocene boundary between Samples 130-805B-28H-4, 74–76 cm, and -28H-7, 40–42 cm; and the lower/middle Miocene boundary between Samples 130-805B-40X-CC and -41X-CC. The hole terminated in lower Miocene strata.

Zones N19–N20 were recognized from abundant, moderately well- to well-preserved foraminifers in Samples 130-805B-7H-CC through -9H-CC by the presence of *Sphaeroidinella dehiscens* combined with coiling trends in *Pulleniatina.* The left-to-right coiling change of *Pulleniatina* at 3.8 Ma within this zone was located between Samples 130-805B-9H-CC (left) and -8H-CC (right). *Sphaeroidinella* was not observed below Sample 130-805B-7H-CC. All Pliocene-Pleistocene samples examined contain *Globorotalia tumida,* which has its FO at the base of Zone N18. Sample 130-805B-13H-CC contains *Globorotalia* cf. *tumida* and was assigned to the base of Zone N18.

Upper Miocene Zone N17 was represented in Samples 130-805B-14H-CC through -20H-CC by assemblages containing *Globorotalia plesiotumida* and *G. merotumida.* The presence of *Pulleniatina,* which has been used to divide the zone into A and B units, was noted as low as Sample 130-805B-16H-CC; therefore, its FO at 5.8 Ma falls within Core 130-805B-17H. Except for the assemblages at the base of this zone that show considerable fragmentation, the planktonic foraminifers are moderately well to well preserved. This high degree of fragmentation was also noted in the uppermost core of Zone N16, below which the planktonic foraminifer assemblages are well preserved. Zone N16, recognized through the presence of *Globorotalia merotumida* in the absence of *G. plesiotumida* includes Samples 130-805B-21H-CC through -28H-4, 74–76 cm. *Globorotalia acostaensis* is well represented in these samples; morphologies transitional from *G. continuosa* are present in the lowest sample. Specimens of *Streptochilus* are well represented in this zone. The change from *S. subglobigerum* to *S. latum,* which occurs in about the middle of Zone N16 (Resig, 1989), takes place in Sample 130-805B-24H-CC.

Middle Miocene Zone N14, with abundant *Globorotalia siakensis* (LO at top of N14), was recognized in Samples 130-805B-28H-7, 40–42 cm, through -31X-CC. Only the last sample shows the concurrence of *Globigerina nepenthes* and *G. siakensis,* which defines the zone. This last sample also marks a change in consolidation of the sediment from nannofossil ooze above to nannofossil chalk below. Zones N9 through N12 were assigned to Samples 130-805B-32X-CC through -39X-CC based on the phylogenetic series *Globorotalia peripheroronda, G. peripheroacuta, G. praefohsi,* and *G. fohsi* and its variants, which occur in stratigraphic succession. Planktonic foraminifers are abundant in this interval and their preservation is moderate. Sample 130-805B-40X-CC is assigned to Zone N8 or N9 on the presence of *Globorotalia archeomenardii* and *Praeorbulina sicana. Catapsydrax unicavus* appears to be reworked into this assemblage.

Lower Miocene Zones N6 and N7 cannot be differentiated in Sample 130-805B-41X-CC, which, like the sample above, contains many small specimens of undetermined stratigraphic significance. The age assignment of the sample was based on the absence of *P. sicana* (FO in Zone N8) and of *Globoquadrina binaiensis* (LO in Zone N5). *Catapsydrax unicava* (LO in Zone N6) is rare in the assemblage but may have been reworked as it appears to have been in the stratigraphically next higher sample. *Globigerinatella insueta,* used to define these zones, is not present in the samples from this site. Samples 130-805B-42X-CC through -46X-CC were assigned to Zone N5 based on the presence of *Globoquadrina binaiensis* and the absence of *Globorotalia kugleri.* Within this zone, radiolarians are particularly abundant in Sample 130-805B-43X-CC and horizons of strong fragmentation of specimens are present in Samples 130-805B-42X-CC and -46X-CC. Zone N4 is represented in Samples 130-805B-47X-CC through -50X-CC, the bottom of the hole, based on the presence of common *Globorotalia kugleri* s.s. Many small planktonic specimens are present in these samples. The preservation of the tests is moderate to good.

Hole 805C

The repeated section of this hole into Zone N4 closely parallels that of Hole 805B in planktonic foraminifer abundance, preservation, and stratigraphy, but a few of the zonal boundaries are slightly offset. In this section, an unusual Zone N16 assemblage, in which there are no keeled species, is present in Sample 130-805C-22H-CC. This may reflect a climatic change, as the foraminifers in the sample are well preserved. In a departure from the stratigraphy of Hole 805B, Samples 130-805C-30X-CC through -32X-CC were tentatively assigned to Zone N13 based on the presence of *Globorotalia siakensis* in the absence of *Globigerina nepenthes.* Because *G. nepenthes* is not consistently present, this assignment is preliminary.

The boundary between lower Miocene Zones N4 and N5 is between Samples 130-805C-47X-CC and -48X-CC based on the LO of *Globorotalia kugleri* s.s. The Oligocene/Miocene boundary was placed between Samples 130-805C-55X-CC and -56X-CC, based on the FO of *G. kugleri* s.s. Below this boundary to Sample 130-805C-58X-CC, specimens of similar morphology to *G. kugleri* are present. These specimens are differentiated from *G. kugleri* s.s. by the greater convexity of their spiral sides and their less inclined sutures. The upper part of Zone P22 is characterized by these *G. kugleri* ancestors, which occur with *Globorotalia opima nana. G. opima opima,* which marks the top of Zone P21b, is present in Sample 130-805C-61X-CC and the remainder of the core-catcher samples to the bottom of the hole. No *Chiloguembelina* are present in these samples from Zone P21b. Only a few specimens of planktonic foraminifers are present in the lowermost Miocene and in the Oligocene section from Sample 130-805C-55X-CC to the bottom of the hole. These samples contain abundant radiolarians.

Benthic Foraminifers

The core-catcher samples from the Quaternary to lower Miocene section of Hole 805B were examined for benthic foraminifers, which were found to be present in all samples. In addition, a single sample from Hole 805C (Sample 130-805C-60X-CC) was examined to evaluate the upper Oligocene benthic assemblage. Preservation of the benthic tests generally is good, even when the planktonic foraminifers show fragmentation. However, Samples 130-805B-14H-CC (top of the Miocene), -42X-CC, -43X-CC, -46X-CC, and -48X-CC (lower Miocene), and Sample 130-805C-60X-CC (upper Oligocene) contain 50% or more broken benthic tests. Large concentrations of radiolarians in these samples, as well as a low planktonic foraminifer content, indicate carbonate dissolution has occurred. The intervals of increased dissolution appear to be fewer than at Site 803, which lies 200 m deeper, but parts of the lower Miocene and upper Oligocene section at both sites experienced extensive dissolution, resulting in a concentration of benthic tests.

At Site 805, as at Site 803, the benthic assemblages represent lower bathyal to abyssal biofacies. No evidence of transported tests was noted. Articulated whole ostracode valves in Samples 130-805B-13H-CC (lower Pliocene) and -17H-CC (upper Miocene) indicate *in-situ* assemblages.

The stratigraphic succession of assemblages is similar to that at Site 803; the upper Oligocene and lower Miocene assemblages are transitional in that they contain species common in the Paleogene such as *Cibicidoides grimsdalei* and *Buliminella grata* along with a high percentage of *Nuttallides,* a genus that is generally prominent in the Neogene assemblages. The Quaternary assemblages examined from Sites 805 and 803 differ significantly in that *Uvigerina* is better represented at Site 805 and *Nuttallides umbonifera* and *Pseudoparrella exigua* are better represented at Site 803. This may be a result of differences between the two sites in deep-water masses or in surface productivity, hence organic input, or to a combination of these environmental factors. At 3200-m water depth, Site 805 is close to the modern boundary between Pacific Deep Water and Pacific Bottom Water that lies at approximately 3000 m. The Site 805 Quaternary assemblage may be at least partly controlled by the deep-water mass, whereas the Site 803 assemblage has bottom-water affiliation. However, Site 805 (1°13′N) lies nearer the band of equatorial upwelling and may receive more organic flux than Site 803 (2°26′N), which would also favor uvigerinid populations. Although the organic content of the carbonate sediment in the Ontong Java Plateau is low, a small increase in organic carbon from <0.01% to 0.35% was linked to an onset of uvigerinids in the Pliocene section at DSDP Site 586 (Hermelin, 1989).

Listed in Table 4 are the most frequent benthic species present in sand fraction (>0.063 mm) samples representative of the various time-stratigraphic units. Their percent frequencies among the benthic fauna are given, as well as the names of some less frequent members of the assemblages. The following data also are given: B = the percent representation of benthic specimens relative to total foraminiferal content; N = the number of specimens counted for the percent frequency data; and T = the total number of benthic specimens in each approximately 20-cm^3 core-catcher sample, calculated from the sample split used for the census data.

Diatoms

Diatoms were examined in Hole 805B (Samples 130-805B-20H-CC through -50X-CC) and in Hole 805C (Samples 130-805C-1H-CC through -20H-CC and Samples 130-805C-50X-CC through -64X-CC). Quaternary through Oligocene diatoms are present. The assignment of samples to a low-latitude diatom zonation is summarized in Figure 15.

Diatoms are few (rare) and poorly preserved in the Pleistocene sediments (Samples 130-805C-1H-CC through -3H-CC). Between 45 (Sample 130-805C-5H-CC, upper Pliocene) and 426.5 mbsf (Sample 130-805B-45X-CC, middle early Miocene), diatoms are

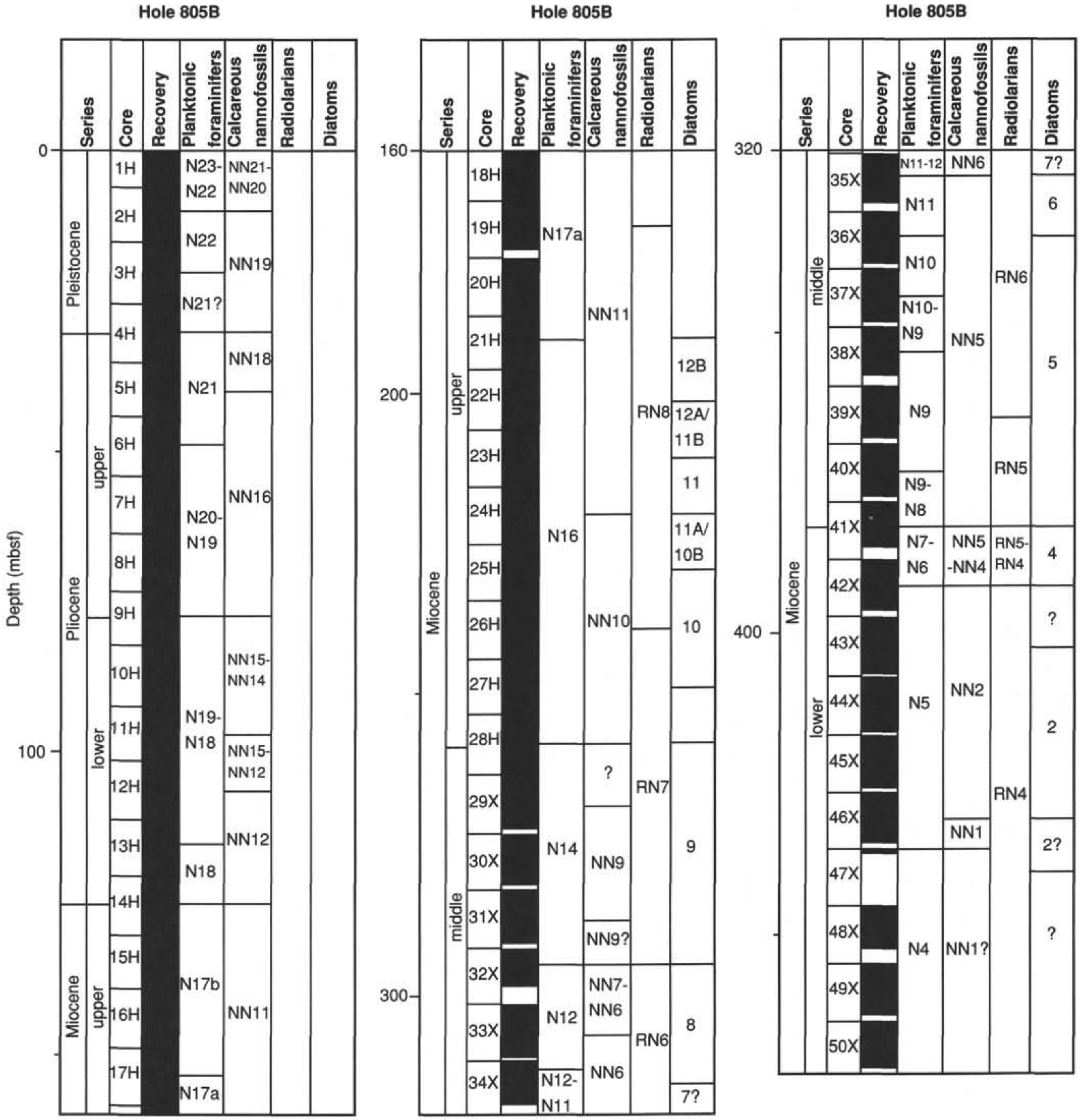

Figure 15. Biostratigraphic hole summaries, Holes 805B and 805C. RN = radiolarian Neogene zone, NTD = Neogene tropical diatom zone, RP = radiolarian Paleogene zone, and NN = nannofossil Neogene zone.

common to abundant, and preservation is generally good. A sharp decrease in abundance and preservation was observed in the early Miocene (Samples 130-805B-46X-CC through -50X-CC) and upper Oligocene (Samples 130-805C-56X-CC through -64X-CC).

Site 805 is the first site on this depth transect with an apparently complete sediment sequence, from the Quaternary NTD *Pseudoeunotia doliolus* Zone (Sample 130-805C-1H-CC) through the Oligocene *Rocella vigilans* Zone (Sample 130-805C-62X-CC). However, poor preservation and low diatom abundances prevented the precise dating of the sediment in the lower Miocene (Samples 130-805B-47X-CC through -50X-CC) and across the Miocene/Oligocene boundary (Sample 130-805C-55X-CC; the *Rocella gelida* Zone may be missing).

Unlike Sites 803 and 804, Site 805 has a complete Miocene sediment sequence (Fig. 15), which includes diatom Zones NTD 13 *Thalassiosira convexa* (Sample 130-805C-14H-CC) through NTD 1 *Rosiella paleacea* (Sample 130-805C-54X-CC). The late Miocene/middle Miocene boundary is located in Sample 130-805B-28H-CC at the top of the NTD 9 *Actinocyclus moronensis*

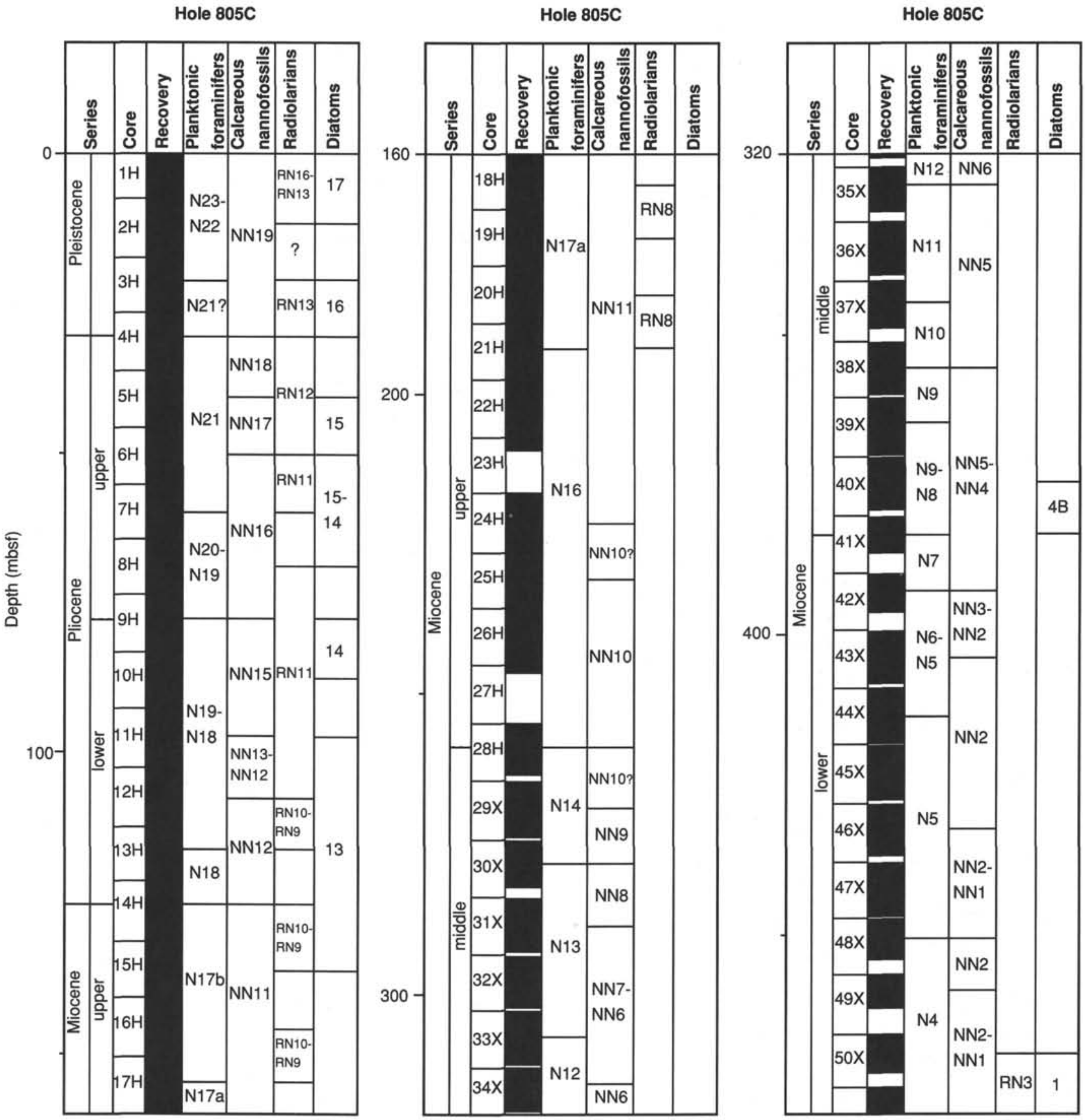

Figure 15 (continued).

Zone. The middle/early Miocene boundary is difficult to locate at Site 805. It may be contained in the basal NTD 5 *Cestodiscus peplum* Zone in Sample 130-805B-40X-CC. The next sample downhole (Sample 130-805B-41X-CC) was assigned to the NTD 4 *Denticulopsis nicobarica* Zone (upper early Miocene). This zone was missing at Sites 803 and 804. The NTD 3 *Triceratium pileus* Zone may be compressed, and the next dated sample (Sample 130-805B-44X-CC) falls within the NTD 2 *Craspedodiscus elegans* Zone.

Diatoms are poorly preserved in the Oligocene samples. Samples 130-805C-56X-CC and -57X-CC are assigned to the *Borgorovia veniamini* Zone, and Samples 130-805C-58X-CC through -62X-CC fall within the *Rocella vigilans* Zone. The age of the last core-catcher sample (Sample 130-805C-64X-CC) could not be determined because of the poor preservation of the diatom assemblage.

Radiolarians

Samples from the three holes at Site 805 were combined to examine a continuous stratigraphic sequence. The following core-catcher samples were examined: 130-805A-1H-CC and -2H-CC; 130-805B-20H-CC through -50H-CC; 130-805C-1H-CC

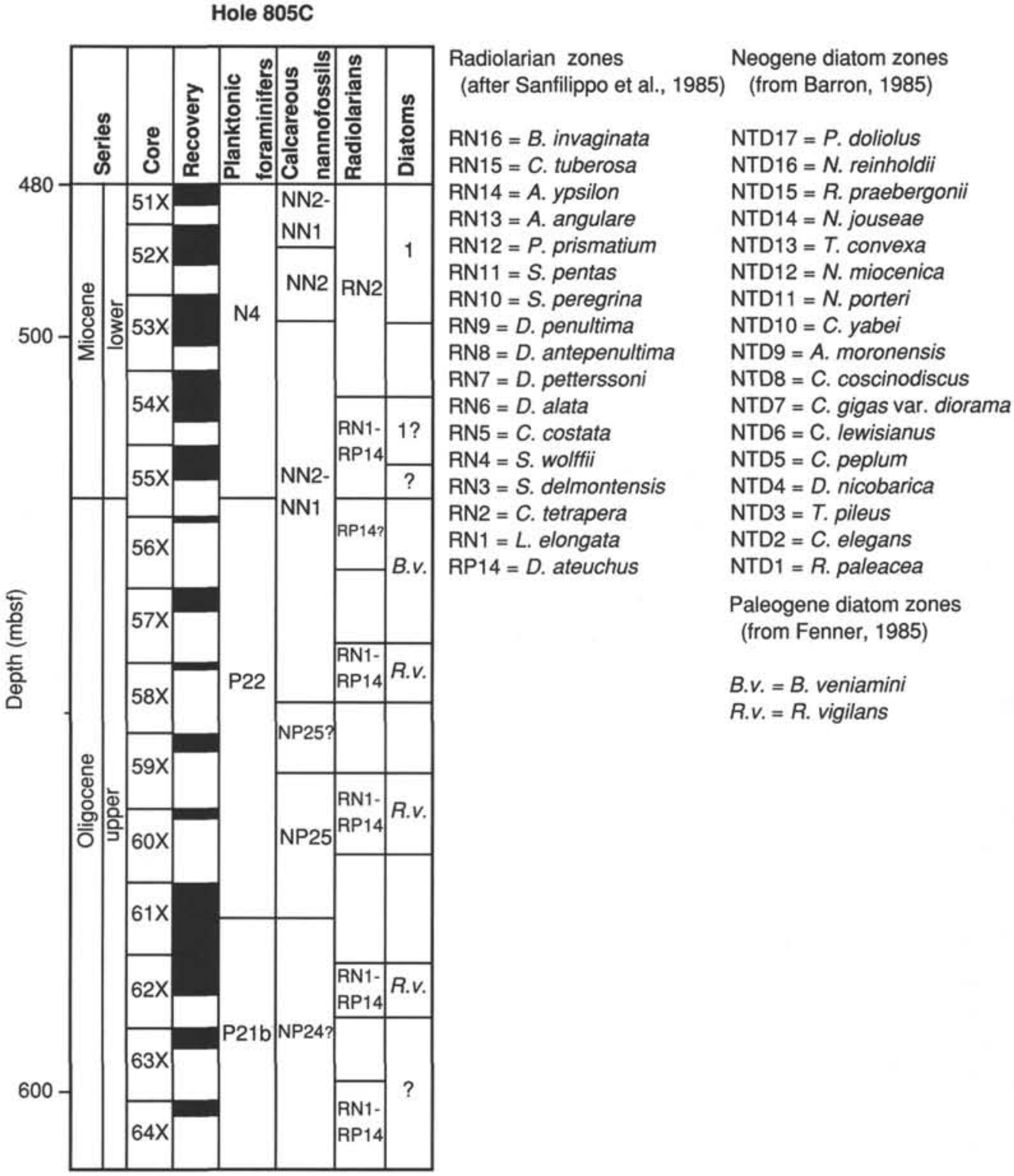

Figure 15 (continued).

through -20H-CC; and 130-805C-50X-CC through -64X-CC (611.0 mbsf). These samples contain radiolarians in variable states of preservation. For most intervals, age assignments based on radiolarians were possible. Radiolarian preservation in Samples 130-805C-1H-CC and -2H-CC was extremely poor, which made age determination uncertain. However, the core-catcher samples from the uppermost two cores of Hole 805A provided useful age information as the radiolarians are preserved in moderate and good condition, respectively.

The following discussion pertains to the zonal assignment of the core-catcher samples examined and their stratigraphically important taxa. Figure 15 summarizes the radiolarian zonation of Holes 805A, 805B, and 805C and correlates these zonations with the zones of other taxa. Evidence for sediment reworking is also discussed.

Quaternary

Sample 130-805A-1H-CC was assigned to the *Buccinosphaera invaginata* Zone, which extends from 0.21 Ma to the present as it contains *B. invaginata*. Significant amounts (18%–19%) of radiolarians are considered to be reworked (see "Sediment Reworking" section below, this chapter). Sample 130-805A-2H-CC belongs to the *Anthocyrtidium angulare* Zone, which is indicated by the presence of *A. angulare* and *Theocorythium trachelium trachelium*. The same zone extends to Sample 130-805C-3H-CC, which contains *Lamprocyrtis heteroporos*.

Pliocene Through Upper Miocene

Sample 130-805C-4H-CC was placed in the *Pterocanium prismatium* Zone because of the presence of *Lamprocyrtis neoheteroporos, L. heteroporos,* and *Pterocanium prismatium*. The presence of both species of *Lamprocyrtis* indicates that this sample belongs to the uppermost part of the assigned zone because the change from *Lamprocyrtis heteroporos* to *L. neoheteroporos* is evolutionary. Sample 130-805C-5H-CC was also placed in that zone, but it contains reworked *Stichocorys peregrina* and *Didymocyrtis antepenultima* from upper Miocene and lower Pliocene intervals. Samples 130-805C-6H-CC through -11H-CC were assigned to the *Spongaster pentas* Zone because of the presence of *S. pentas* and *Didymocyrtis avita*.

Table 4. Benthic foraminifers as a percentage of total foraminifers, Site 805.

Age and sample data	Species name	Sample (%)
Quaternary (N22)	*Oridorsalis umbonatus*	10%
Sample 130-805B-2H-CC	*Pullenia bulloides*	8%
B = 1%	*Uvigerina bradyana*	8%
N = 211	*Pseudoparrella exigua*	7%
T = 3,376	*Cassidulina* sp.	6%
	Pacinonion novozealandicum	6%
	Melonis pompilioides	5%
	(Others: *Cibicidoides mundulus*)	
early Pliocene (N18)	*Nuttallides umbonifera*	10%
Sample 130-805B-13H-CC	*Globocassidulina subglobosa*	7%
B = <1%	*Pullenia bulloides*	5%
N = 296	*Eggerella bradyi*	5%
T = 2,368	(Others: *Cibicidoides mundulus*)	
late Miocene (N17)	*Siphouvigerina* sp.	10%
Sample 130-805B-18H-CC	*Melonis affinis*	6%
B = <1%	*Pleurostomella acuminata*	6%
N = 195	*Nuttallides umbonifera*	5%
T = 780	(Others: *Cibicidoides mundulus*)	
middle Miocene (N11)	*Nuttallides umbonifera*	10%
Sample 130-805B-35X-CC	*Oridorsalis umbonatus*	9%
B = 1%	*Eggerella bradyi*	7%
N = 172	*Globocassidulina subglobosa*	6%
T = 1,376	*Cibicidoides mundulus*	6%
	Brizalina pusilla	5%
	(Others: *Bolivinopsis cubensis*)	
early Miocene (N4)	*Nuttallides umbonifera*	17%
Sample 130-805B-50X-CC	*Oridorsalis umbonatus*	14%
B = <1%	*Globocassidulina subglobosa*	13%
N = 174	*Linaresia pseudogrosserugosa*	6%
T = 348	*Pullenia bulloides*	6%
	(Others: *Cibicidoides grimsdalei, Buliminella grata, Bolivinopsis cubensis*)	
late Oligocene (P22)	*Globocassidulina subglobosa*	24%
Sample 130-805C-60X-CC	*Oridorsalis umbonatus*	10%
B = 5%	*Linaresia pseudogrosserugosa*	7%
N = 375	*Pseudoparrella* aff. *exigua*	6%
T = 375	*Siphonodosaria* sp.	6%
	Gyroidinoides girardanus	6%
	Cassidulina spinifera	6%
	(Others: *Cibicidoides* cf. *subhaidingeri, Bolivinopsis cubensis*)	

Notes: B = the percentage of representation of benthic specimens relative to total foraminifer content; N = the number of specimens counted for the percent frequency data; and T = the total number of benthic specimens in each approximately 20-cm^3 core-catcher sample, calculated from the sample split used for the census data.

Samples 130-805C-12H-CC, -14H-CC, and -16H-CC are in either the *Didymocyrtis penultima* Zone or the *S. peregrina* Zone as these zones cannot be differentiated. The samples contain *D. penultima, S. peregrina, Spongaster berminghami,* and *Solenosphaera omnitubus.* Samples 130-805C-18H-CC through -25H-CC were placed in the *Didymocyrtis antepenultima* Zone, based on the presence of *Diartus hughesi* and/or *Didymocyrtis antepenultima.*

Middle Miocene

Sample 130-805B-26X-CC was placed in the upper part of the *Diartus petterssoni* Zone because of the presence of *Didymocyrtis laticonus* and *D. petterssoni.* Samples 130-805B-28X-CC, -30X-CC, and -31X-CC also belong to the *D. petterssoni* Zone, an assignment further substantiated by the presence of *Lithopera neotera,* in addition to the two taxa already mentioned. Samples 130-805B-32X-CC through -38X-CC were placed in the *Dorcadospyris alata* Zone as they all contain *D. alata* and/or *Lithopera renzae.*

Lower Miocene Through Oligocene

Samples 130-805B-39X-CC and -40X-CC were placed in the *Calocycletta costata* Zone because it can be bracketed by *Calocycletta costata* and *Dorcadospyris forcipata.* Sample 130-805B-41X-CC belongs to either the *Calocycletta costata* Zone or the upper part of the *Stichocorys wolffii* Zone as it contains *Dorcadospyris dentata.* Samples 130-805B-42X-CC through -50X-CC (473.3 mbsf) were placed in the *Stichocorys wolffii* Zone because of the presence of *Dorcadospyris simplex, S. wolffii,* and *Cyclampterium pegetrum.* Sample 130-805C-50X-CC (475.5 mbsf) was placed in the *Stichocorys delmontensis* Zone as it can be bracketed by the presence of *Cyrtocapsella cornuta* and *Cyclampterium leptetrum.* The presence of *Cyrtocapsella tetrapera* and *Theocyrtis annosa* brackets Samples 130-805C-51X-CC, -52X-CC, and -53X-CC in the *Cyrtocapsella tetrapera* Zone. Samples 130-805C-54X-CC through -64X-CC belong to either the *Lychnocanoma elongata* or the *Dorcadospyris ateuchus* zones. They typically contain *Dorcadospyris papilio, D. forcipata, D. ateuchus, and T. annosa.* Sample 130-805C-56X-CC was assigned to the *D. ateuchus* Zone because a specimen of *Lychnocanoma* cf. *trifolium* was found. However, this specimen does not have feet, although the rest of the features are conformable with *L. trifolium,* and therefore the zonal assignment is tentative.

Sediment Reworking

A significant number of radiolarians in the uppermost core catcher have been reworked. The extent of reworking can be estimated by counting radiolarians of two different refractive indexes, as reworked specimens have significantly different indexes. Sample 130-805A-1H-CC, mounted in Canada Balsam (refractive index, ND = 1.53), contains abundant and moderately preserved radiolarians. Most radiolarians have low refractive indexes, which makes them nearly transparent under a transmission light microscope. In this sample, there are many reworked specimens of late Miocene radiolarians such as *Stichocorys peregrina, S. delmontensis,* and *Didymocyrtis antepenultima.* More than 20 of these specimens appear to have significantly higher refractive indexes than upper Pleistocene and/or Holocene radiolarians. No reworked specimens of significantly older age with low refractive indexes have been found thus far. Therefore, we assumed that all of the specimens with the high index are reworked.

There are many species of Quaternary, Pliocene-Quaternary, and even longer ranging taxa with high indexes also admixed in the sample. These are also considered to be reworked. Based on counting the specimens in three different areas (N = 139 specimens in each area) at 100× magnification of each slide, the following percentages of radiolarians are considered to be reworked: from 63 to 125 μm, N = 18.3% and standard deviation (SD) = 1.5%; greater than 125 μm, N = 19.1% and SD = 3.3%.

The reworked radiolarians must have been buried once (probably upslope somewhere) as they remain well preserved. At a later time (<0.21 Ma, during the *Buccinosphaera invaginata* Zone), these specimens were transported to the present site. Because these radiolarians were buried once and probably have a cation coating on their skeletal surfaces, they were not subjected to further dissolution to a significant extent.

PALEOMAGNETISM

Introduction

Paleomagnetic analysis in Hole 805B began in Cores 130-805B-1H and -2H at 1-cm intervals, with measurement of both the natural remanent magnetization (NRM) and the remanence

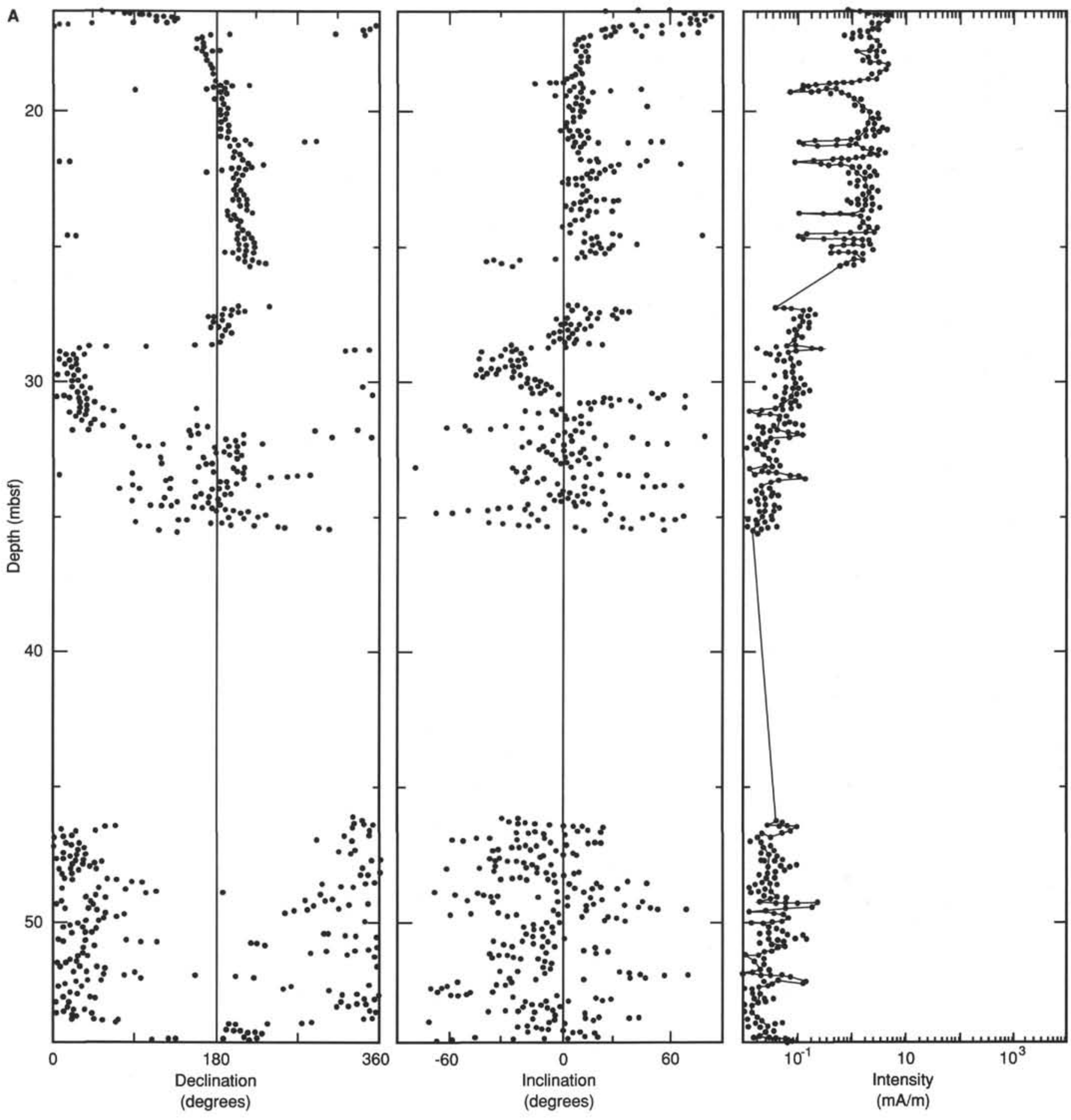

Figure 16. Oriented declination, inclination, and intensity plots for **(A)** Cores 130-805B-3H to -6H and **(B)** Cores 130-805C-3H to -5H. Note the difference in the depth scales.

after 15-mT alternating field (AF) demagnetization. Measurement intervals were increased to 3 cm at Core 130-805B-3H, to 5 cm at Core 130-805B-5H, and to 10 cm at Core 130-805B-10H. Magnetization intensity after AF demagnetization in Hole 805B drops to less than 0.1 mA/m at depths below 32 mbsf (Fig. 16). This corresponds to a magnetic moment less than 1 order of magnitude greater than that of the sample holder, and thus below the practical limit of measurement on the shipboard cryogenic magnetometer. Therefore, AF demagnetization in this hole was limited to one section per core after Core 130-805B-10H. The behavior of each demagnetized section, and of the NRM of the whole core, was monitored throughout the remainder of Hole 805B for evidence of an increase in intensity and/or an improvement in the magnetization direction record. Most cores below Core 130-805B-4H show evidence of a magnetic overprint, with a steep negative inclination (between $-60°$ and $-80°$), that was largely removed by 15-mT AF demagnetization. Intensities after demagnetization are frequently $<10\%$ of the NRM

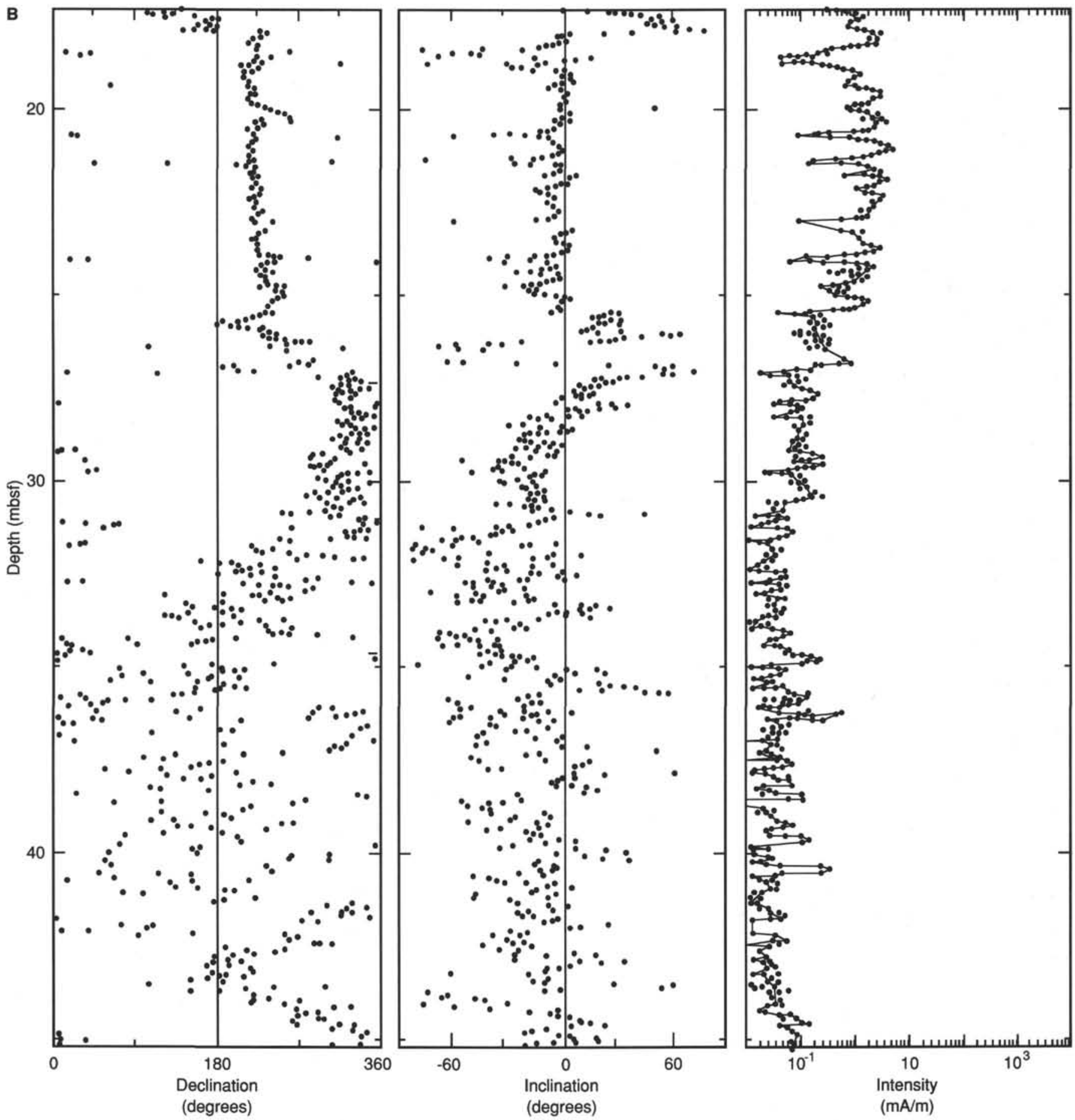

Figure 16 (continued).

intensity. It is suspected that this component was acquired during or after drilling, possibly within the regions near the base and the top of the drill string where the ambient field is concentrated. No consistent primary magnetizations are present below Core 130-805B-5H. Demagnetization of the first few cores of Hole 805C follows a similar pattern to that of Hole 805B (Fig. 16). It was clear that nothing would be gained by the measurement of cores from Hole 805C over most of the Miocene sequence, so measurement was discontinued after Core 130-805C-10H. Measurement in Hole 805C began again at Core 130-805C-58X and continued to 130-805C-64X, but no consistent primary magnetization could be determined from this interval.

Cores from the dedicated Hole 805A were not to be demagnetized and thus were not included in the routine paleomagnetic analysis. The NRM of whole-round Cores 130-805A-3H and -4H was measured, however. Both cores show evidence of overprinting, resulting in anomalously high negative inclinations. Polarities can be tentatively identified in Core 130-805A-3H and in part of Core 130-805A-4H, but these are subject to confirmation by demagnetization.

Pliocene-Holocene Magnetostratigraphy and Sedimentation Rate

Only the Brunhes Chron and part of the Matuyama Chron can be confidently identified in the three holes at Site 805 (Fig. 17). A normal interval within Core 130-805B-4H from 28.6 to 31.6 mbsf correlates with the Olduvai Subchron; the lower boundary of this subchron is the oldest datable magnetic event in the sequence. Although recognizable polarity extends for a further 3.9 m to the bottom of Core 130-805B-4H, neither of the two Réunion events can be recognized. The Jaramillo Subchron can be tentatively identified in Holes 805B and 805C, but it unfortunately spans the core break between Cores 2H and 3H in both holes. Flow-in at the top of the first section of Core 130-805B-3H prevented recognition of the top of the Jaramillo Subchron in Hole 805B, and a similar disruption in Core 130-805C-3H obscured the base of the Jaramillo Subchron in Hole 805C.

Both the top and the base of what has been provisionally interpreted as the Jaramillo Subchron were identified in Hole 805A within Core 130-805A-3H from 15.4 to 16.9 mbsf. Below this interval, a second interval of normal polarity in the NRM record is present within Core 130-805A-3H from 18.8 to 19.6 mbsf. Although this event does not appear in the record for either of the two other holes at this site, it does correlate with a normally polarized interval seen at Site 804 in Core 130-804B-2H from 11.5 to 11.7 mbsf and in Core 130-804C-2H from 12.3 to 12.5 mbsf. This normally polarized interval may correspond to the Cobb Mountain Event (Mankinen et al., 1978; Jacobs, 1984, p. 165).

Three minor events of apparently normal polarity within the Matuyama Reversed Chron can be correlated between Cores 130-805B-3H and 130-805C-3H; two of these also appear to be present in Core 130-805A-3H. A minor event, <1 m below the base of the Brunhes Chron, can be correlated from Core 130-805B-2H to 130-805C-2H. Two other minor events near the base of Core 130-805B-2H have no equivalent in the other two holes. The nature of all these minor events, and their relation (if any) to the global polarity record, is unclear. However, the three minor events seen in Cores 130-805B-3H and 130-805C-3H are all marked by sudden decreases in intensity from a background of 2–3 mA/m to a value at the event of 0.1–0.2 mA/m (Fig. 18). This behavior may suggest a relationship between events of this sort and zones of increased reduction potential in which magnetite has been removed by solution.

Age controls on the sedimentation rate in Hole 805B are provided by the base and top of the Olduvai Subchron, the base of the Jaramillo Subchron, and the Brunhes/Matuyama boundary. The three youngest age-depth data are nearly collinear, and their line of best fit intersects the origin, indicating a sedimentation rate of 17.1 m/m.y. from about 1.7 Ma to the present day (Fig. 19). Age controls in Holes 805A and 805C are consistent, but very limited, with this rate.

SEDIMENTATION RATES

The biostratigraphic age-depth indicators observed in the cored sediments at Site 805 suggest a continuous depositional history from the present to approximately the lower Oligocene/upper Oligocene boundary at about 30 Ma. The rates by which these sediments were deposited varied by a factor of 3; the average rate over the entire 30-m.y. interval was estimated to be 23 m/m.y.

All age-depth indicators observed in the three holes cored are listed in Table 5, and the results from Holes 805B and 805C are shown graphically in Figures 20 and 21, respectively. In the 5–15-Ma interval, the data from Hole 805C appear somewhat more coherent than the corresponding plots from Hole 805B, which simply reflects the fact that more (and more widely spread) data were available from Hole 805B. When comparing the age-depth distribution of the calcareous indicators alone, this results in highly similar patterns of the age-depth progression in the two holes, also in the 5–15-Ma interval.

The maximum penetration of the stratigraphic column was obtained in Hole 805C, and shorter intervals from this hole are plotted in Figures 22 and 23, respectively. The particular events used as control points for sedimentation rate changes are listed in Table 6. The distribution of the age-depth indicators clearly indicates a rate change at about 2 Ma (Fig. 22) in the late Pliocene. The stepwise increase in sedimentation rate from that point and back to 8.7 Ma is perhaps less well constrained, as the distribution of points in principle would allow a uniform rate (36.5 m/m.y.) to be drawn from 2.07 to 8.7 Ma. The distribution of the age-depth indicators in the lower Neogene–upper Oligocene interval, however, offers many possible alternative sedimentation rates to the ones suggested in Table 6; the inferred constant rate from 18.8 to 29.9 Ma, for example, presumably contains more variability than is indicated in Table 6.

The rate histories from Holes 805B and 805C are compared in Figure 24. The two largest changes occur close to 2 and 9 Ma, respectively. The 7-m.y. interval between these points of major change is characterized by high sedimentation rates (about 25–40 m/m.y.), and the surrounding intervals are characterized by medium high rates (about 10–20 m/m.y.).

The transition period into the high sedimentation rate regime just after 9 Ma appears to be shorter than the transition out of this regime, which clearly is smoother and perhaps even occurred in a stepwise fashion throughout most of the Pliocene (5, 3.5, and 2 Ma, respectively). This Pliocene change from high to medium high sedimentation rates is considered to be well constrained biochronologically, a fact that cannot be claimed for the sharp change at 8.7 Ma. Yet, both the shape and timing of change of this curve closely mimic paleomagnetically constrained sedimentation rate curves that recently have been obtained from the western equatorial Indian Ocean (Peterson and Backman, 1990). This suggests that the productivity and preservation patterns changed on an interbasinal scale, presumably from related causes and hence that these changes were synchronous. If this is true, the change from lower early-middle Miocene rates to higher late Miocene rates indeed was sharp, occurring over a few hundred thousand years, and the change probably occurred closer to 8 than to 9 Ma.

INORGANIC GEOCHEMISTRY

We collected 24 interstitial water samples at Site 805: 11 from Hole 805B at depths ranging from 183.7 to 469.2 mbsf, and 13 from Hole 805C at depths ranging from 6.0 to 165.7 mbsf and from 449.3 to 578.2 mbsf. For the purpose of this report, these are considered to constitute a single depth profile. Interstitial water samples cover most of the depth range drilled of the nannofossil ooze and chalk of Unit I, the single lithologic unit recognized at Site 805 (see "Lithostratigraphy" section, this chapter). Chemical gradients in the interstitial waters at this site (Table 7) are generally similar to those at Sites 803 and 804, being governed by the biogenic, organic-carbon-poor character of the sediments and by diffusive influence of basalt alteration reactions at depth. The magnitude of the chemical gradients at Site 805, the shallowest of the first three sites drilled on Leg 130, are generally equal to or larger than those at Site 803. The chemical gradients in Site 803 are, in turn, larger than those at the deepest site, Site 804. These differences are consistent with more organic carbon burial at shallower water depths; or, because Site 805 is closer to the equator, the sedimentation rate at Site 805 is the highest of the first three sites.

Chlorinity increases almost 3% to 570 mM at 32.8 mbsf (Core 130-805C-4H) and increases further to values greater than

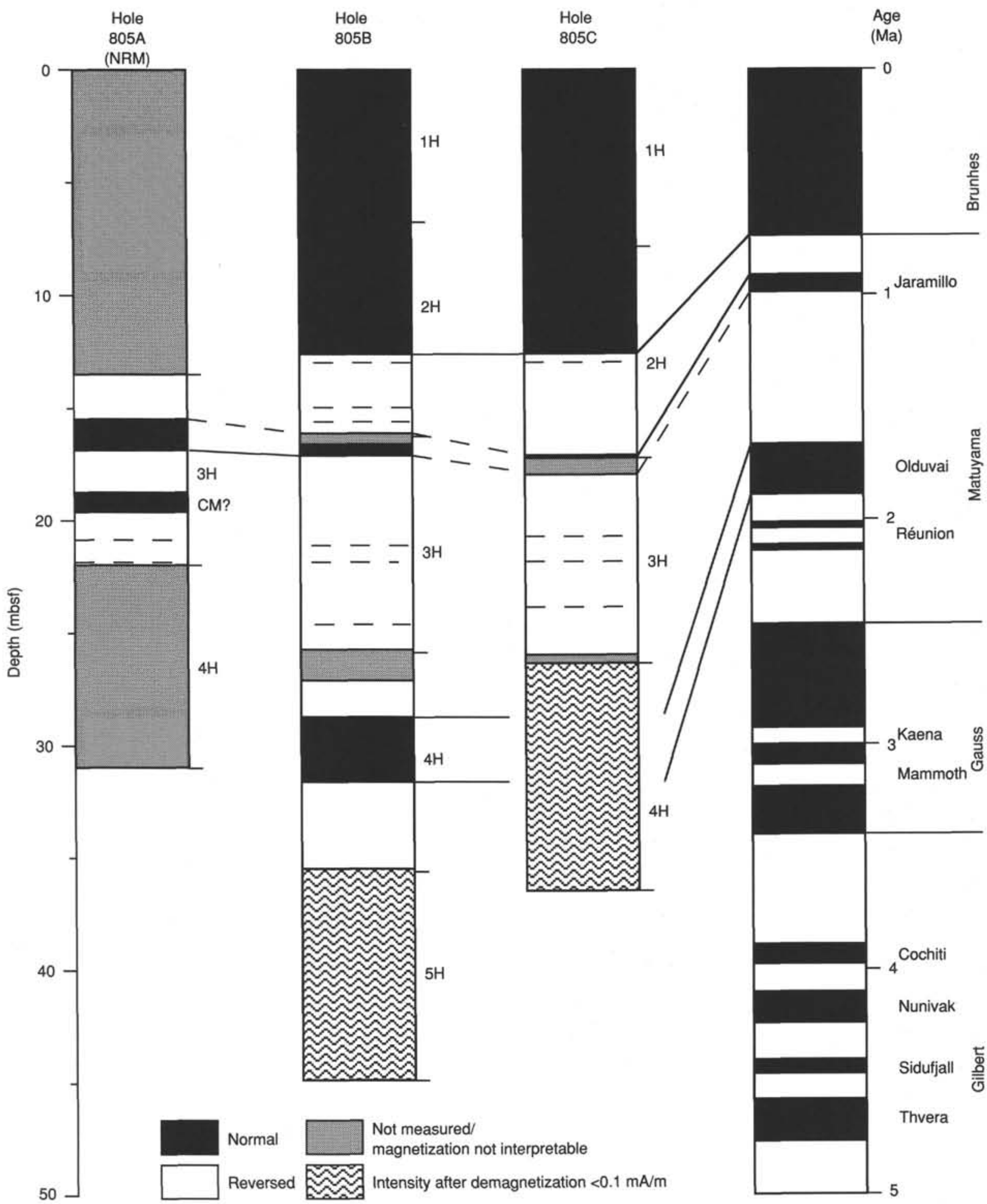

Figure 17. Pliocene-Holocene magnetostratigraphy for holes at Site 805, with a reference magnetostratigraphy after Berggren et al. (1985). Black intervals indicate normal polarization; white, reversed polarization. Half-tone shading indicates unknown polarity. Dashed lines within columns are short events; areas with wavy lines indicate that intensity after demagnetization is <0.1 mA/m. Confident ties between columns are shown by an unbroken line; dashed lines indicate ties between minor events.

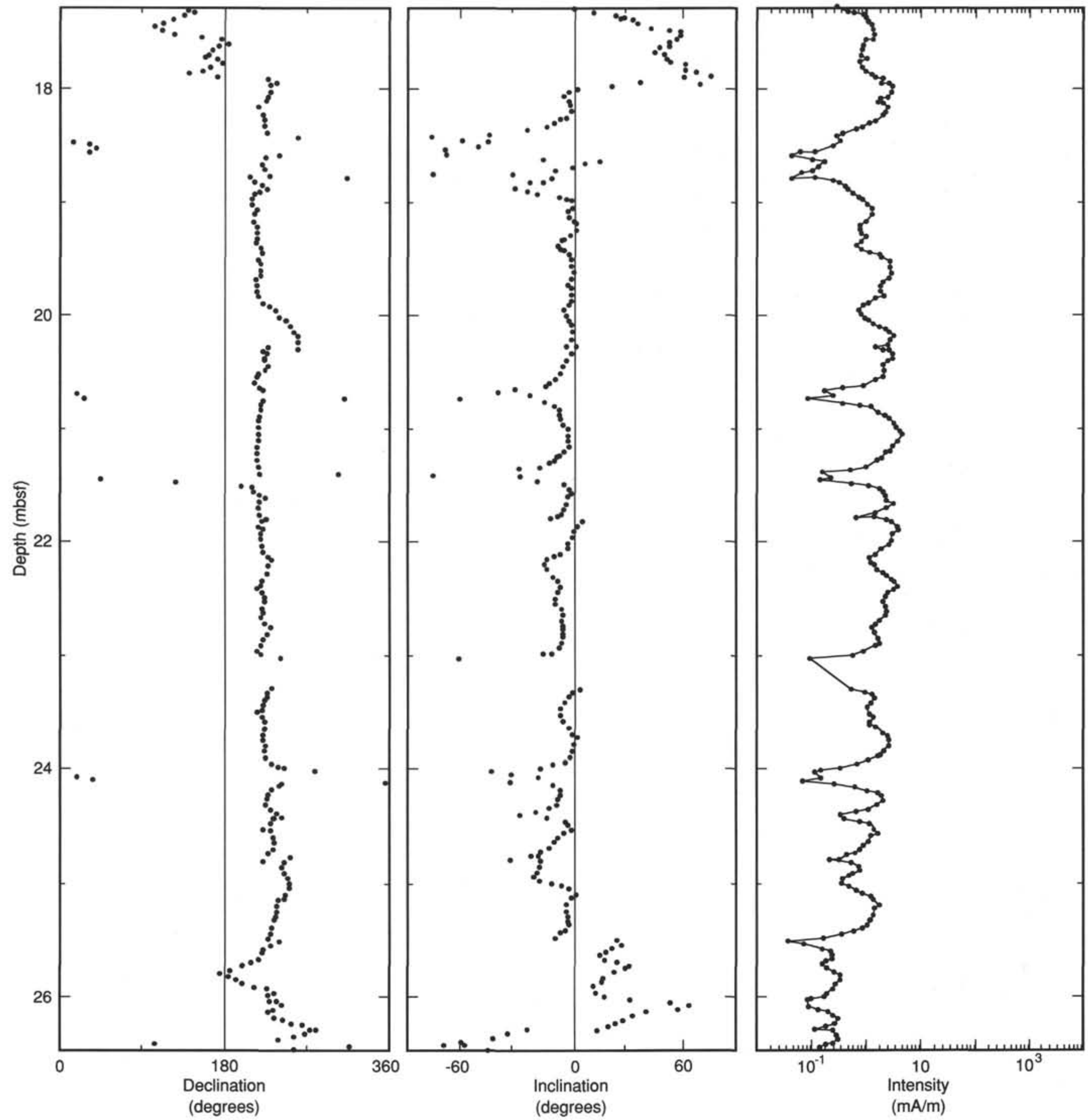

Figure 18. Oriented declination, inclination, and intensity plots for Core 130-805C-3H. Note the three apparent polarity events at 20.7, 21.4, and 24.1 mbsf, and the large decrease in intensity associated with each.

580 mM by 165.7 mbsf (Core 130-805C-18H) and as high as 590 mM at depths below 450 m, for a total increase of 6.5% (Fig. 25). Chlorinity at Site 805 is greater than that at Site 804, with a depth profile roughly similar to that at Site 803. Salinity, measured refractively as total dissolved solids, increases with depth from 35.0 to 36.5 g/kg (Table 7). Sodium concentrations measured by flame emission spectrophotometry (Table 7) and those estimated by charge balance calculations generally agree to within <1.5%. Sodium concentrations increase 4% to 500 mM from 6.0 to 578.2 mbsf and are higher than those at Sites 803 and 804. Alkalinity increases from ~3 mM to a peak of 5 mM at 80.3 mbsf, then decreases to values around 4 mM. There is a small secondary alkalinity maximum of 4.8 mM at 324.9 mbsf, and a further decrease to 2.6 mM at 578.2 mbsf (Fig. 25). Alkalinity values at Site 805 are consistently larger, and the peak value occurs at a greater depth than at Site 804, the deepest site drilled. Alkalinity values at Site 805 are generally similar to those at Site 803, but the maximum is larger here at Site 805.

Sulfate concentrations decrease by nearly 25% from 28.5 mM at 6.0 mbsf to values around 22 mM by 165.7 mbsf and

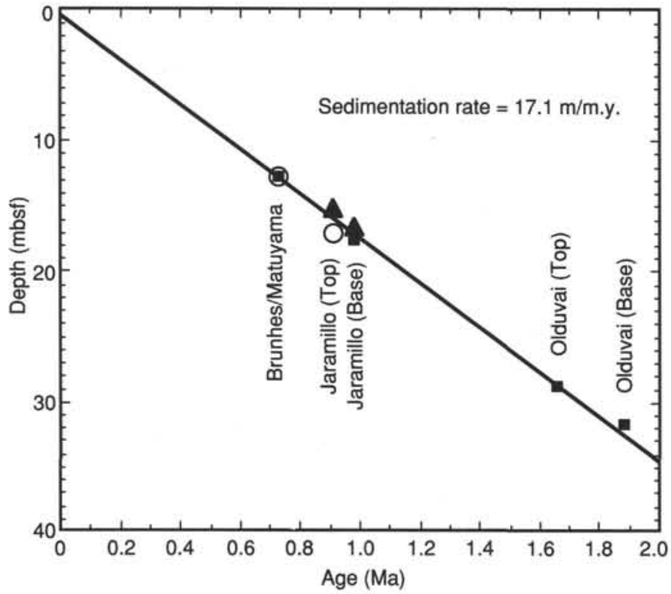

Figure 19. Age vs. depth plot, Site 805, with linear sedimentation rate fitted to Hole 805B data for the Brunhes/Matuyama boundary and the base of the Jaramillo and the top of the Olduvai subchrons. Filled triangle = Hole 805A, filled square = Hole 805B, and open circle = Hole 805C.

then are fairly constant with depth (Fig. 25). The extent of sulfate depletion at Site 805 is greater than at Site 804 and is similar to that at Site 803. Phosphate concentrations are below the detection limit of 1–2 μM in all samples analyzed (Table 7). Ammonia concentrations reach a maximum around 250 μM from 183.7 to 295.1 mbsf and decrease to 150–160 μM with depth (Fig. 25). These concentrations are higher than those at Sites 803 and 804, suggesting that more organic matter was oxidized or that the sedimentary sinks for ammonia were more limited at Site 805.

Dissolved silica concentrations increase with depth to around 1200 μM at 578.2 mbsf (Fig. 25). The depth profile, both in shape and concentration, is similar to those at Sites 803 and 804, despite the absence at Site 805 of the intervals enriched in radiolarians found at Sites 803 and 804 (see "Lithostratigraphy" section, this chapter). There are no obvious dissolved Si decreases corresponding to the occurrence of small chert nodules found at depths of 344.35 mbsf (Core 130-805C-37X-2, 135–137 cm) and 370.6 mbsf (Core 130-805C-40X-1, 0–10 cm) in Hole 805C (but not in Hole 805B; see "Lithostratigraphy" section, this chapter). The extent of chert formation is probably limited. Manganese concentrations are generally below the detection limit ($<$2–3 μM), with the exception of the two shallowest samples (Table 7). No increase in dissolved Mn is apparent with the increase in dissolved Si, despite previous reports suggesting this correlation (Gieskes, 1981).

Calcium concentrations increase with depth, with an average gradient of 4 mM/100 m (Fig. 26), similar to that observed at Site 804. The Ca depth profile is generally similar to that at Site 803 as well, except below 500 mbsf. The profile at Site 803 is steeper than that from Site 805, presumably because of decreased diffusion coefficients as sediment porosity decreases. Magnesium concentrations decrease with depth, with a gradient of -3.4 mM/100 m (Fig. 25), similar to those at Sites 803 and 804. Magnesium and Ca concentrations are linearly correlated (R^2 = 0.98), with a $\Delta Ca/\Delta Mg$ ratio approximately equal to -1.2. The linear correlation is indicative of the conservative

Table 5. Bio- and magnetostratigraphic events determined at Site 805.

Event	Upper depth (mbsf)	Lower depth (mbsf)	Age (Ma)
130-805A-			
FO *E. huxleyi* (N)	0	3.0	0.28
LO *P. lacunosa* (N)	3.0	12.5	0.46
LO *C. tuberosa* (R)	3.0	12.5	0.50
LO *G. tosaensis* (F)	3.0	12.5	0.60
LO *N. reinholdii* (D)	3.0	12.5	0.65
LO *C. macintyrei* (N)	22.0	31.5	1.45
LO *D. brouweri* (N)	22.0	31.5	1.89
OA *D. triradiatus* (N)	22.0	31.5	2.07
FO *G. truncatulinoides* (F)	12.5	22.0	1.90
LO *D. surculus* (N)	41.0	50.5	2.45
FO *G. tosaensis* (F)	41.0	50.5	3.10
130-805B-			
LO *P. lacunosa* (N)	6.7	16.2	0.46
LO *G. tosaensis* (F)	6.7	16.2	0.60
Brunhes (O)	12.6	12.6	0.73
LO *C. macintyrei* (N)	33.9	35.2	1.45
Olduvai (T)	28.6	28.6	1.66
Olduvai (O)	31.6	31.6	1.88
LO *D. brouweri* (N)	33.9	35.7	1.89
OA *D. triradiatus* (N)	33.9	35.7	2.07
FO *G. truncatulinoides* (F)	16.2	25.7	1.90
LO *D. pentaradiatus* (N)	43.4	44.7	2.35
LO *D. surculus* (N)	43.4	44.7	2.45
LO *D. tamalis* (N)	44.7	54.2	2.65
LO *G. altispira* (F)	54.2	63.7	2.90
FO *G. fistulosus* (F)	63.7	73.2	2.90
LO *Sphaeroidinellopsis* spp. (F)	54.2	63.7	3.00
FO *S. dehiscens* (F)	63.7	73.2	3.00
LO *R. pseudoumbilica* (N)	73.2	82.7	3.56
LO *G. nepenthes* (F)	92.2	101.7	3.90
LO *C. acutus* (N)	101.7	111.2	4.6
LO *D. quinqueramus* (N)	120.7	130.2	5.0
FO *G. tumida* (F)	120.7	130.2	5.2
FO *P. spectabilis* (F)	120.7	130.2	5.2
LO *G. conglobatus* (F)	120.7	130.2	5.3
FO *P. primalis* (F)	149.2	158.7	5.8
FO *S. omnitubus* (R)	196.7	206.2	6.4
FO *Amaurolithus* (N)	196.7	206.2	6.7
LO *N. porteri* (D)	196.7	206.2	6.7
LO *T. burckliana* (D)	215.7	225.2	7.0
FO *G. plesiotumida* (F)	177.7	187.2	7.1
LO *N. porteri* (D)	196.7	206.2	7.2
LO *D. hughesi* (R)	196.7	206.2	7.2
FO *D. quinqueramus* (N)	215.7	225.2	7.5
LO *C. yabei* (D)	234.7	244.2	7.5
LO *T. burckliana* (D)	215.7	225.2	8.0
FO *S. berminghami* (R)	234.7	244.2	8.0
LO *D. pettersoni* (R)	253.7	263.2	8.2
LO *S. wolfii* (R)	282.5	292.2	8.2
FO *N. dutertrei* s.l. (F)	187.2	196.7	8.0
LO *C. yabei* (D)	234.7	244.2	8.6
LO *D. hamatus* (N)	263.2	272.9	8.7
LO *Catinaster* (N)	263.2	272.9	8.8
LO *A. moronensis* (D)	253.7	263.2	8.9
FO *D. neohamatus* (N)	272.9	282.5	9.0
FO *N. acostaensis* (F)	260.4	263.1	10.2
LO *G. siakensis* (F)	260.4	263.1	10.4
LO *L. thornburgi*	292.2	301.4	10.5
FO *D. hamatus* (N)	282.5	292.2	10.5
LO *D. punctata* f. *hustedtii* (D)	320.5	330.0	10.7
LO *C. coscinodiscus* (D)	292.2	301.4	10.7
FO *H. cuneiformis* (D)	292.2	301.4	11.2
LO *A. moronensis* (D)	253.7	263.2	11.3
FO *G. nepenthes* (F)	292.2	301.4	11.3
LO *G. fohsi lobata/robusta* (F)	292.2	301.4	11.5
LO *C. cornuta* (R)	301.4	311.0	11.8
LO *D. punctata* f. *hustedtii* (D)	320.5	330.0	12.2
LO *C. coscinodiscus* (D)	292.2	301.4	12.2
FO *H. cuneiformis* (D)	292.2	301.4	12.6
LO *C. nitescens* (N)	301.4	311.0	12.8
LO *C. lewisianus* (D)	320.5	330.0	12.9
LO *C. floridanus* (N)	311.0	320.5	13.1

Table 5 (continued).

Event	Upper depth (mbsf)	Lower depth (mbsf)	Age (Ma)
130-805B- (Cont)			
LO *C. lewisianus* (D)	320.5	330.0	13.5
LO *S. heteromorphus* (N)	320.5	330.0	13.6
FO *G. praefohsi* (F)	330.0	339.7	13.9
LO *C. peplum* (D)	330.0	339.7	14.1
LO *G. peripheroronda* (F)	330.0	339.7	14.6
FO *G. peripheroacuta* (F)	349.4	359.0	14.9
FO *C. peplum* (D)	368.7	378.3	16.4
LO *C. dissimilis* (F)	397.7	407.3	17.6
FO *S. heteromorphus* (N)	388.0	397.7	18.6
LO *C. elegans* (D)	407.3	417.0	18.7
LO *S. belemnos* (N)	388.0	397.7	18.8
FO *S. belemnos* (N)	407.3	417.0	20.0
LO *G. kugleri* (F)	436.0	445.5	21.8
130-805C-			
LO *P. lacunosa* (N)	0	7.8	0.46
Brunhes (O)	12.7	12.7	0.73
LO *L. neoheteroporus* (R)	17.3	26.8	1.11
LO *C. macintyrei* (N)	26.8	36.3	1.45
LO *D. brouweri* (N)	26.8	36.3	1.89
OA *D. triradiatus* (N)	26.8	36.3	2.07
FO *G. truncatulinoides* (F)	17.3	26.8	1.90
LO *D. pentaradiatus* (N)	36.3	45.8	2.35
LO *D. surculus* (N)	45.8	55.3	2.45
FO *L. neoheteroporus* (R)	36.3	45.8	2.52
LO *D. tamalis* (N)	45.8	55.3	2.65
LO *G. altispira* (F)	45.8	55.3	2.90
FO *G. fistulosus* (F)	55.3	64.8	2.90
LO *Sphaeroidinellopsis* spp. (F)	64.8	74.3	3.00
LO *G. margaritae* (F)	64.8	74.3	3.40
LO *Sphenolithus* (N)	64.8	74.3	3.45
LO *P. doliolum* (R)	74.3	83.8	3.54
LO *R. pseudoumbilica* (N)	74.3	83.8	3.56
LO *S. pentas* (R)	64.8	74.3	3.78
FO *A. ypsilon* (R)	74.3	83.8	3.78
LO *S. berminghami* (R)	93.3	102.8	3.86
FO *S. pentas* (R)	112.3	121.8	4.25
LO *C. acutus* (N)	102.8	112.3	4.6
LO *S. omnitubus* (R)	102.8	112.3	4.8
LO *D. quinqueramus* (N)	121.8	131.3	5.0
LO *S. corona* (R)	55.3	64.8	5.1
FO *G. tumida* (F)	112.3	121.8	5.2
FO *P. spectabilis* (F)	121.8	131.3	5.2
LO *G. conglobatus* (F)	140.8	150.3	5.3
FO *G. cibaoensis*	140.8	150.3	5.3
LO *A. tritubus* (R)	169.3	178.8	5.4
FO *P. primalis* (F)	150.3	159.8	5.8
LO *C. caepa* (R)	169.3	178.8	6.4
FO *Amaurolithus* (N)	197.8	207.3	6.7
FO *G. plesiotumida* (F)	188.3	197.8	7.1
FO *D. quinqueramus* (N)	216.8	235.8	7.5
FO *A. tritubus* (R)	188.3	197.8	7.7
LO *D. laticonus* (R)	169.3	178.8	8.2
LO *D. hamatus* (N)	264.7	274.4	8.7
LO *Catinaster* (N)	264.7	274.4	8.8
FO *D. neohamatus* (N)	264.7	274.4	9.0
FO *N. acostaensis* (F)	255.1	264.7	10.2
LO *G. siakensis* (F)	255.1	264.7	10.4
FO *D. hamatus* (N)	274.4	284.0	10.5
FO *Catinaster* (N)	284.0	293.7	11.1
FO *G. nepenthes* (F)	274.4	284.0	11.3
LO *G. fohsi lobata/robusta* (F)	302.9	312.6	11.5
LO *C. nitescens* (N)	312.6	322.3	12.8
LO *C. floridanus* (N)	312.6	322.3	13.1
LO *S. heteromorphus* (N)	322.3	331.8	13.6
FO *G. praefohsi* (F)	341.5	351.2	13.9
LO *G. peripheroronda* (F)	351.2	360.9	14.6
FO *G. peripheroacuta* (F)	351.2	360.9	14.9
LO *P. sicana* (F)	351.2	360.9	14.9
FO *P. sicana* (F)	380.3	389.9	16.6
LO *C. dissimilis* (F)	389.9	399.5	17.6
FO *S. heteromorphus* (N)	389.9	399.5	18.6
LO *S. belemnos* (N)	389.9	399.5	18.8
FO *S. belemnos* (N)	399.5	409.1	20.0

Table 5 (continued).

Event	Upper depth (mbsf)	Lower depth (mbsf)	Age (Ma)
130-805C- (Cont)			
LO *G. kugleri* (F)	447.7	457.4	21.8
FO *R. paleacea* (D)	523.9	533.5	22.7
LO *R. vigilans* (D)	523.9	533.5	22.7
FO *G. kugleri* (F)	523.9	533.5	23.7
FO *B. veniamini* (D)	543.2	552.9	24.0
LO *S. ciperoensis* (N)	552.9	562.6	25.2
LO *S. distentus* (N)	572.3	582.0	27.5
LO *G. opima* (F)	572.3	582.0	28.2

Notes: The depth uncertainty predominantly represents sample intervals used. References for the age estimates are presented in the "Explanatory Notes" chapter (this volume). N = nannofossil, F = foraminifer, D = diatom, R = radiolarian, FO = first occurrence, LO = last occurrence, and OA = onset acme. Magnetostratigraphic reversal boundaries followed by the designation (T) or (O) refer to "termination" and "onset," respectively.

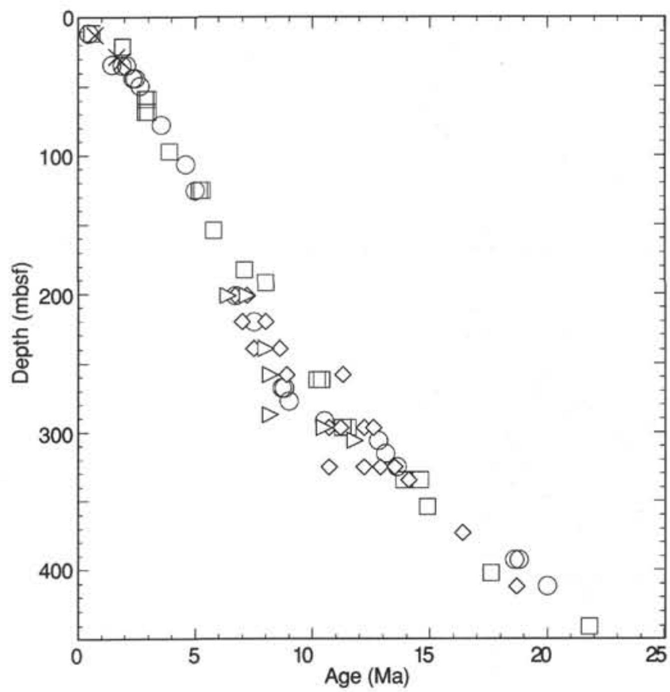

Figure 20. Age-depth relationships of bio- and magnetostratigraphic markers, Hole 805B. Sample interval uncertainties correspond closely to the symbol size used. Circle = nannofossil, square = foraminifer, diamond = diatom, triangle = radiolarian, and × = magnetostratigraphic reversal boundary.

nature of these profiles, with Ca and Mg gradients primarily controlled by reactions in the underlying basalt and diffusion between this boundary and overlying seawater (McDuff and Gieskes, 1976; McDuff, 1981).

Strontium concentrations increase with depth to maximum values >900 μM by 108.8 mbsf and persist to 578.2 mbsf, the deepest sample (Fig. 25). Strontium concentrations at this site are always larger than those at the deeper Site 804, where sediments accumulate more slowly. The Sr increase with depth at this site is steeper than that at Site 803, with the maximum con-

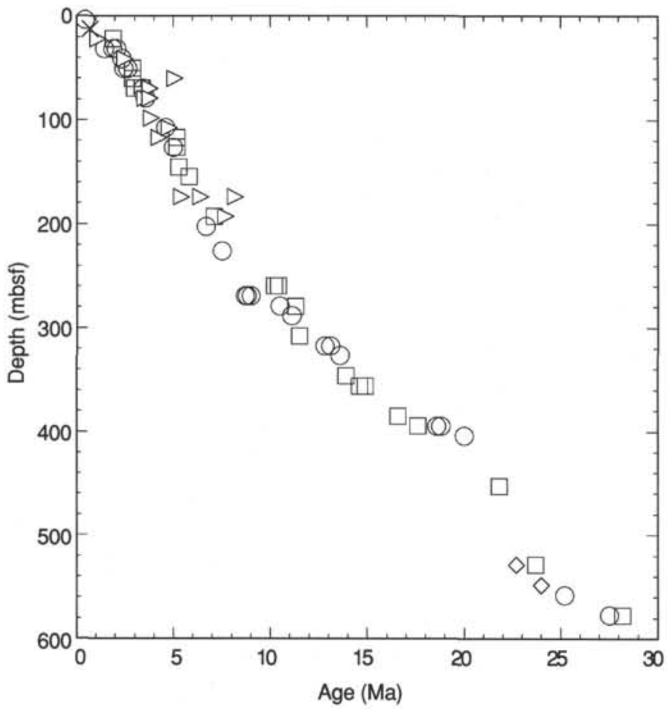

Figure 21. Age-depth relationships of biostratigraphic markers, Hole 805C. Sample interval uncertainties correspond closely to the symbol size used. Symbols used are as in Figure 20.

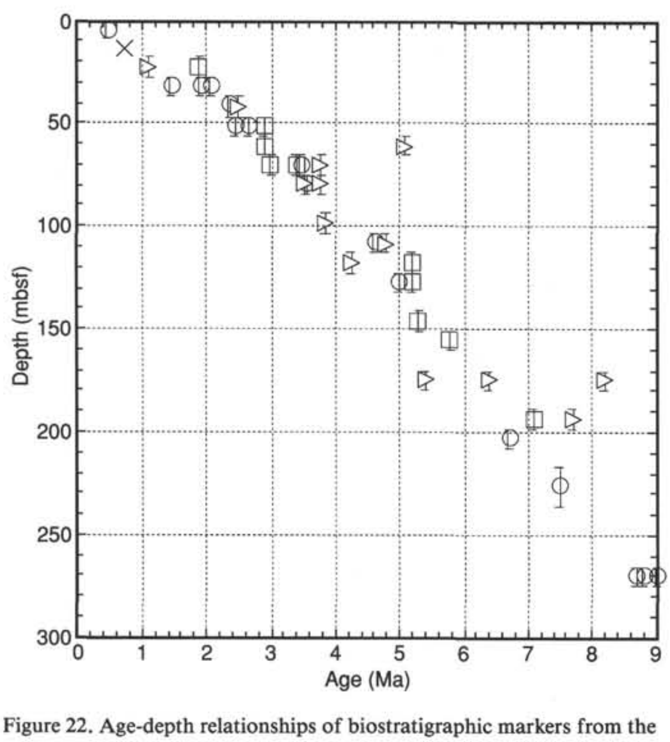

Figure 22. Age-depth relationships of biostratigraphic markers from the upper Miocene through Holocene interval in Hole 805C. Error bars show sample interval uncertainties. Symbols used are as in Figure 20.

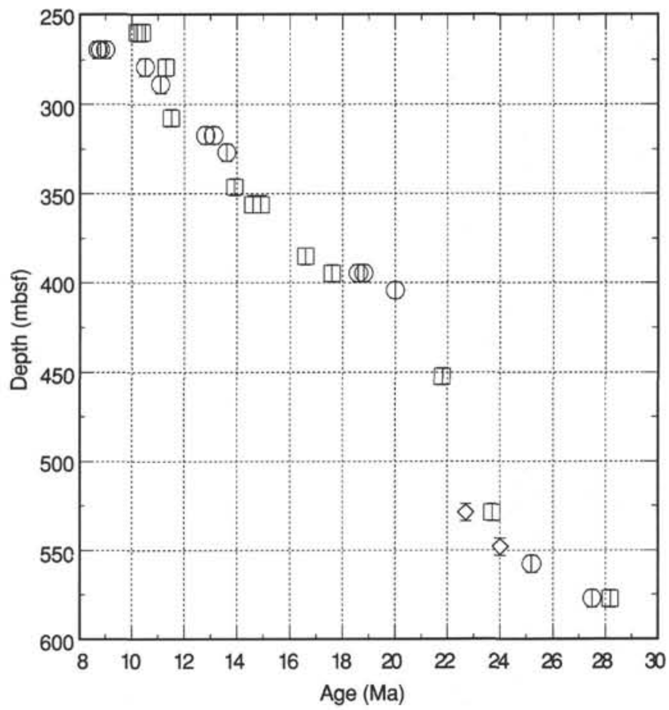

Figure 23. Age-depth relationships of biostratigraphic markers from the upper Oligocene through the lower upper Miocene interval, Hole 805C. Error bars show sample interval uncertainties. Symbols used are as in Figure 20.

Table 6. Estimated sedimentation rates, Site 805, and the control points determining those rates.

Control point	Depth (mbsf)	Age (Ma)	Sedimentation rate (m/m.y.)
130-805B-			
Top section	0	0	
Olduvai (O)	31.60	1.88	16.8
LO *R. pseudoumbilica* (N)	77.95	3.56	27.6
LO *D. quinqueramus* (N)	125.45	5.00	33.0
LO *D. hamatus* (N)	268.05	8.70	38.5
LO *S. heteromorphus* (N)	325.25	13.60	11.7
LO *S. belemnos* (N)	392.85	18.80	13.0
LO *G. kugleri* (F)	440.75	21.80	16.0
Terminal depth	473.30	23.84	
130-805C-			
Top section	0	0	
OA *D. triradiatus* (N)	31.55	2.07	15.2
LO *R. pseudoumbilica* (N)	79.05	3.56	31.9
LO *D. quinqueramus* (N)	126.55	5.00	33.0
LO *D. hamatus* (N)	269.55	8.70	38.6
LO *S. heteromorphus* (N)	327.05	13.60	11.7
LO *S. belemnos* (N)	394.70	18.80	13.0
LO *G. opima* (F)	577.15	28.20	19.4
Terminal depth	611.00	29.94	

Notes: References for the age estimates are presented in the "Explanatory Notes" chapter (this volume), as well as the Leg 130 philosophy for determining the sedimentation rates. N = nannofossil, F = foraminifer, FO = first occurrence, LO = last occurrence, and OA = onset acme. Magnetostratigraphic reversal boundaries followed by the designation (T) or (O) refer to "termination" or "onset," respectively.

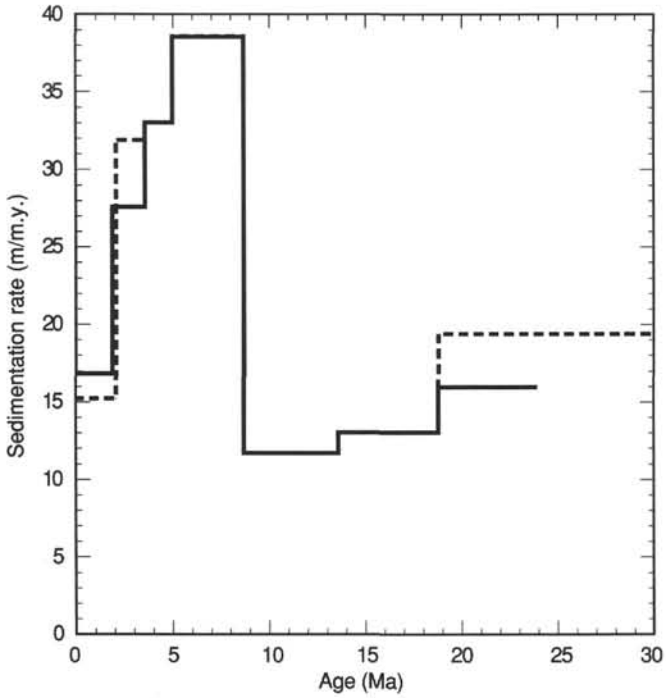

Figure 24. Sedimentation rate history, Site 805. Solid line = Hole 805B and dashed line = Hole 805C.

centrations at Site 803 similar to these, but not reached until >300 mbsf. This is consistent with previous observations for carbonate-rich sites, suggesting that the depth of the Sr maximum, although not necessarily its concentration, is inversely related to sedimentation rate, with deeper maxima for slower sedimentation rates (Gieskes, 1981).

Lithium concentrations decrease from 22.5 μM near the top of the sediment column to a minimum of 14.6 μM at 165.7-12.2 mbsf. The Li profile then increases to 22.2 μM at 578.2 mbsf (Fig. 25). The profile is similar to those at Sites 803 and 804, suggesting that the controls on these profiles must also be similar. Potassium concentrations decrease from 12 mM at 6.0 mbsf to 6.8 mM at 578.2 mbsf (Fig. 25). Rubidium concentrations decrease from 1.9 μM at 6.0 mbsf to 1.1 μM at 578.2 mbsf (Fig. 25). Potassium and Rb concentrations linearly correlate with Ca (R^2 = 0.95 and 0.85, respectively) and have similar depth profiles at this site as at Sites 803 and 804. Lithium, at all three sites, clearly behaves differently than the other two alkalis, K and Rb. Increases in Ca, K, and Rb and decreases in Mg with depth at all three sites are apparently a result of the diffusive influence of basalt alteration reactions on interstitial water composition; the similarities between the sites suggests that the general histories of basalt alteration at these sites must be comparable.

ORGANIC GEOCHEMISTRY

Shipboard carbon geochemical analyses of samples from Site 805 consisted of determinations of inorganic carbon on 510 samples, 40 determinations of volatile hydrocarbons in sediments, and 10 Rock-Eval analyses. Total carbon (TC), nitrogen, and sulfur were not measured because the NCS-elemental analyzer was inoperable during drilling at Site 805. More detailed descriptions of analytical methods are outlined in the "Explanatory Notes" chapter (this volume) and given by Emeis and Kvenvolden (1986). The volatile hydrocarbon gases were extracted from the bulk sediment, using the headspace-sampling technique, and routinely were monitored for abundances of methane, ethane, and propane. As in the previous sites of Leg 130, no significant amounts of these gases were detected.

Analyses of total inorganic carbon (IC) were performed on physical properties samples. Percent $CaCO_3$ is calculated as IC · 8.334. The data are presented in Table 8 (microfiche, back pocket) and are plotted vs. depth in Figure 6. The sediments at Site 805 generally show very high carbonate contents ranging from 85% to 95%. Compared with Site 804, carbonate values at Site 805 are less variable, which may reflect lower carbonate dissolution because of the shallower water depth at Site 805.

The Rock-Eval pyrolysis (Espitalié et al., 1977) was used to determine the total organic carbon (TOC) content. The values, however, are below the detection limit of the shipboard Rock-

Table 7. Interstitial water geochemical data, Holes 805B and 805C.

Core, section, interval (cm)	Depth (mbsf)	pH	Alk. (mM)	Sal. (g/kg)	Cl^- (mM)	Na (mM)	SO_4^{2-} (mM)	PO_4^{3+} (μM)	NH_4^+ (μM)	SiO_2 (μM)	Mn (μM)	Ca2+ (mM)	Mg^{2+} (mM)	Sr (μM)	Li (μM)	K (mM)	Rb (μM)
130-805C-1H-4, 145-150	5.95	7.5	2.90	35.0	554	480	28.5	LD	28	528	10	10.6	50.4	175	22.5	12.1	1.92
130-805C-2H-4, 145-150	13.75	7.5	3.59	35.0	561	482	28.5	LD	54	530	4	11.7	50.2	281	21.0	11.4	1.79
130-805C-3H-4, 145-150	23.25	7.4	3.60	35.0	567	483	26.9	LD	83	558	LD	12.7	49.2	407	21.0	11.5	1.71
130-805C-4H-4, 145-150	32.75	7.2	3.91	35.0	569	484	25.8	LD	105	585	LD	13.6	48.1	495	20.1	11.2	1.75
130-805C-5H-4, 145-150	42.25	7.2	4.09	35.5	570	491	26.0	LD	127	625	LD	14.6	47.1	603	19.1	11.0	1.70
130-805C-6H-4, 145-150	51.75	7.5	4.14	35.0	570	490	24.8	LD	146	678	LD	15.3	45.2	672	18.6	11.2	1.75
130-805C-9H-4, 145-150	80.25	7.1	5.36	35.5	575	483	23.6	LD	178	736	LD	17.7	42.8	837	16.6	10.6	1.67
130-805C-12H-4, 145-150	108.75	7.6	4.48	35.5	569	492	22.8	LD	209	835	LD	21.3	40.1	939	15.1	10.4	1.72
130-805C-15H-4, 140-150	137.20	7.6	4.57	35.5	575	493	22.6	LD	222	865	LD	22.0	38.7	989	15.1	10.1	1.63
130-805C-18H-4, 140-150	165.70	7.1	4.43	36.0	581	494	21.5	LD	231	893	LD	23.6	37.3	963	14.6	9.68	1.60
130-805B-20H-4, 145-150	183.65	7.7	4.33	35.5	575	506	22.0	LD	247	931	LD	24.3	36.4	959	14.7	10.1	1.61
130-805B-23H-4, 145-150	212.15	6.9	4.34	36.0	582	497	22.9	LD	252	965	LD	26.2	35.1	959	14.7	9.25	1.52
130-805B-26H-4, 145-150	240.65	7.5	3.76	36.0	582	495	21.8	LD	251	1032	LD	26.8	34.6	932	15.3	9.41	1.62
130-805B-29X-4, 145-150	269.15	7.6	ND	36.5	582	493	22.4	LD	260	960	LD	28.7	34.1	923	15.8	8.79	1.47
130-805B-32X-2, 140-150	295.10	7.1	4.19	36.5	582	491	22.7	LD	247	975	LD	29.0	33.4	904	16.8	8.88	1.47
130-805B-35X-3, 140-150	324.90	7.1	4.80	36.5	583	487	21.9	LD	238	1008	LD	29.5	33.2	904	17.3	8.56	1.43
130-805B-38X-3, 140-150	353.80	7.1	3.82	36.5	584	493	21.8	LD	234	1043	LD	30.3	32.9	921	18.4	8.45	1.43
130-805B-41X-3, 140-150	382.70	7.6	3.24	36.5	585	493	21.8	LD	206	1084	LD	29.6	33.0	888	21.0	8.46	1.34
130-805B-44X-5, 140-150	414.70	ND	ND	36.5	577	494	21.7	ND	202	1077	LD	30.8	32.2	924	18.4	7.94	1.35
130-805B-48X-3, 140-150	449.90	ND	ND	ND	585	497	23.3	ND	195	1092	LD	32.2	31.6	952	20.0	7.65	1.26
130-805B-50X-3, 140-150	469.20	ND	ND	ND	596	497	22.5	ND	ND	1075	LD	32.3	32.6	937	20.0	7.55	1.24
130-805C-53X-3, 140-150	499.30	7.6	2.90	36.5	588	505	22.4	ND	166	1138	LD	32.8	31.8	979	21.1	7.28	1.17
130-805C-57X-2, 0-10	535.00	ND	ND	ND	593	500	22.7	ND	158	1158	LD	32.7	31.3	940	21.1	7.14	1.18
130-805C-61X-4, 140-150	578.20	7.6	2.59	36.5	590	500	22.3	ND	153	1205	LD	33.9	30.8	952	22.2	6.82	1.08

Notes: LD = concentration lower than detection limit, and ND = not determined.

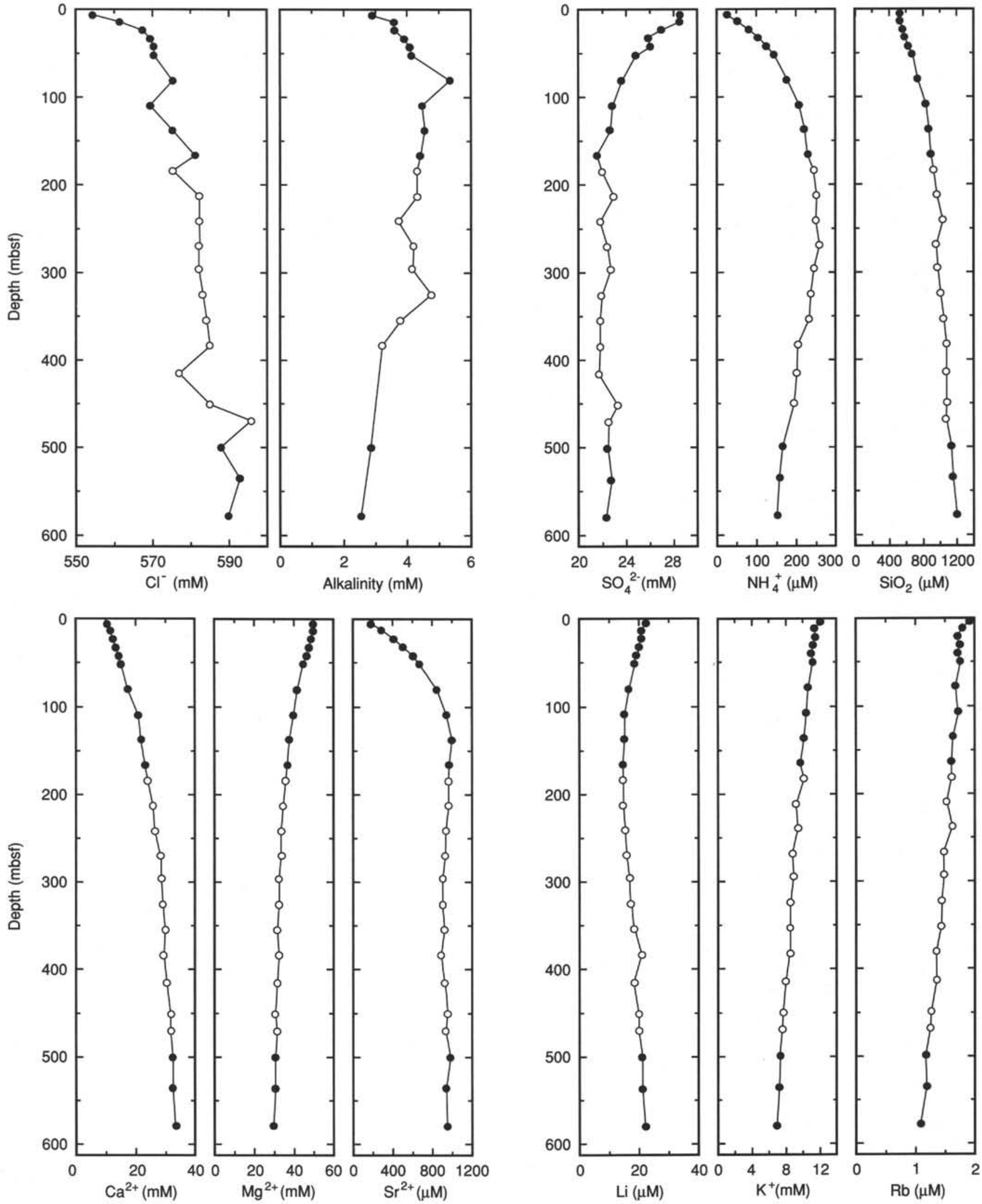

Figure 25. Interstitial water geochemical data vs. depth, Holes 805B and 805C. Open circles = samples from Hole 805B; closed circles = samples from Hole 805C. The depth at the base of the plots is that of the deepest sediment drilled.

Eval instrument (0.05%) and have to be verified by other analytical methods (see "Organic Geochemistry" section, "Site 803" chapter, this volume).

PHYSICAL PROPERTIES

The physical properties program at Site 805 included whole-round measurements (multisensor track and needle-probe thermal conductivity) on the cores from the three holes at Site 805. Split-core measurements (vane shear strength and velocity probe measurements) were performed on the split cores of Holes 805B and 805C. Samples were obtained from the split cores for analysis of index properties. The resulting physical properties data are compared with the downhole logging data obtained at Site 805 and are used in the construction of synthetic seismograms (see "Seismic Stratigraphy" section, this chapter).

Drilling disturbance (flow-in) in many of the piston cores obtained in Hole 805C prevented meaningful physical properties measurements in the affected sections. This disturbance involved the upper five sections of Core 130-805C-7H, all of Core 130-805C-8H, and shorter intervals in Cores 130-805C-10H, -11H, -13H, -14H, -16H, and -17H. A malfunction of the vane shear strength electronics prevented shear strength measurements in Cores 130-805B-1H through -21H.

Multisensor Track

All core sections of the three holes drilled at Site 805 were run through the multisensor track (MST). Because of time constraints, no MST data from Site 805 were processed at sea. These data will be presented in the *Scientific Results* volume.

Thermal Conductivity

Thermal conductivity was measured in three sections per core at Site 805. However, as was the case for results from Site 803 and 804, considerable work is still required to adjust the values for improper probe calibration. This effort has been postponed and will be completed post-cruise. Therefore, thermal conductivity data are not presented here.

Vane Shear Strength

Undrained shear strength was measured using a motorized minivane on split-core sections (see the procedures outlined in the "Explanatory Notes" chapter, this volume). Vane measurements were made in APC cores and in competent biscuits of XCB cores until the sediment became too stiff for insertion of the vane, near 240 mbsf. Table 9 (microfiche, back pocket) presents peak and residual vane shear data for Site 805. Residual shear strengths were obtained where cracking of the sediment did not dominate failure (see the discussion of vane shear strength data interpretation in the "Physical Properties" section, "Site 803" chapter, this volume). Figure 26 presents peak vane shear strength for Hole 805C and mean grain size for Hole 805B (taken from the "Lithostratigraphy" section, this chapter).

As noted above, equipment malfunction prevented vane shear measurements in most of Hole 805B. Many data gaps also exist in the Hole 805C profiles because of coring disturbance. Measurements were obtained in the apparently undisturbed lower sections in some of those cores where flow-in was observed in the upper sections; however, in some cases these lower sections also were disturbed (e.g., the measurement at 91 mbsf, Section 130-805C-10H-5, yielded a peak shear strength of 2.3 kPa). As observed for Sites 803 and 804, the shear strength profile at Site 805 is strongly influenced by disturbance of the calcareous sediments during coring, resulting in core-length cycles. These problems with the vane shear strength data set at Site 805 make it difficult to interpret the data with respect to changes in grain size or carbonate content.

Shear strength values at Hole 805C generally range between 5 and 20 kPa, with considerable variation between these two end members. Shear strength in silt-sized sediment is largely dependent on grain size (see more detailed discussion in the "Physical Properties" section, "Site 803" chapter, this volume). The observed variations are likely the result of high-frequency grain-size fluctuations in the upper 300 m (see "Lithostratigraphy" section, this chapter). Unfortunately, shipboard grain-size samples were not taken at the same intervals as vane shear measurements, so verification of this correlation is not possible at present.

Low-frequency variations in grain size also appear to have some effect on vane shear strength. For example, the slightly higher shear strength values in the interval from 20 to 45 mbsf may correspond to a slight increase in grain size (Fig. 26). Over the next 80 m, correlation between grain size and shear strength is limited by data gaps. From approximately 125 to 185 mbsf, peak vane shear strength decreases from near 20 kPa to approximately 8 kPa, and then increases again to near 25 kPa at 220 mbsf. This trend can be correlated loosely with a decrease and increase in mean grain size over this interval.

Index Properties

Samples were obtained from the split cores for index properties analyses. The index properties calculated from the wet and dry weights and dry volume of these samples are wet-bulk density, grain density, water content (based on dry weight), porosity, and dry bulk density (see "Explanatory Notes" chapter, this volume). The data for the four holes at Site 805 are presented in Table 10 (microfiche, back pocket).

As observed at Sites 803 and 804, the high calcite content of these sediments (generally >85%) results in grain densities that are constant with depth, with values near 2.7 g/cm^3. The slight scatter observed in the grain density values is within the scope of measurement error, with a few exceptions that are unexplainable at this time. For example, a low grain density (2.47 g/cm^3) at 45 mbsf in Hole 805C is possibly a result of an improperly recorded weight. Low bulk density and high water content were also calculated for this sample. We have resisted the temptation to discard unexplainable data spikes at this time; the GRAPE profile for this interval will be examined as part of a shore-based study so that this and similar data spikes can be verified or discarded.

Bulk-density data for Holes 805B and 805C are plotted vs. depth in Figure 27. Porosity and water content for these holes are presented in Figures 28 and 29, respectively. In the upper 10 m of the sediment column, there are steep gradients in index properties, associated with the consolidation of young sediment. Over this interval, bulk density increases from 1.45 g/cm^3 near the seafloor to 1.55 g/cm^3 near 10 mbsf, whereas water content decreases from almost 110% to 80% over the same interval. Between 15 and 180 mbsf, the gradients are not as high, with bulk density increasing gradually from values near 1.55 g/cm^3 at approximately 10 mbsf to 1.72 g/cm^3 near 190 mbsf. High-frequency variations are seen in the index property profiles in both holes of this site, and may be the result of fluctuations in the carbonate content ("Lithostratigraphy" section, this chapter). To verify this relationship, bulk density must be corrected for porosity rebound caused by the removal of overburden; this study will be completed post-cruise.

Near 190 mbsf there is a change in the bulk density profile (Fig. 27) from a trend of increasing density with depth (the expected trend for a normally consolidating sediment sequence) to one of decreasing density with depth. A similar change was observed at Site 803 at approximately 110 mbsf and at Site 804 near 50 mbsf. This trend continues to 260 mbsf. As discussed for Site 803, this phenomenon appears to be associated with a

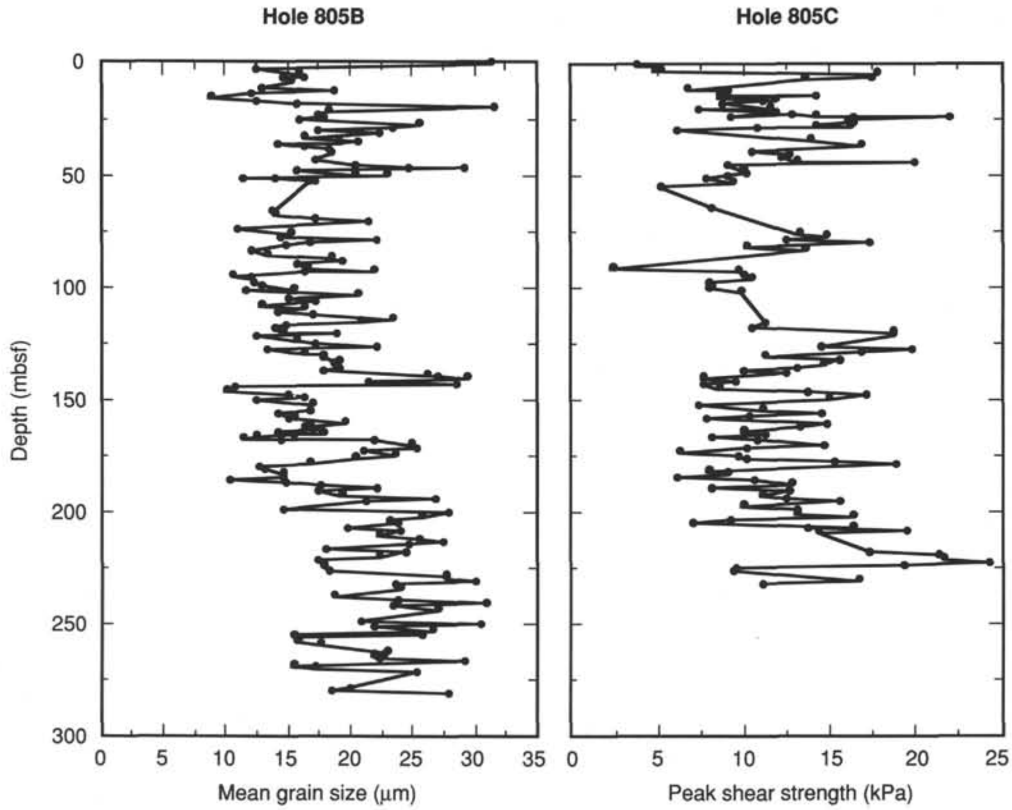

Figure 26. Laboratory vane peak shear strength vs. depth, Hole 805B, and mean grain size vs. depth, Hole 805C.

major dissolution event and corresponds to a notable decrease in carbonate content over this interval.

Bulk density begins to increase with depth again below 260 mbsf, from values of approximately 1.72 g/cm^3 near 260 mbsf to 1.77 g/cm^3 near 390 mbsf. Porosity decreases from 60% to 55% and water content decreases from 55% to 45% over this interval. This zone of fairly constant index property gradients crosses the ooze-chalk boundary, near 290 mbsf (see "Lithostratigraphy" section, this chapter). The decreases in porosity may be a result, in part, of consolidation as a consequence of overburden and, in part, of chemical cementation. Alternations between softer ooze and more cemented sediments in the ooze-chalk transition zone probably result in much of the variation seen in the profiles of index properties.

At 390 mbsf, bulk density values increase sharply to 1.9 g/cm^3, whereas porosity and water contents measurements show a steplike decrease; porosity values decrease to 50% and water contents to 35%. The index properties values then remain constant at these levels, with a few variations caused by local variations in grain size, to a depth of approximately 500 mbsf. The slight scatter observed may be the result of local grain-size variations. This interval of constant index properties is possibly a result of increased cementation, which prevents continued mechanical consolidation.

Between 500 and 600 mbsf bulk density values increase again but with less of a gradient than in the zones of increasing bulk density discussed above. Near 600 mbsf, bulk density values reach levels near 2 g/cm^3, whereas porosity values decrease to 45% and water contents decrease to 30%. These changes in the properties of already-cemented sediments probably represent the result of infilling of voids by calcite overgrowths. The explanations given for the various zones of physical properties will be tested by post-cruise crystallinity analyses and scanning electron microscope (SEM) studies.

Velocity

Compressional wave (*P*-wave) velocities were measured on split cores both perpendicular to (vertical) and parallel with (horizontal) bedding. Measurements were performed using the Digital Sediment Velocimeter (DSV) or the Hamilton Frame, depending on the degree of lithification of the sediment (see "Explanatory Notes" chapter, this volume).

Profiles of vertical and horizontal *P*-wave velocity with depth for Holes 805B and 805C are shown in Figure 30 and listed in Table 11 (microfiche, back pocket). Data gaps in the upper 100 m of Holes 805C are the result of coring disturbance, as previously discussed. As at Sites 803 and 804, velocities remain close to 1550 m/s in the upper 200 m of sediment at Site 805, similar to the previous two sites. Detailed examination of variations within this interval must await shore-based investigation of grain size, carbonate content, crystallinity, and isotopes.

Velocities begin to increase near 240 mbsf, indicating the upper limit of lithification, reaching 1700 m/s near 310 mbsf. After this initial increase in velocity, there is a sharp decrease to values below 1550 m/s near 330 mbsf. Shipboard grain size data are not available deeper than 280 mbsf, and thus the reason for this decrease in velocity is unknown at this time.

Velocity increases sharply from 1550 m/s at 325 mbsf to near 2000 m/s at 380 mbsf. This increase corresponds to a marked increase in bulk density over this interval and can be attributed to increased cementation. Fluctuations in velocity are possibly the results of variations in the degree of cementation of the

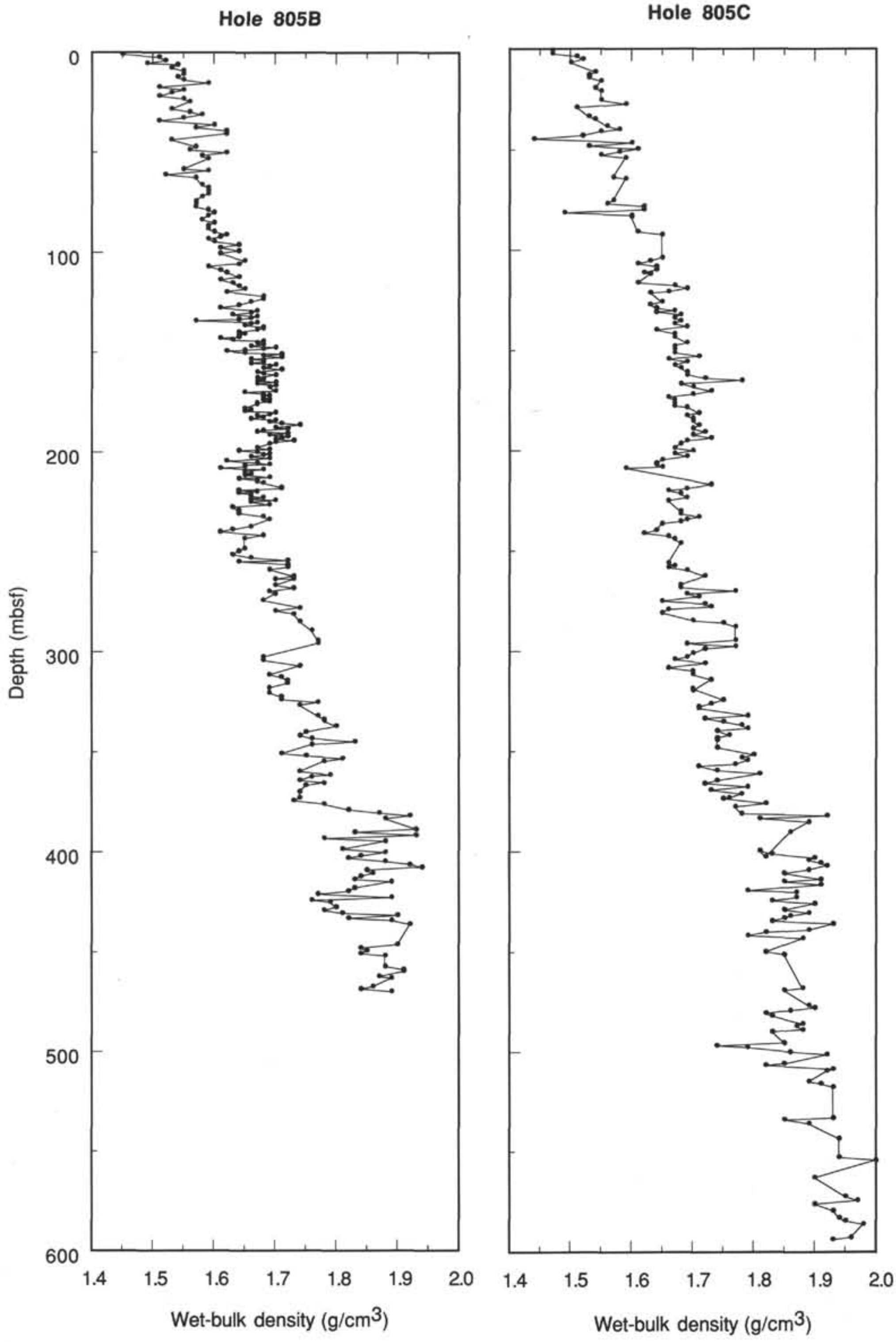

Figure 27. Laboratory bulk density vs. depth, Holes 805B and 805C.

measured samples. The interval between approximately 400 and 500 mbsf may represent a zone in which cementation is sufficient to prevent further consolidation, as discussed above with regard to the index properties data.

A zone of velocity anisotropy (with vertical velocities significantly greater than horizontal velocities) was observed between 440 and 490 mbsf. This, however, may be an artifact of testing. If small horizontal cracks exist in the sample, the force of the Hamilton Frame transducers applied in the vertical direction may close the fractures, thus increasing the measured velocity. Conversely, the force of the transducers applied in the horizontal direction may open the fractures and decrease the measured velocity.

Velocity increases over the interval from 500 to 600 mbsf. This increase in velocity would be expected if calcite is filling the voids in this interval, thus increasing the rigidity of the sedi-

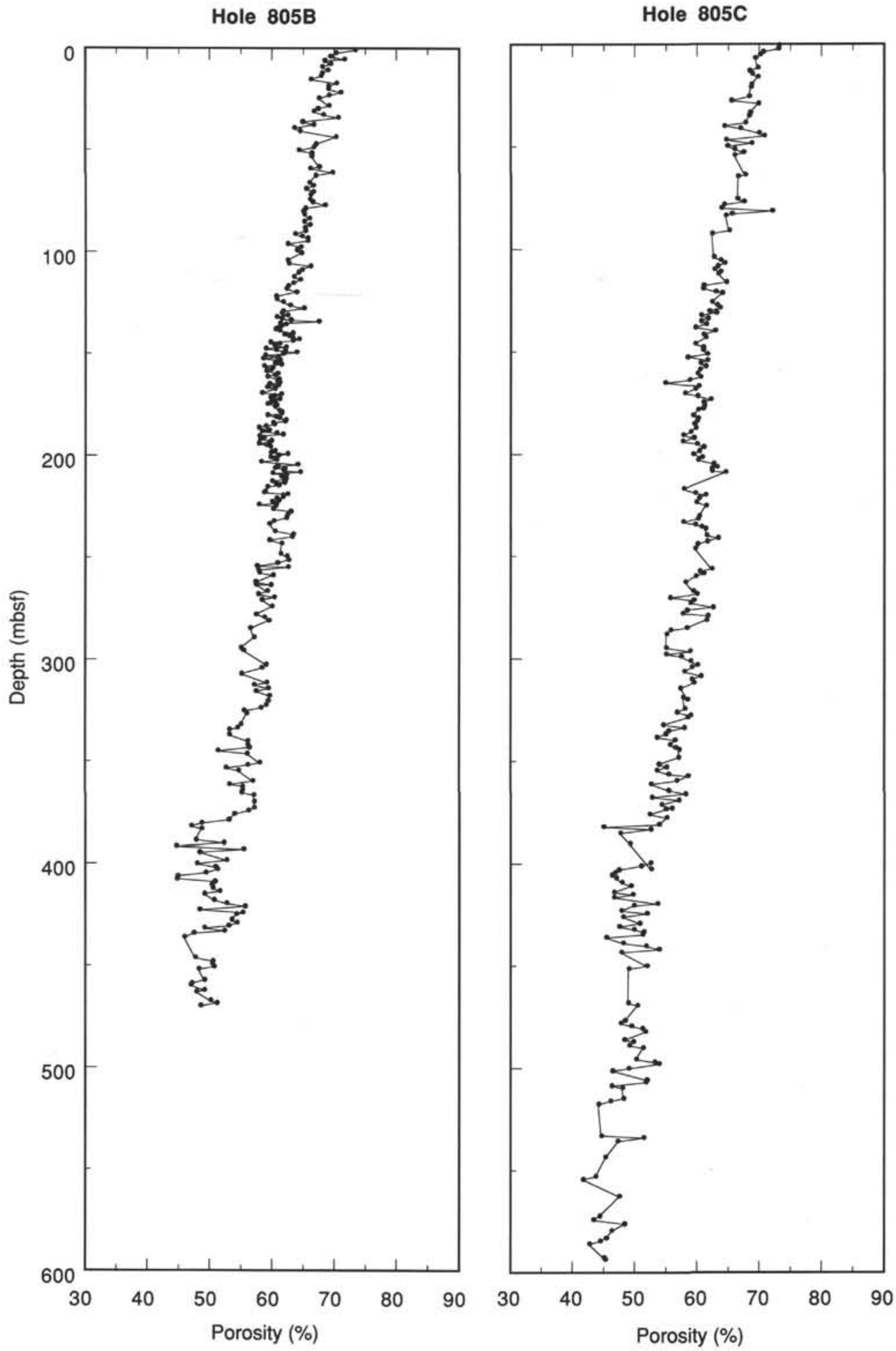

Figure 28. Laboratory porosity vs. depth, Holes 805B and 805C.

ment. Laboratory *P*-wave velocities reach values near 2000 m/s at the bottom of the hole, near 600 mbsf.

Laboratory velocity data for Site 805 are compared with log sonic velocity data for this site in the "Logging" section (this chapter). In general, there is good agreement in the shape of the curves, although laboratory velocities are lower than log velocities because of coring disturbances and the removal of overburden that resulted in porosity rebound of the cored sediments.

Summary

This brief examination of the shipboard physical properties data for Site 805 identifies the major trends in peak vane shear strength, index properties, and *P*-wave velocity. Detailed study of the high-frequency variations observed will be performed post-cruise with the aid of additional analyses such as grain size, crystallinity, SEM, triaxial shear strength, and consolida-

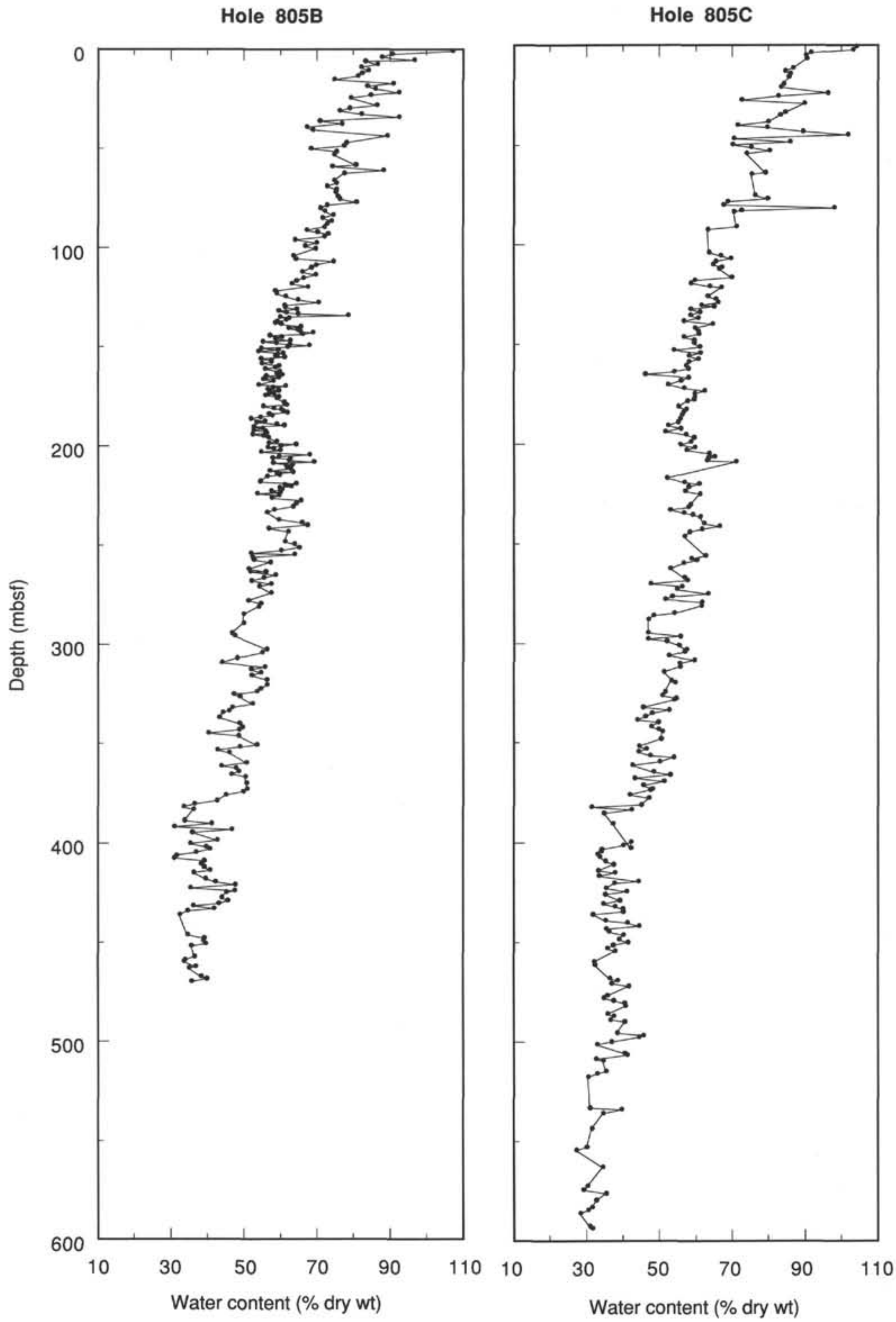

Figure 29. Laboratory water content vs. depth, Holes 805B and 805C.

tion. The major physical properties trends in the carbonate ooze appear related to dissolution events that are also evident in grain size and carbonate content data. Observed trends in the chalk sequences appear closely related to the degree of lithification and diagenesis.

LOGGING

Logging Operations

Logging at Site 805 went much more smoothly than at Site 803. Nevertheless, logging of Hole 805C was not without its

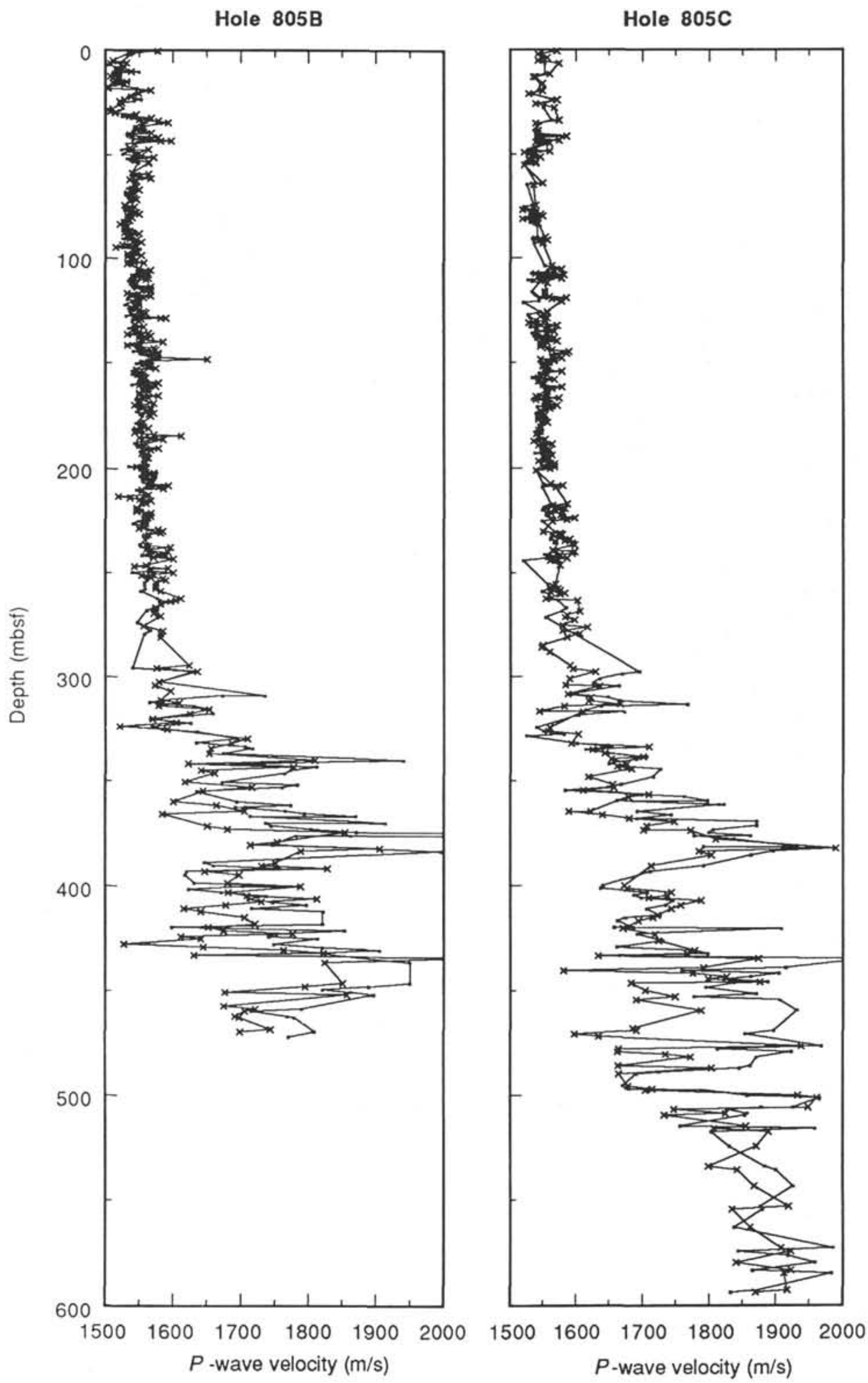

Figure 30. Laboratory compressional wave velocity vs. depth, Holes 805B and 805C. Lines with squares represent vertical (longitudinal) measurements (perpendicular to bedding), and lines with crosses represent horizontal (transverse) measurements (parallel to bedding).

problems. Table 12 lists the sequence of events during the logging of Hole 805C, and Table 13 lists the acronyms used in that table and this chapter. The first logging run consisted of a sonic velocity tool (LSS), resistivity tool (DITE), and the natural gamma-ray tool (NGT). The geophysical tool string was lowered to within 2 m of the bottom of the hole (609 mbsf), and it collected data up to the drill pipe at 100 mbsf. The section between 200 and 100 mbsf was logged a second time to establish the repeatability of the measurements. All tools functioned well on this run.

Table 12. Sequence of events during logging, Site 805.

Local day	Local time	Cumulative hour	Depth (mbsf)	Comments
2/16/90	9:00			Last core on deck
2/16/90	16:00	0.0		RIH with geophysical string tool (NGT/DIT/LSS)
2/16/90	17:02	1.0		At mud line
2/16/90	17:47	1.8	609.0	On bottom of hole, <2 m fill
2/16/90	17:50	1.8	609.9	Main log pass; NGT/DIT/LSS all working; up at 900 ft/hr
2/16/90	19:25	3.4	100.3	Tool in pipe at 3,300 m (10823 ft); run down for repeat
2/16/90	19:45	3.8	199.9	Start up on repeat section; NGT/DIT/LSS all working; 900 ft/hr
2/16/90	20:10	4.2	100.3	Tool in pipe at 3,300 m (10,823 ft); POOH
2/16/90	21:00	5.0		Tool string on deck
2/16/90	21:44	5.7		RIH with geochemical string tool (NGT/ACT/HLDT/GST)
2/16/90	22:34	6.6		POOH; put bullnose on to lock back flapper
2/16/90	23:12	7.2		RIH with geochemical string tool (NGT/ACT/HLDT/GST)
2/17/90	0:49	8.8	609.3	At bottom of hole; start log up
2/17/90	2:29	10.5	331.6	Trouble with GST after 11,900 ft (428 m); stop log
2/17/90	2:41	10.7	443.8	Dropped back to this depth; start repeat log up
2/17/90				GST misbehaving; not putting out many neutrons for this run
2/17/90	4:55	12.9	100.3	Enter pipe; end repeat geochemical string tool
2/17/90	5:32	13.5	199.9	Second repeat; go down to 11,150 ft to see if formation activated
2/17/90	5:59	14.0	100.3	No sign of neutrons; POOH with geochemical string tool
2/17/90	8:25	16.4		Rigged down from logging runs

Note: Depth is based on a seafloor depth of 3199 mbrf.

Table 13. Acronyms used in describing logging at Hole 805C.

Acronym	Description
ACT	Aluminum clay tool
API Units	American Petroleum Institute standard unit for gamma-ray activity
BHC	Borehole compensated sonic tool
DIT	Phasor dual induction resistivity tool
FMS	Formation microscanner
GST	Geochemical spectral tool
HLDT	High temperature lithodensity tool
LSS	Long-spaced sonic digital tool
NGT	Natural gamma-ray tool
TLT	LDGO temperature logging tool
fbrf	Feet below rig floor
mbrf	Meters below rig floor
mbsf	Meters below sea floor
POOH	Pull out of hole
RIH	Run (tool) into hole

The second logging run was the combined geochemical tool string (geochemical spectral tool [GST], aluminum clay tool [ACT], and the natural gamma tool [NGT]), the lithodensity tool (HLDT), and the Lamont temperature tool (TLT). The tool string was lowered almost halfway to the mud line before we realized that the bullnose (which insures that the flapper valve on the XCB bit locks out of the way) was not attached to the base of the tool. The string was pulled back to the surface, the bullnose was attached, and the tool string was sent down again, to within 2 m of the base of Hole 805C. During the upward logging run, the GST went out of tolerance near 428 mbsf, and the up log was stopped at 331 mbsf. The tool was lowered again to 443 mbsf, and an attempt was made to calibrate the GST. The GST continued to malfunction and failed to obtain any new data for the rest of the logging run. The ACT, NGT, HLDT, and TLT continued to function for the remainder of the upward logging run to pipe. After the tool string entered pipe (100 mbsf), we pulled it from the hole and concluded logging 23.5 hr after the last core was on deck.

Even though the GST malfunctioned, the other logs are of excellent quality and most cover the entire hole from 609 to 100 mbsf. The density log is good only between 609 and 120 mbsf because the upper hole was broadened by washing. A step in the velocity profile at 240 mbsf also may be traced to bad hole conditions, as is discussed in more detail below. An ash layer was recorded at 544 mbsf in both NGT runs that provides a stratigraphic tie point between the two logs. Unfortunately, because this interval was poorly recovered by coring, we were unable to tie the logs definitively to core.

Log Stratigraphic Units

The lithology of the recovered section at Site 805 was described as a monotonous single unit (subdivided at the ooze chalk boundary; see "Lithostratigraphy" section, this chapter) but the detailed resolution of the logs showed a wide range of sedimentological changes at a number of scales. Following the procedure established at Site 803, the logging results were divided into log stratigraphic units based on internal consistencies within the logging records. These log stratigraphic units were then compared with the lithostratigraphic units and the basis for their similarities or differences were evaluated. Figure 31 presents the primary geophysical log data (velocity, density, resistivity, and natural gamma ray), and Figures 32 through 37 present the geochemical log results (calcium, silica, and aluminum). Because the GST only worked properly between 600 and about 400 mbsf, the log stratigraphic units were based solely on the geophysical log suite.

The logging data were divided into four log stratigraphic units (A, B, C, and D) based on the geophysical logs, with the exception of the natural gamma-ray log. Although changes in velocity, density, and resistivity generally correlate with each other, their relationship to the gamma-ray data is unclear. As discussed in the logging section of Site 803 (this volume), the natural gamma-ray levels in these sediments are extremely low (probably representing the low content of clay or ash) and, therefore, do not significantly influence the other parameters.

Logging Unit A

Unit A begins at the depth of the shallowest log data (100 mbsf) and continues to between 240 and 260 mbsf, depending on which log is being examined. This unit has fairly constant resistivity and density profiles, and a gently increasing velocity profile (the low-velocity zone between 140 and 160 mbsf is probably an artifact of poor hole conditions; see the comparison with laboratory data below). The numerous low-amplitude, high-frequency changes in all properties may be related to changes in

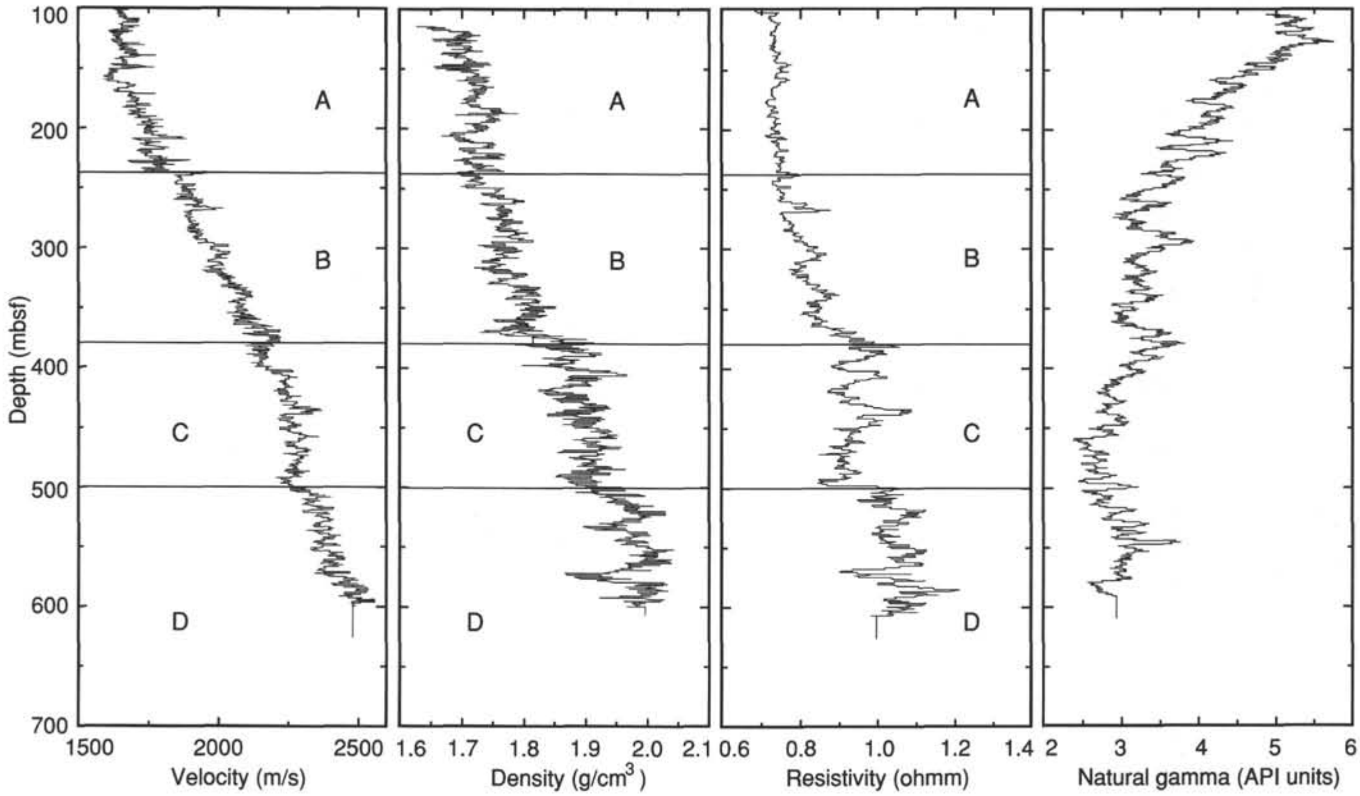

Figure 31. Logs of velocity, density, resistivity, and natural gamma-ray activity vs. depth, Site 805, with log-stratigraphic units marked. See text for description of units.

foraminifer content, although detailed correlations are not possible at this point. Below about 200 mbsf, high-amplitude changes in density and velocity are seen. These appear to be related to changes in induration noted by the sedimentologists (see "Lithostratigraphy" section, this chapter). As at Site 803, there are small zones of high resistivity (low porosity) that correspond to increases in velocity and density (e.g., between 210 and 240 mbsf).

Logging Unit B

Unit B is marked by an offset (increase) in velocity, density, and resistivity. This offset occurs at slightly different depths depending on the log: 240 mbsf in the velocity log, 250 mbsf in the density log, and 260 mbsf in the resistivity log. Analyses of the borehole sonic data indicate that this offset may be an artifact of a rapid change in borehole diameter. The velocity data shallower than 240 mbsf should be considered suspect. The change in borehole conditions is, in itself, probably indicative of changes in the properties of the sediment; thus, we have chosen to maintain this boundary as a log-stratigraphic-unit boundary. This offset roughly corresponds to a time of transition from high to low sedimentation rates (see "Sedimentation Rates" section, this chapter).

Beneath the offset, density, velocity, and resistivity values all increase slowly with depth, probably because of compaction. Superimposed on this steady increase with depth are high-frequency, low-amplitude fluctuations in all parameters, probably related to changes in sediment properties in response to variations in oceanographic conditions.

Logging Unit C

Unit C begins with another offset, an increase in velocity, density, and resistivity. The log profiles are characterized by high-amplitude excursions, particularly resistivity. Within the unit, the gradients decrease with depth. The top of Unit C (380 mbsf) is the depth at which there is a sharp decline in foraminifer content from about 30% to about 10% (see "Lithostratigraphy" section, this chapter). The decrease in grain size associated with the disappearance of foraminifers is consistent with the increase in velocity, density, and resistivity (resulting from decreased pore space) that is seen in the logs. The high-amplitude fluctuations are probably related to changes in the induration of the sediment.

Logging Unit D

Unit D is marked by another offset (increase) in velocity, density, and resistivity. Within this unit are several high-amplitude, low-frequency excursions in all properties, resulting in decreases in density and resistivity. Although recovery was poor in these intervals, the logs imply that these zones are probably less indurated than the surrounding material.

Correlation with Lithostratigraphy

Examination of the logs has revealed much variability, more than can be noted in the visual description of the cores. Given the internal consistency between the logs, the variations observed are probably significant in terms of changes in paleoceanographic conditions. The section at Site 805 was divided into a single lithologic unit with a subdivision at the ooze-chalk transition that was placed between 283 and 293 mbsf (see "Lithostratigraphy" section, this chapter). The logs indicate that this transition began somewhat higher in the section. The velocity log shows a shift to higher values at about 240 mbsf, the density log at 250 mbsf, and the resistivity log at 260 mbsf. Although we have discussed that this may, in part, be an artifact of borehole conditions, the different logs apparently reflect different stages

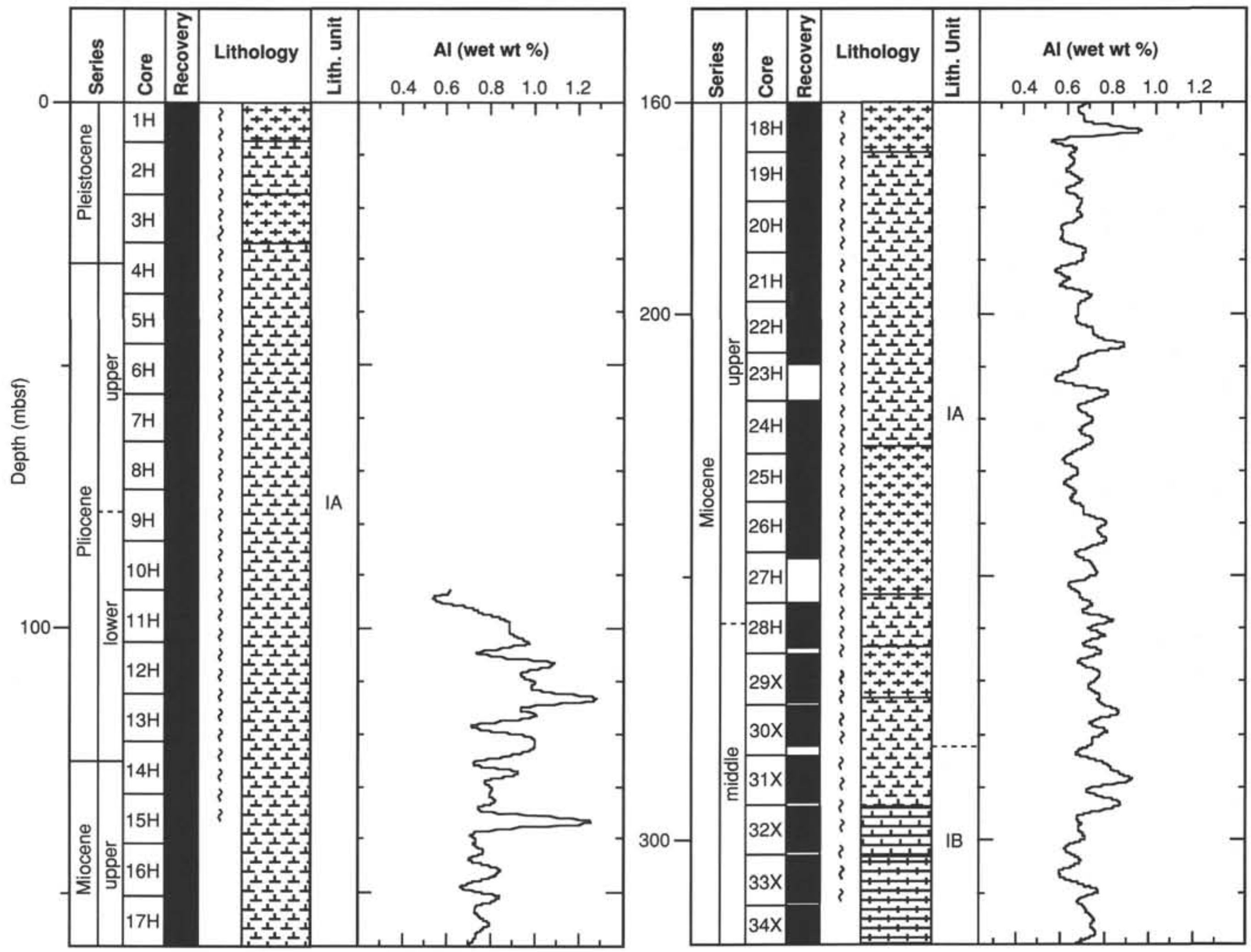

Figure 32. Log-derived aluminum record and lithologic column, Hole 805C.

of lithification. At the onset of cementation (240 mbsf), the rigidity of the sediment is rapidly changed (and thus the velocity) without substantial change to the density or resistivity. At a more advanced stage (250 mbsf), cementation begins to affect the density and then finally (at 260 mbsf) the resistivity. The alterations of induration noted by the sedimentologists above the zone of the ooze-chalk transition are clearly seen on the logs.

A major break in the logs takes place at 380 mbsf (Units B/C boundary), correlating with a change in foraminifer content downhole. This level also corresponds to a change in the style of recovery; below this depth the recovered material consists of disjointed chunks and chips whereas above it recovery is more continuous. The offset in the logs at 500 mbsf has no counterpart in the lithologic description, but this is a zone of poor recovery. The logs imply that there are significant changes in the sediment in the deepest log stratigraphic unit (D).

Small nodules of chert were recovered in Hole 805C at 344 mbsf, but there is no evidence of massive chert layers in the logs at this depth. Chert was not recovered from Hole 805B at this depth, supporting the notion that the chert is patchy.

Comparison with Laboratory Data

Figure 38 shows the comparison of log velocity and density data to uncorrected and corrected laboratory values (for details of the correction procedure, see "Seismic Stratigraphy" section, "Site 803" chapter, this volume). As was noted at Site 803, these comparisons serve to test the quality of both laboratory and log values. Wherever the high-frequency components of the curves have the same shape, we can be reasonably confident that both sets of measurement are good. When there is a discrepancy between the two, we must examine each to see where the problem could lie. The lack of a low-velocity zone between 140 and 160 mbsf in the laboratory data led us to question the log values over this interval. Examination of caliper data here suggests that borehole conditions may have been poor.

Chemical Logs

Three separate logs provided *in-situ* chemical information in Hole 805C: the natural gamma-ray tool, the aluminum clay tool, and the geochemical spectral tool. Presented below are preliminary observations on aluminum distribution (ACT) from 100 to 580 mbsf (Fig. 32) and the calcium data (GST) for the lower 200 m of the hole (Fig. 33).

Aluminum and Natural Gamma Logs

The aluminum data in Figure 32 are presented as wet-weight percent. The profile has been smoothed by a 15-point Gaussian filter to remove noise associated with the low absolute aluminum content. The aluminum concentration in Hole 805C is low and has high-frequency variability, but only subtle low-frequency

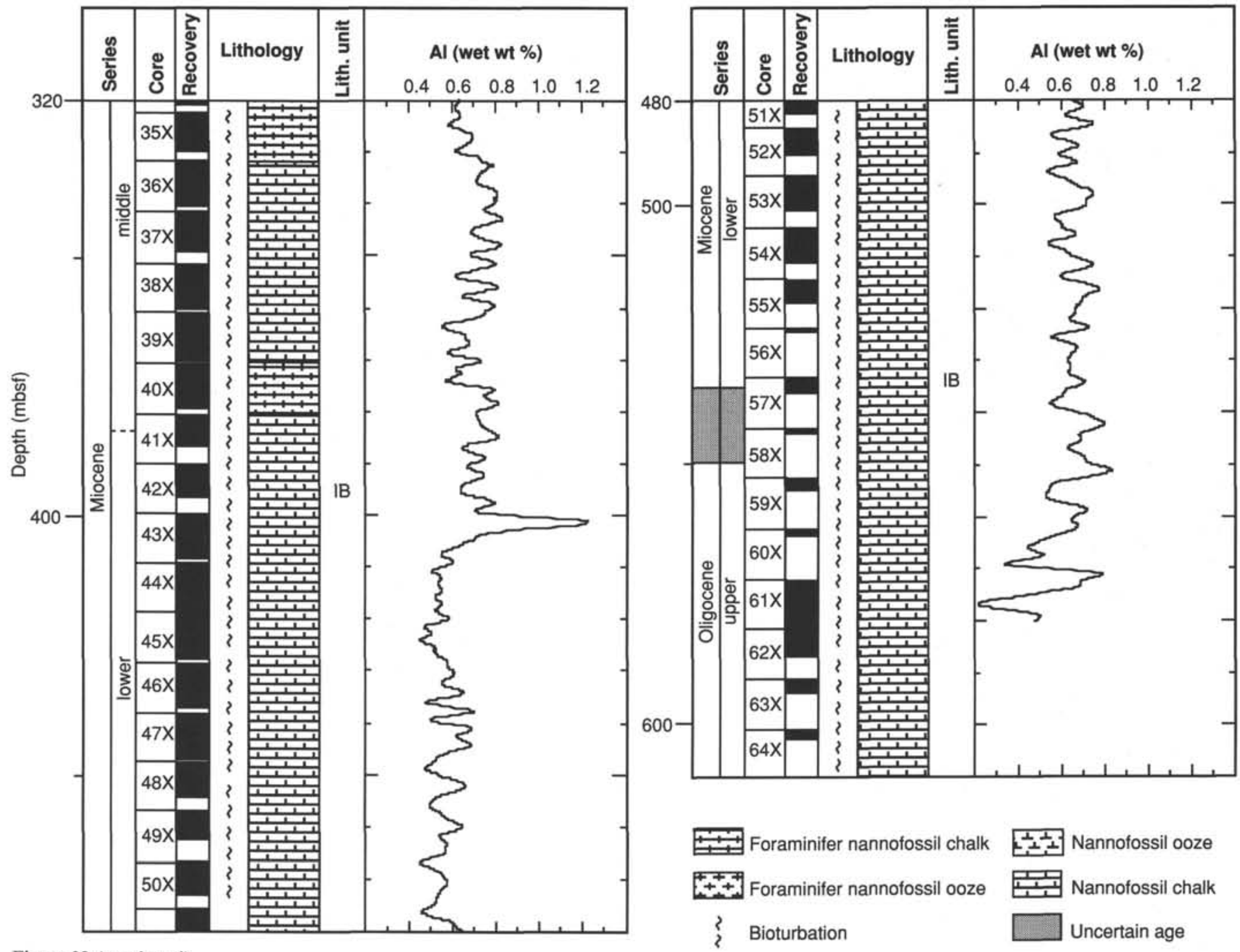

Figure 32 (continued).

trends. In Figure 34, the aluminum data are compared with the natural-gamma information. Because Al and natural gamma-ray activity both indicate the amount of terrigenous debris, one would expect that the two should be correlated. Below 260 mbsf we do see such a correlation between the two records. Between 160 and 260 mbsf the logs diverge strongly for reasons not yet well understood.

As calcite dilutes the other sediment fractions in these sediments, there should be a perfect correlation between the noncalcite fraction in the sediment and the aluminum content, provided that the aluminum content of the noncalcite fraction is constant. Figure 35 is a plot of these two parameters vs. depth in Hole 805C. The noncalcite fraction was determined by subtracting core measurements of calcite from 100%. As illustrated in the figure, there is general agreement between the two variables. The comparison suffers, however, from differences in sampling density. The log information was collected at 15-cm intervals, whereas the core data were collected on a meter spacing at best. Downhole, where recovery became poorer, the core data are more widely spaced. Better comparisons and more rigorous validation of the aluminum log must await shore-based studies.

The GST Calcium Log

Only preliminary processing of the GST data was available on board the ship. The GST collects data for Ca, Si, Fe, K, Ti, S, Gd, Cl, and H. However, the sediments of Hole 805C are so highly calcareous that only Ca and Si in the solid phases and Cl and H in the pore waters will most likely be above detection limits. We present the data for the shipboard comparison as counts of Ca/(Ca + Si) to normalize any variations in neutron capture by the solid phases.

Figure 33 shows the calcium log plotted vs. the lithologic column from 405 mbsf to the base of the hole. The uppermost port of the section (~425–405 mbsf) was logged as the tool began to exceed its tolerances and may be invalid. It is obvious that most of the variation seen on the profile is in the higher frequency range, even though fluctuations at periodicities of several million years are also apparent. The Ca/(Ca + Si) data and the aluminum data (Fig. 36) are inversely correlated, at least for lower frequencies. At shorter periods, on the order of 1–5 m, the correlation is not good, probably because of the low aluminum content.

A comparison of the log of Ca/(Ca + Si) to the core carbonate data is presented in Figure 37. The two data sets compare in a general way through the interval from 405 to 510 mbsf, where core recovery was quite good. Below 510 mbsf the core and log records diverge, but as core recovery was poor in this interval, one must be concerned about the positioning of core data in terms of depth below seafloor as well as whether the recovered core represents a biased sample of the sedimentary record (e.g., lithified sections only).

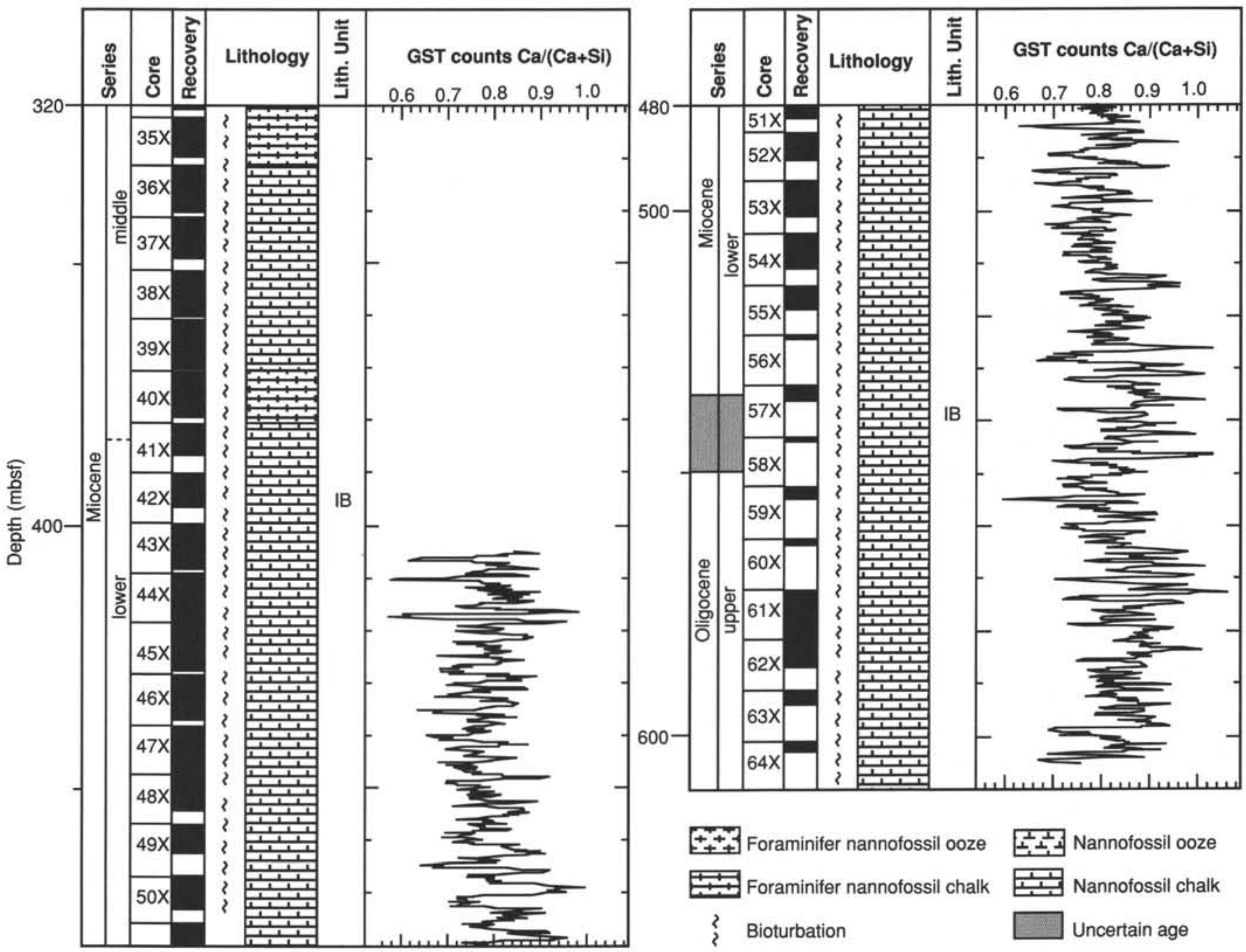

Figure 33. Log-derived calcium/(calcium + silica) ratio and lithologic column, Hole 805C.

The data records presented in Figure 37 cover an interval that has major sedimentation rate changes; in addition, they provide a way to check if the high-frequency information in the calcite log is consistent across the interval of sedimentation rate changes. Between 404 and 453 mbsf, the sedimentation rate is estimated to be 26.8 m/m.y., based upon the LO of the foraminifer *Globorotalia kugleri* and the FO of the nannofossil *Sphenolithus belemnos* (Table 5, "Sedimentation Rates" section, this chapter), as is shown in Figure 37 by the bar representing 1 m.y. of time. During a typical 1-m.y. interval in this section, 9–10 high-amplitude calcium cycles occur, perhaps equivalent to the 100-k.y. period observed in Pacific Pleistocene carbonate sediments.

Between 453 and 529 mbsf, the estimated sedimentation rate based upon the FO and LO of *G. kugleri* is 40.1 m/m.y. (Fig. 37). The high-amplitude calcium cycles continue to occur at frequencies of about 9–10/m.y., even though the cycles are much broader when viewed along a depth axis. Below 529 and above 558 mbsf, the sedimentation rate (based upon the LO of the nannofossil *S. ciproensis* and the FO of *G. kugleri*) is estimated to be 19.4 m/m.y. Here too, calcium variations occur at frequencies of 9–10 cycles/m.y. These observations are very encouraging with regard to carbonate cycle information contained in these records, which will be investigated after shore-based reprocessing of the data sets.

SEISMIC STRATIGRAPHY

The seismic section at Site 805 has the "layer-cake" appearance of the thick, shallow regions of the Ontong Java Plateau. Despite the similarity in appearance to the top of the plateau, the section here is approximately 25% thinner than that at Sites 289/586 (see Mayer et al., this volume). As discussed in Mayer et al., it is not possible to trace individual reflectors from the top of the plateau beyond depths of about 3000 m. Nonetheless, a preliminary analysis of the site survey seismic records indicates that the majority of the thinning takes place in the Miocene and Pliocene intervals and in the pre-Oligocene. Although the section in the vicinity of Site 805 is fairly flat-lying and undisturbed, displacements and faulting can be seen on either side of the site. In addition, a small MSR (see Mayer et al., this volume) is located slightly downslope from the site (Fig. 39).

As at the previous sites, we used the results of laboratory and log measurements to convert seismic traveltime to depth-in-section as well as seismic modeling to check on the accuracy of this traveltime-to-depth conversion. For Site 805, laboratory measurements of velocity and density were made approximately every 75 cm (see "Physical Properties" section, this chapter), and velocity and density logs (15-cm sample interval; around 60-cm sensor spacing) were run for the section between 100 and 609

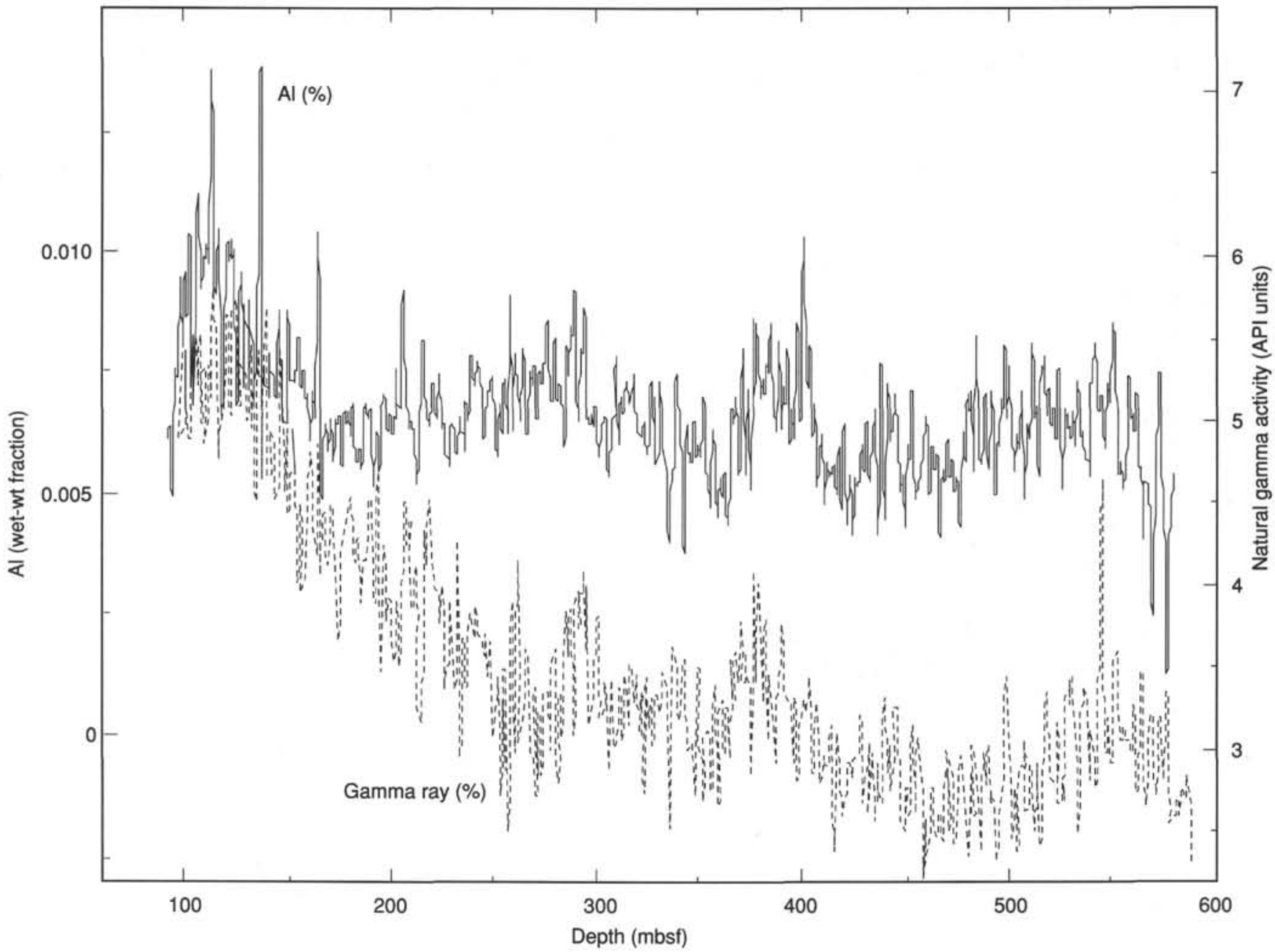

Figure 34. Wet-weight fraction of aluminum (solid line) compared with natural gamma-ray activity (dashed line), Hole 805C.

mbsf (see "Logging" section, this chapter). Laboratory measurements of velocity and density were converted to *in-situ* values using the methods described in Mayer et al. (1985) and merged with the log data. If we assume that the log measurements represent *in-situ* values, then the good match seen between the corrected laboratory measurements and log data implies that the *in-situ* correction is reasonable (Fig. 38). A comparison of log and corrected laboratory data also reveals that between 140 and 160 mbsf there is a zone where log velocity values decrease but laboratory values do not. A close examination of the log data over this interval suggests that the borehole in this section was extremely wide and thus the log data may be questionable; log data, therefore, were replaced by corrected laboratory data over this interval.

The merged, corrected laboratory and log data (velocity and density) were used to calculate acoustic impedance (Fig. 40), which was then convolved with a seismic source signature to generate a synthetic seismogram (see "Site 803" chapter, this volume, or Mayer et al., 1985, for details). The synthetic seismogram is compared to the field seismic profile to evaluate the accuracy of the traveltime-to-depth conversion. The field records used for this study are those collected by the *Thomas Washington* (ROUNDABOUT Cruise 11) during the site surveys for Leg 130 (see Mayer et al., this volume).

As is typical for equatorial Pacific deep-sea carbonates, the seismic record at Site 805 is composed of numerous closely spaced reflectors (there are more than 90 at Sites 289/586). It would be far beyond the scope of this report to discuss the possible origin of each of these reflectors. Instead, we select a few representative reflectors and look at their origin and stratigraphic significance. The criteria for selection of these reflectors is simply that they have high amplitudes and are laterally coherent within the immediate area of Site 805. No effort has been made to select reflectors that are regionally correlatable (e.g., see Mayer et al., this volume) and thus the regional paleoceanographic significance of the selected reflectors remains uncertain.

A comparison of the synthetic seismogram to the field record at Site 805 (Fig. 41) produces a reasonable match, although not one that is without ambiguities. In the absence of a clear tie point like basement or chert (as at Site 803), there are several possible fits of the synthetic record to the field data. We have chosen a fit that maximizes the number of matches, particularly in the deeper part of the section (Fig. 41). We have selected 11 reflectors in the 611-m thick section; their traveltimes, depths, and ages are listed in Table 14. To facilitate discussion, the seismic section has been divided into six groups (Panama, Tethys, Antarctic, Drake, Texas, and Ontong Java). These groups have been given labels based on major oceanographic events that influence oceanographic processes during the time of their formation. The rationale for this naming scheme is discussed in the "Summary and Conclusions" section of this chapter.

The high Pleistocene sedimentation rates at Site 805 allow us to pick the first Pleistocene reflector of Leg 130 (at Sites 803 and 804 all of the Pleistocene was obscured by the signal of the

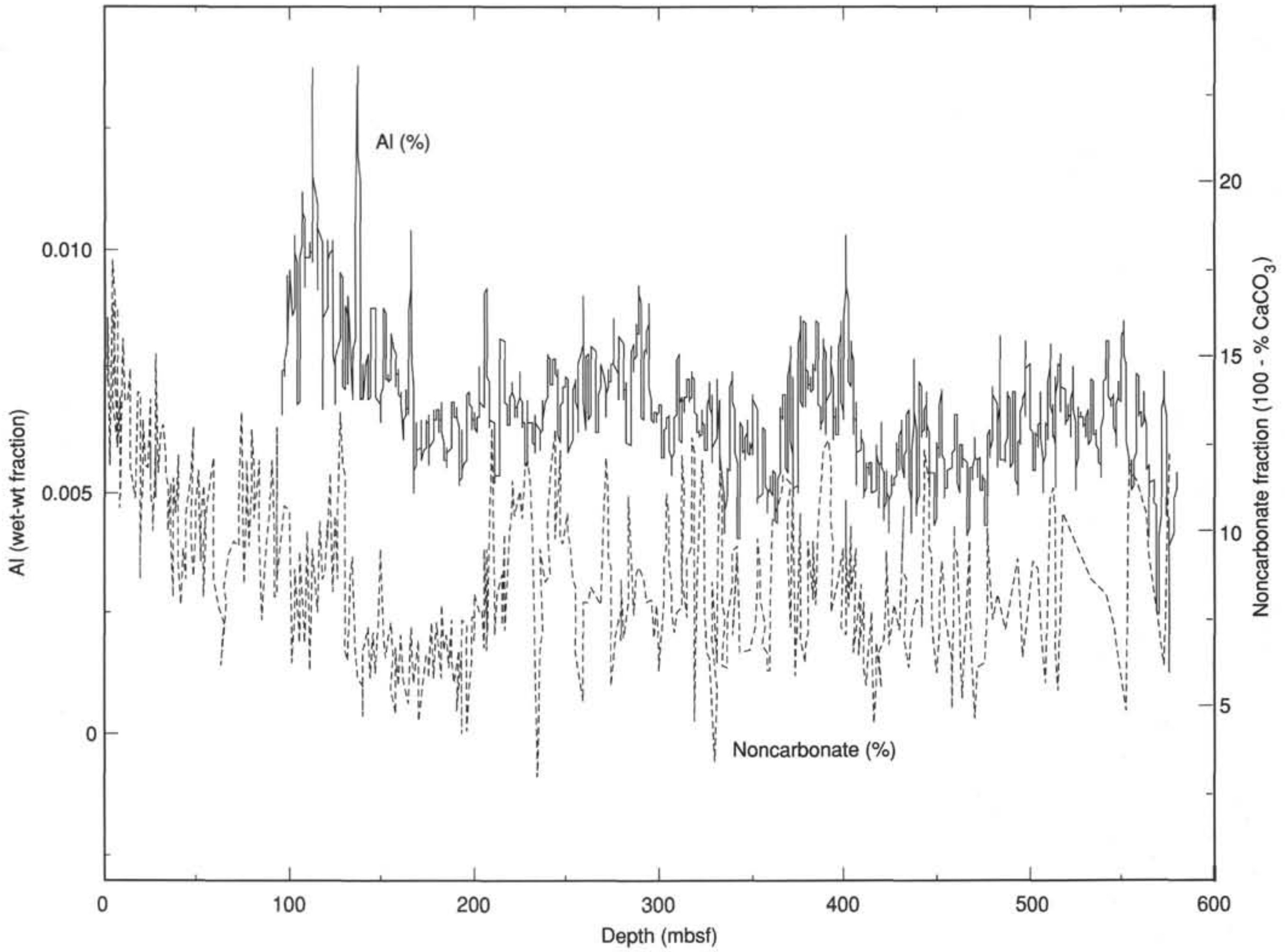

Figure 35. Log-derived aluminum wet-weight fraction (solid line) compared with shipboard measurements of the noncarbonate fraction (100 − %$CaCO_3$) (dashed line), Hole 805C.

outgoing pulse). Reflector 5-1 (0.026 s below seafloor [sbsf], 20 mbsf, 1.2 Ma) is characterized by an increase in density and velocity (and thus acoustic impedance; Fig. 41). These changes correlate with an increase in grain size and a decrease in carbonate content (Fig. 42). The association of increased grain size with decreased carbonate content is unusual and may indicate the removal of nannofossils by currents. The same set of physical property relationships characterize the next two deeper reflectors (5-2, 45 mbsf, 2.4–2.5 Ma, and 5-3, 80 mbsf, 3.7 Ma) assigned to the "Panama" series of reflectors (see "Summary and Conclusions" section, this chapter).

In the next three deeper reflectors (5-4, 101 mbsf, 4.4–4.5 Ma; 5-5, 218 mbsf, 7.1–7.3 Ma; and 5-6, 280 mbsf, 10.3–10.6 Ma), members of the "Tethyan Series" (see "Summary and Conclusions" section, this chapter), grain size no longer appears to play a dominant role. Here, velocity and density seem to be responding to changes in carbonate content that may be a function of variations in productivity and dissolution. All records begin to show cyclic, moderate-amplitude fluctuations (particularly evident in the density record) that give rise to the numerous closely spaced reflectors that characterize this interval. Within this reflector series is the ooze-chalk transition, at about 282 mbsf, roughly at Reflector 5-6 (see "Lithostratigraphy" section, this chapter). The alternations in induration state noted by the sedimentologists are evident in the physical property records and are expressed as high-amplitude peaks in density and particularly in velocity.

In the middle of this interval, there is a large offset in the log-derived velocity (237 mbsf) that results in a high impedance contrast and a large reflector on the synthetic seismogram (Figs. 40 and 41). A depth below seafloor of 237 m should correspond to a seismic traveltime of approximately 0.280 s, a time at which we do not see a high-amplitude, well-developed reflector on the field profile. Laboratory velocity data over this interval do not show a similar effect, and several quality control parameters in the log imply that this velocity offset may be an artifact of poor borehole conditions (see "Logging" section, this chapter). It should be noted, however, that variations in hole conditions often correspond to variations in lithology. Closer examination of this interval will be a subject of shore-based study.

The next four reflectors (5-7, 5-8, 5-9, and 5-10), associated with the "Drake" and "Antarctic" series (see "Summary and Conclusions" section, this chapter), are all the result of rapid, high-amplitude increases in velocity that are superimposed on lower frequency velocity and density excursions (Fig. 40). Carbonate data are sketchy in this interval, but carbonate content apparently plays no role here. Velocity and density fluctuations are perfectly in phase, indicating that cementation and induration are becoming more advanced. The deepest selected reflector (5-11, 530 mbsf, 23.7–23.9 Ma) is also the result of a high-

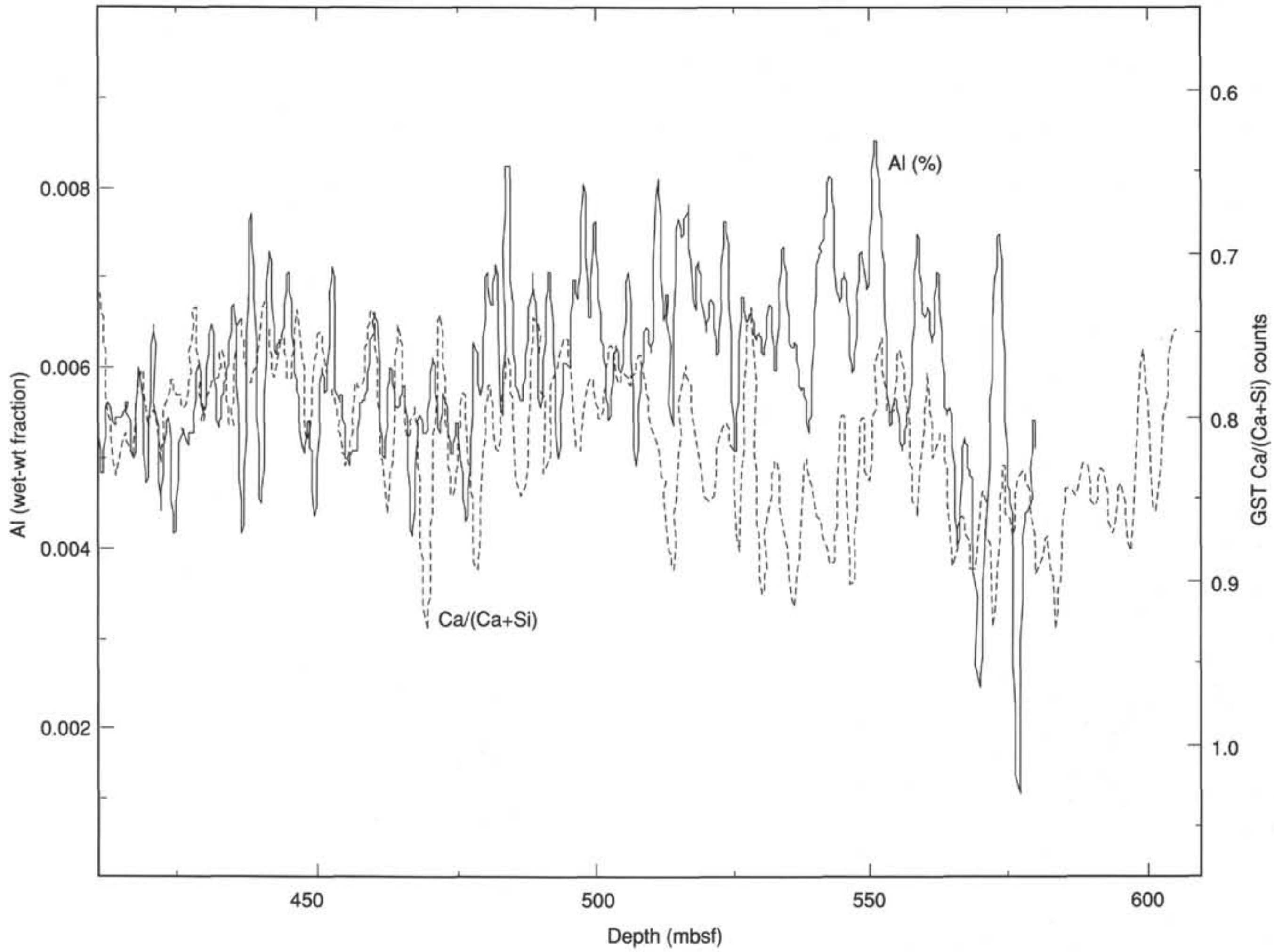

Figure 36. Log-derived calcium/(calcium + silica) ratio (dashed line) compared with log-derived aluminum wet-weight fraction (solid line).

amplitude change in velocity, but, in this case, a decrease rather than an increase.

Drilling stopped at Site 805 at 611 mbsf. Using the results of Site 803, we can estimate that the Eocene/Oligocene boundary should be found at approximately 0.650 sbsf (660 m) and that the strongly reverberant reflectors of the "Ontong Java Series" (see "Summary and Conclusions" section, this chapter) represent the large fluctuations in carbonate content and induration (alternations between limestone and chert) typical of many Eocene sections. Acoustic basement at this site is complex; there are two very strong reverberant zones, one at 0.758 sbsf and the second at 0.845 sbsf. The upper zone may represent massive chert and the lower one basalt, or we may be seeing two basaltic flow units separated by sediments.

The ultimate goal of our seismic stratigraphic effort was to use the seismic record as a paleoceanographic tool by producing detailed maps of the distribution, in time and space, of various parameters that reflect paleoceanographic processes. The achievement of this goal involved, among other things, the careful mapping of selected seismic horizons over large distances, a project well beyond the scope of a shipboard report. We have, however, already noticed identifiable patterns in the seismic character of the Ontong Java Plateau sites and, to facilitate future discussions, have given these reflector patterns names. Reflectors have been grouped and the groups given labels based on the major geographic events that influenced oceanographic processes at that time. Thus, we adopt (tentatively) the hypothesis of Mayer et al. (1985, 1986), which proposes that certain central Pacific-wide seismic reflectors were the result of global oceanographic events. We do not imply, however, by this naming, that our analyses of Ontong Java seismic stratigraphy suffices for ascribing particular reflectors to particular events.

The youngest named group of reflectors (4–2 Ma) are called the Panama Series because of the influence of the closing of the Isthmus of Panama on global oceanography at this time. Also dominating global oceanographic processes during this period was the onset of Northern Hemisphere Glaciation and associated reorganizations of North Atlantic Deep Water. The next group, the Tethyan Series, spans a time interval (10.5–4 Ma) affected by the closing of the Tethyan Seaway and including the isolation of the Mediterranean and a fundamental change in the partitioning of silica and carbonate between the Atlantic and the Pacific.

The Antarctic Series (19–10.5 Ma) represents that period of time dominated by the buildup of ice in Antarctica and perhaps the initiation of Norwegian Sea overflow into the Atlantic. This is followed, downsection, by the Drake Series (22.5–19 Ma), during which the Drake Passage opened up and steep north-south thermal gradients and circumpolar circulation began. Beneath the Drake Series are the Texas Interval (35–23 Ma), a long period of comparatively little oceanographic change that resulted in a reflector-free seismic interval, and the Ontong Java

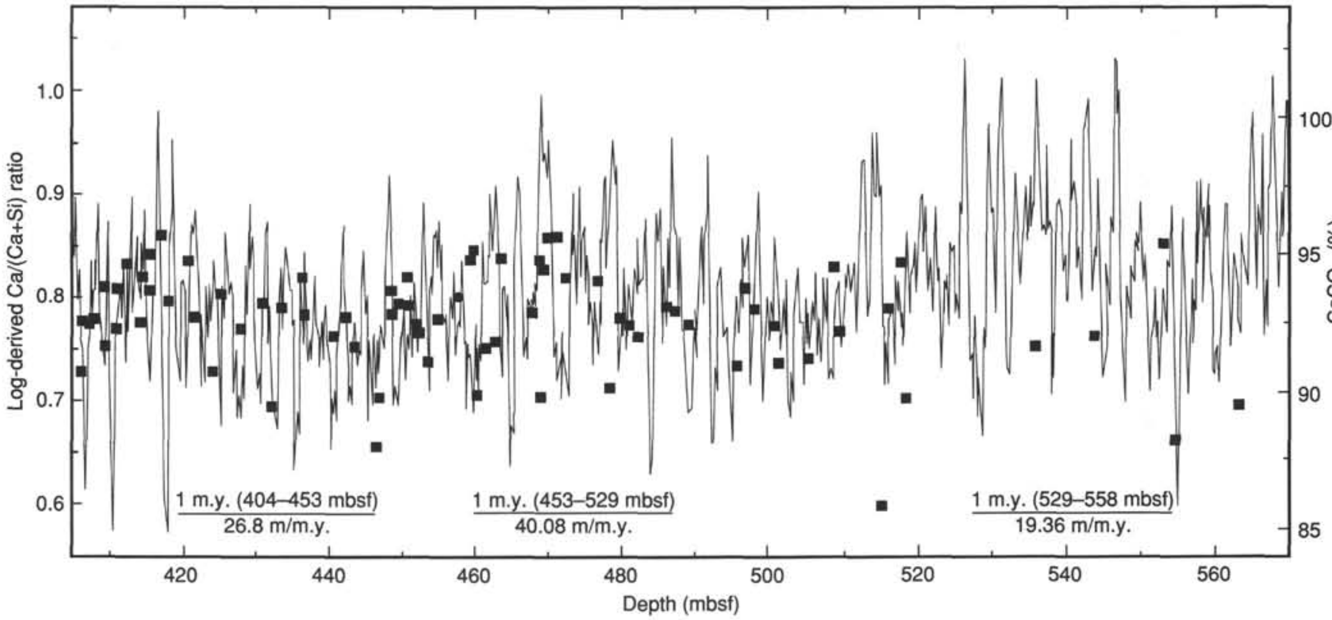

Figure 37. Log-derived calcium/(calcium + silica) ratio (solid line) compared with shipboard measurements of $\%CaCO_3$ (squares) for the interval from 400 to 590 mbsf, Hole 805C. Bars represent 1-m.y. time intervals. Note change in spacing of cyclicity as sedimentation rate changes.

Series (middle and late Eocene), which is characterized by strongly reverberant reflectors that are indicative of the large fluctuations in carbonate content and induration typical of the Eocene. Further discussion of the rationale for these divisions can be found in the "Summary and Conclusions" section of this chapter.

SUMMARY AND CONCLUSIONS

Site 805 is located in the western equatorial Pacific on the northeastern margin of the Ontong Java Plateau (latitude 1°13.7′N, longitude 160°31.8′E) in 3188 m of water. Our objective in drilling this site was to obtain a continuous record that would serve as the intermediate member of a depth transect of Neogene sediments, designed to recover depth-related paleoceanographic signals. We anticipated that we would encounter a high-resolution carbonate record in a near-lysoclinal setting for our studies of dissolution history and biostratigraphy.

The site was positioned based on two intersecting single-channel seismic (SCS) lines acquired by the *Thomas Washington* during ROUNDABOUT Cruise 11 (2130 UTC, 24 December 1989, and 1700 UTC, 25 December 1989). The site was located within a gently sloping valley about 3.5 km wide, flanked by low ridges along either side where the SCS profiles showed continuous reflectors with little or no disturbance.

Coring Results

We spent 6.17 days on this site, drilling three holes and coring 1135 m of sediment, of which 993 m were recovered. Hole 805A, a dedicated hole, was cored with the APC to 50.5 mbsf into upper Pliocene sediments, with 103% recovery. Hole 805B was cored with the APC to 263.2 mbsf, where refusal occurred, at the boundary between upper and middle Miocene sediments; recovery was 103%. The hole was continued with XCB coring to 473.3 mbsf, with 210.1 m of sediment cored and 173.6 m recovered (83% recovery). Coring ended about half-way through a thick section of lower Miocene sediments. Hole 805C was cored with the APC to 235.8 mbsf (100% recovery), at which point XCB coring was initiated. Drilling ended in upper Oligocene sediments at 611.0 mbsf, with 259.1 m cored with the XCB (69% recovery). The hole was then logged.

The sediment retrieved is Neogene in age, except for the nine deepest cores in Hole 805C, which recovered Oligocene chalk. The entire column, from the earliest deposits to the seafloor, was considered to be one lithologic unit and was classified as nannofossil and foraminifer nannofossil ooze and chalk. The average sedimentation rate over the entire interval is ~20 m/m.y. No stratigraphic breaks were detected. However, sedimentation rates fell to rather low values (almost 10 m/m.y.).

Two subunits were recognized in this quite uniform section of bioturbated ooze and chalk. They are separated by the ooze-chalk transition at 282.5 mbsf in Hole 805B (base of Core 130-805B-30X) and at 293.7 mbsf in Hole 805C (base of Core 130-805C-31X) (upper middle Miocene, ca. 11.4 Ma). The transition is gradational and shows alternating layers with varying degrees of lithification.

The younger section of the unit (Subunit IA, 0–293.7 mbsf) comprises Pleistocene to middle Miocene nannofossil ooze, nannofossil ooze with foraminifers, and foraminifer nannofossil ooze. Radiolarian content was low on the whole. The oozes are light gray in the top 30 mbsf, grading into white ooze. Color banding is common throughout the unit and is especially well expressed in the uppermost Miocene. For the most part, color bands are coarse and irregular in Subunit IA. Some large burrows have well-developed concentric color rings ("Liesegang rings"), indicating redox gradients as the cause for color banding. Microfaulting was observed in Core 130-805B-18H at 166 mbsf (middle upper Miocene), and color band tilting was seen at the middle/upper Miocene boundary.

Sediments are generally soft, but in the lowermost portion of Subunit IA (283–293 mbsf) more lithified intervals appear. A shift toward higher velocities occurred near the top of that zone, and another at the ooze-chalk transition at about 294 mbsf.

The older section of the unit, Subunit IB (293.7–611 mbsf), consists of approximately 317 m of nannofossil chalk, nannofossil chalk with foraminifers, and foraminifer nannofossil chalk of middle Miocene to late Oligocene age. The color is dominantly white. Color banding occurs throughout but becomes rare below 504 mbsf in the lowermost Miocene. It includes bundles of pseudolaminae, that is, fine-scale Liesegang banding, that show sharp individual boundaries. Microfaulting is gener-

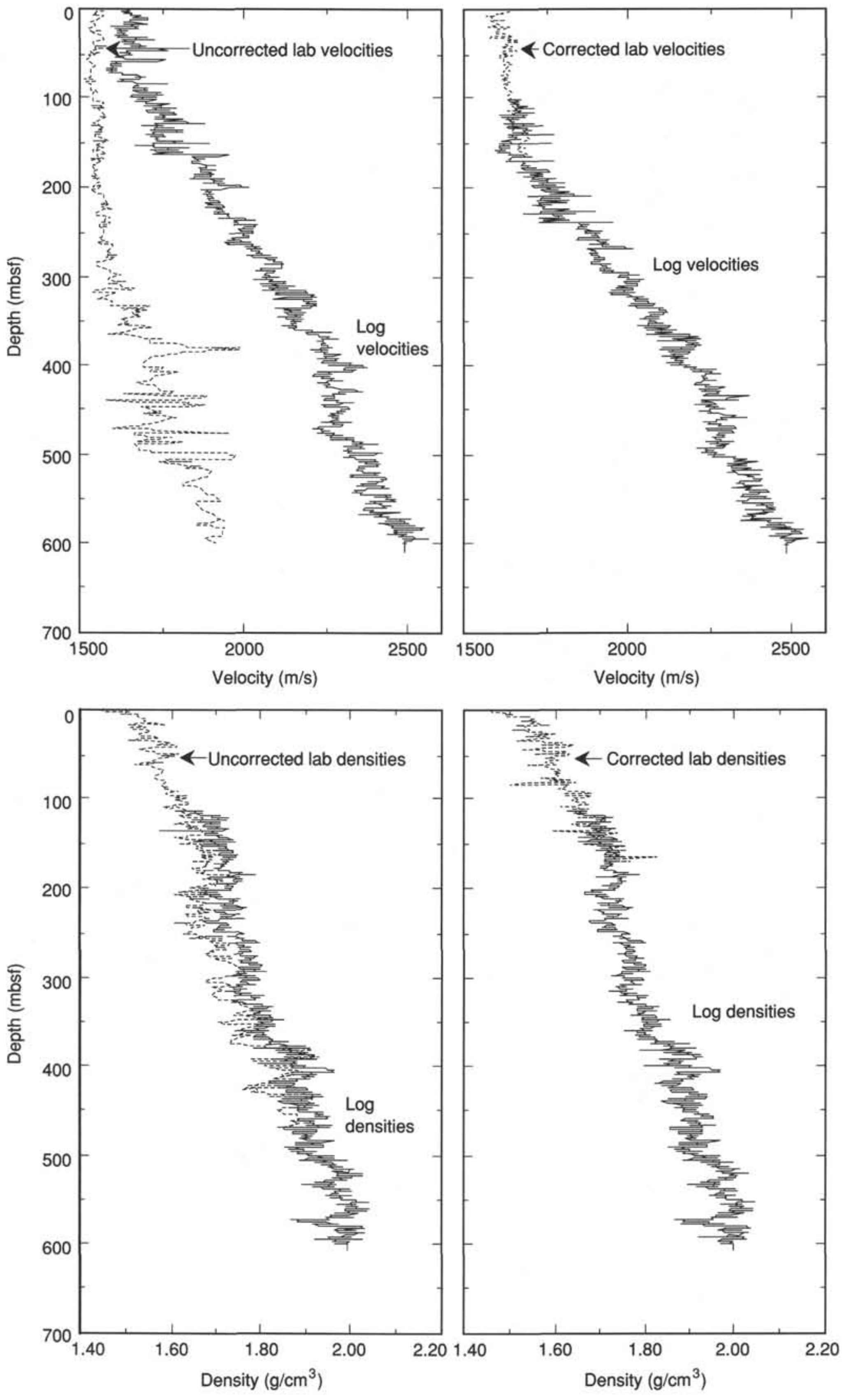

Figure 38. Comparison of velocity and density logs with uncorrected and corrected laboratory measurements, Hole 805C. Dashed line represents laboratory measurements. Comparison of velocity log with corrected laboratory velocity measurements.

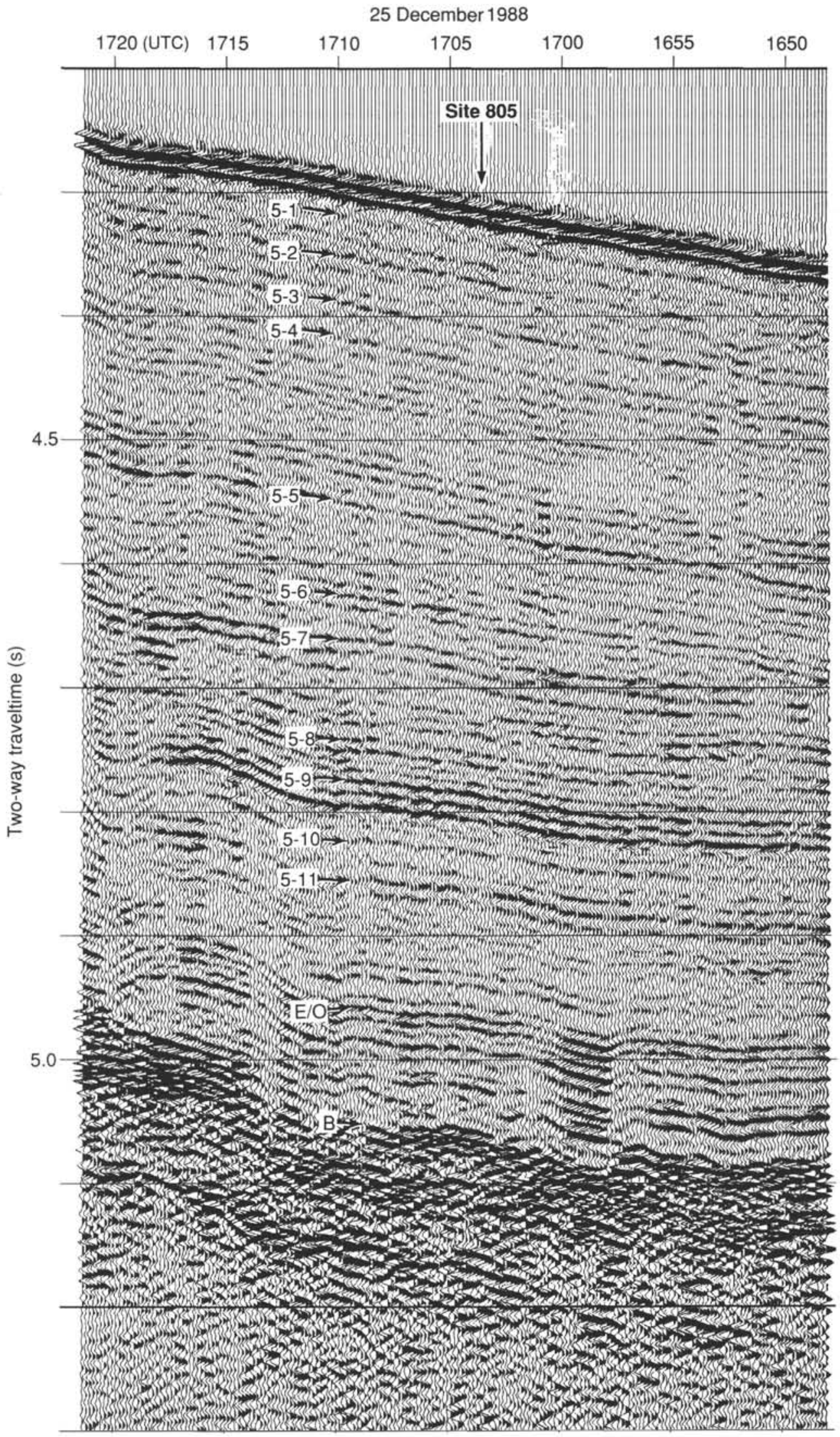

Figure 39. Seismic record collected on ROUNDABOUT Cruise 11 site survey over Site 805 using the 80-in.^{3} water gun, 70–250 Hz band-pass filter. For details of reflectors, see Table 14.

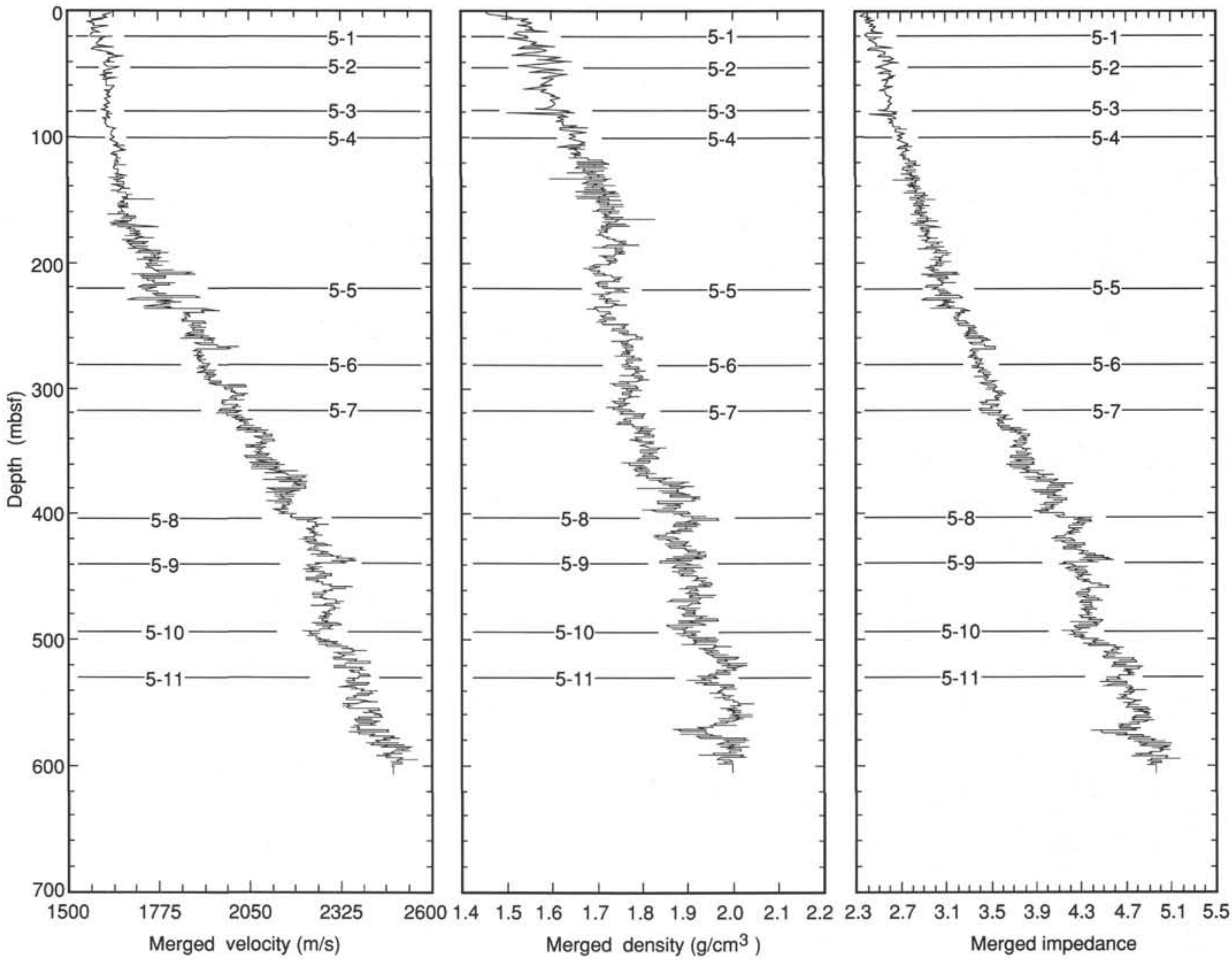

Figure 40. Velocity, density, and acoustic impedance used for generating Site 805 synthetic seismogram.

ally absent, except at ~310 mbsf (ca. 12 Ma), near the top of the subunit.

Recovery in the chalk subunit was good down into lower Miocene sediments. Here it dropped noticeably below 450 mbsf (Core 130-805C-47X) and became quite poor below 520 mbsf (Core 130-805C-55X) near the Oligocene/Miocene boundary. Even where recovery is very good, core contents are largely disjointed chunks and chips, with evidence for grinding of chalk on chalk. This type of recovery is typical for the material below 370 mbsf. The Oligocene/Miocene boundary was located near 525 mbsf and apparently is without hiatus. Sedimentation rates for the deep chalk section are typically between 7 and 30 m/m.y., with the lower rates occurring in the Oligocene and the higher ones in the lower middle Miocene.

Special Studies

Magnetostratigraphy was produced for the uppermost section of Holes 805B and 805C. Only the Brunhes Chron and part of the Matuyama could be identified. The sedimentation rate since 1.7 Ma was determined to be 17.1 m/m.y.

Chemical gradients in the interstitial waters at this site are generally similar to those at Sites 803 and 804, reflecting the calcareous/siliceous nature of the sediments and the paucity of organic material. A somewhat higher supply of organic matter at this shallower site, perhaps a result of the shallower depth, tends to produce slightly stronger gradients. Calcium and magnesium gradients are influenced by basalt alteration reactions at depth and show the usual negative correlation. Strontium concentrations reflect recrystallization processes, which take place in younger sediments at this site than at the other two because of the higher sedimentation rates. Dissolved silica shows a steady increase with depth, except for a minor reversal of this trend just above the ooze-chalk transition.

Seismic Stratigraphy

Site 805 was the first of the Leg 130 sites to deliver a complete stratigraphic record without hiatuses. It is, therefore, of great interest with respect to a central objective of the leg: to determine the nature of the acoustic reflectors seen on seismic profiles. Guidance in attempting this was provided by the velocity and density profiles recovered during logging and by the age controls determined during biostratigraphic analyses.

A great number of reflectors were observed in the profile taken by the *Thomas Washington* during the ROUNDABOUT pre-site survey (Fig. 43). Depth assignment and dating shows that at least some of the reflectors are associated with pale-

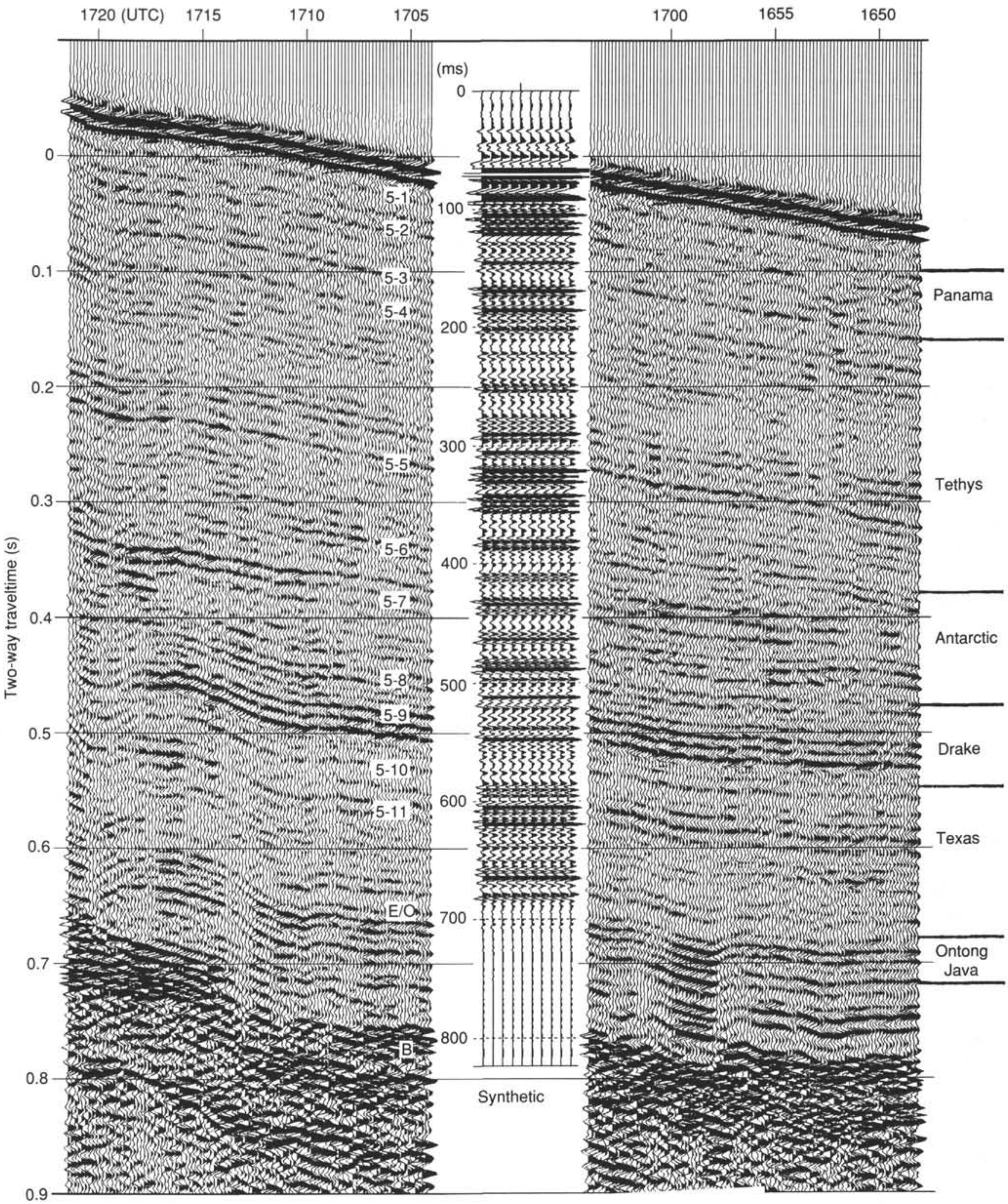

Figure 41. Comparison of synthetic seismogram and field records, Site 805. For details of reflectors (5-1, 5-2, etc.), see Table 14. E/O = Eocene/Oligocene boundary and B = basement. Names to the right refer to distinct groups of reflectors. See text for details.

Table 14. Summary of traveltimes, depths, and ages for Site 805 reflectors.

	Traveltime		Depth		
Reflector	Seismic (s)	Synthetic (s)	Seismic (m)	Synthetic (m)	Age (Ma)
5-1	0.027	0.025	21	20	1.2
5-2	0.060	0.057	48	45	2.4–2.5
5-3	0.100	0.100	80	80	3.7
5-4	0.124	0.124	101	101	4.4–4.5
5-5	0.260	0.267	215	221	7.1–7.36
5-6	0.328	0.332	278	281	10.3–10.6
5-7	0.367	0.368	317	319	12.8–12.9
5-8	0.442	0.449	396	403	19.0–19.9
5-9	0.479	0.482	436	440	21.2–21.3
5-10	0.522	0.530	486	495	22.6–22.9
5-11	0.559	0.561	528	531	23.7–23.9

Notes: Depths and traveltimes to seismic events are picked on both the synthetic seismogram (synthetic) and the field record (seismic). Ages are from sedimentation rate curves (see "Sedimentation Rates" section, this chapter).

oceanographic events, as suggested by Mayer et al. (1986) for the central equatorial Pacific. They proposed the closing of the Panama Isthmus, reorganization of deep circulation in the Atlantic, climatic events surrounding the Antarctic, and the opening of Drake Passage as important paleoceanographic themes reflected in the acoustic properties of Pacific pelagic sediments. Accordingly (but without prejudging the question about origins), we refer to reflectors aged 2–4 Ma as "Panama Series," to those aged 10–19 Ma as "Antarctic Series," and to those aged 19–23 Ma as "Drake Series." These ages are approximate; the criterion is grouping, not dating. The advantage of considering groups of reflectors in addition to single members is that the variability of properties within a given section is being addressed, rather than only an individual excursion of velocity and/or density within the sediment profile.

The interval between the Panama and the Drake reflectors is the "Tethys Interval," which contains sediments deposited during mountain building in the closing Tethys Belt. Below the Drake Series is an acoustically quiet zone, the "Texas Interval," named in appreciation of Texan know-how in deep-sea drilling, which saved enough time in a crowded schedule to allow entering this zone on several occasions during Leg 130. Below the Texas Interval is the "Ontong Java Series," a group of strong re-

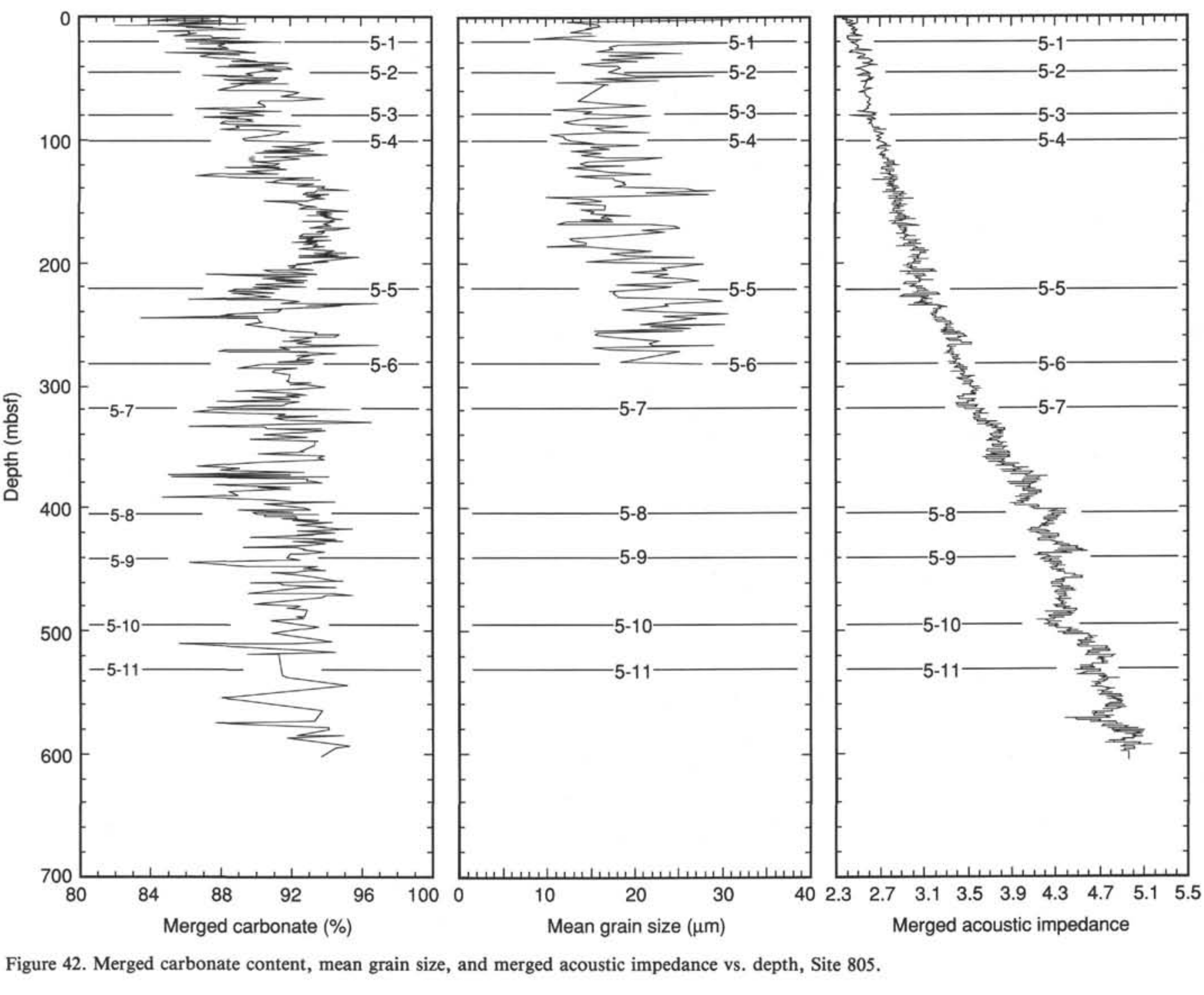

Figure 42. Merged carbonate content, mean grain size, and merged acoustic impedance vs. depth, Site 805.

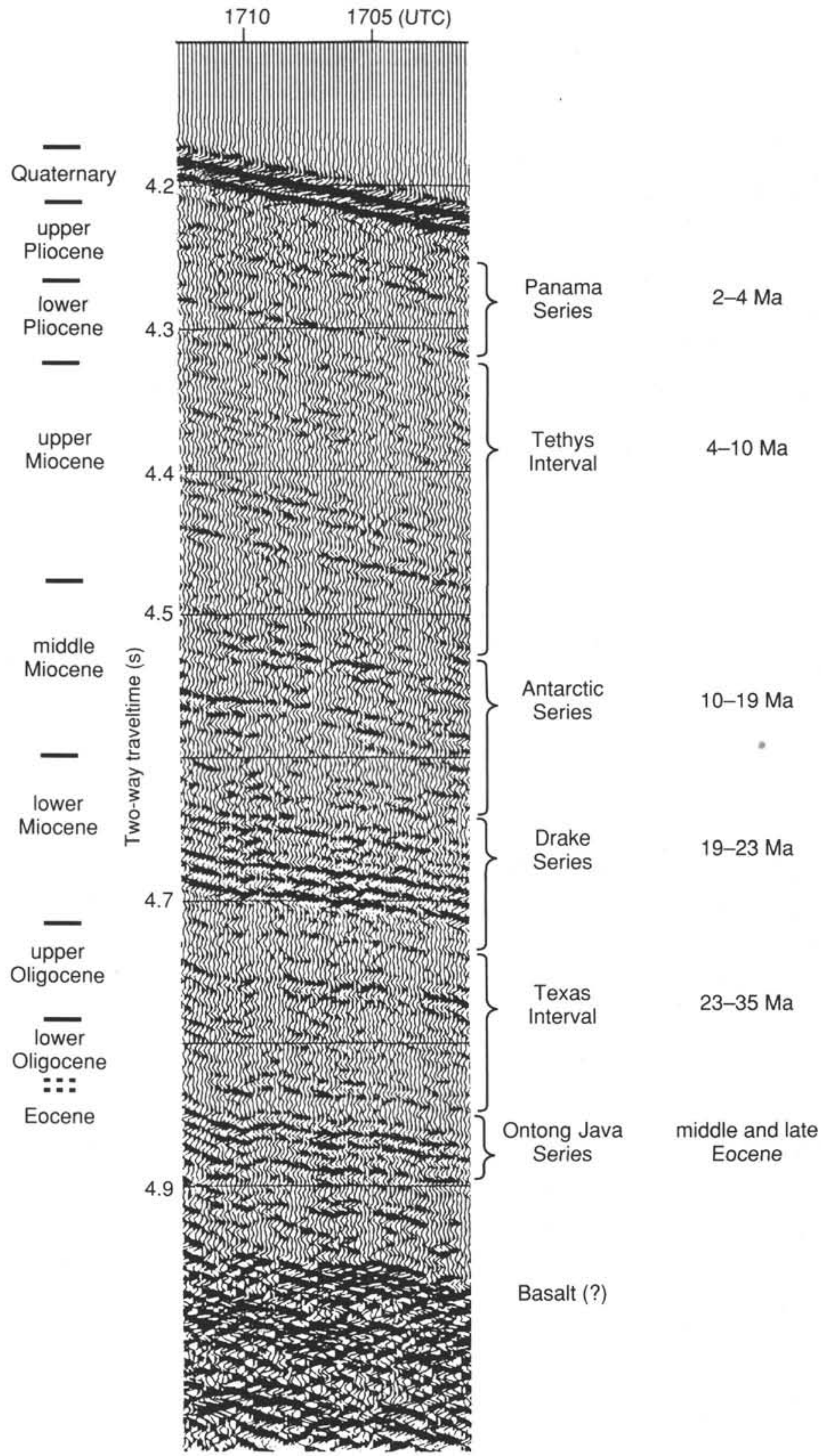

Figure 43. Seismic profile at Site 805, taken on 25 December 1989 on the *Thomas Washington* ROUNDABOUT Cruise 11 (see "Seismic Stratigraphy" section, this chapter), with time scale assigned from drilling and logging results. Names to the right refer to distinct groups of reflectors ("series") and to zones with no distinct groups of reflectors ("intervals"). Three of the names are taken from suggestions by Mayer et al. (1986) regarding the origin of such reflectors (Panama, Antarctic, and Drake Passage). Although these hypotheses are appealing, our use of these names does not imply that we consider them proved. For "Tethys" and "Texas" intervals, see text. Numbers to the left refer to two-way traveltime. Numbers at top refer to time of day.

flectors, ubiquitous on the plateau, that are derived from impedance changes caused by limestone and chert formation.

The Panama Series contains reflectors dated near 2, 2.4, and 3.7 Ma. The age of 2.4 Ma corresponds to a deep-water cooling event and the onset of North Atlantic ice buildup (Backman, 1979; Shackleton et al., 1984). Reflectors dated at 2.4 and 3.7 Ma can be identified in the seismic record across DSDP Site 586 (near Site 289) using the velocity profile obtained from logging that site (Shipboard Scientific Party, 1986a). The Tethys Interval (Fig. 43) contains a number of lesser reflectors, one of which apparently corresponds to lithification (near 210 m, age 7 Ma). The presumed condensed section just below 10 Ma (see "Sedimentation Rate" section, this chapter) has a less than prominent group of reflectors at the base of the Tethys Interval (270–290 mbsf). Also, the ooze-chalk transition does not seem to be strongly expressed, although it is possible to find reflecting horizons in the vicinity of 290 mbsf.

The next group of strong reflectors, going downsection in Figure 43, is the upper part of the Antarctic Series, in the middle of the middle Miocene (13 Ma). It starts with a distinct reflector between 310 and 320 mbsf (dated 12.5–13 Ma). The lower part of this series is somewhat weaker and belongs to the lowermost middle Miocene and uppermost lower Miocene (360–385 mbsf, 15–18 Ma). This entire zone is characterized by a major climatic change and associated excursions in carbonate content and other sediment properties (Barron et al., 1985). These changes, presumably, are associated with the onset of Antarctic Bottom Water production at that time. The group of reflectors immediately below the Antarctic Series, the Drake Series, has the strongest reflector members. Ages range from about 18.5 Ma for the uppermost members of the group (390 mbsf) to 22 Ma for the deepest (460 mbsf).

Below this group there is a thick section, the Texas Interval (up to 180 m thick), which is more or less transparent acoustically. The reason for this is the absence of abrupt changes in sediment properties within the Oligocene. This period was also noted by the biostratigraphers for the paucity of evolutionary events. One lone reflector (Fig. 43; 520–530 mbsf, ca. 23.6 Ma) appears to mark the Oligocene/Miocene boundary. Below this interval, there is a group of strong reflectors, the Ontong Java Series, the top of which is thought to represent the change from chalk to limestone in the lowermost Oligocene and upper Eocene, especially the occurrence of chert in the middle Eocene. The thickness of this acoustic unit is on the order of 100 m. Another 50 m or so down, acoustic basement is reached, which probably consists of basalt or perhaps of chert and limestone.

In summary, the results of Site 805 support, in a general way, the hypothesis that many reflectors represent the effects of global paleoceanographic events and can be correlated across the tropical Pacific. Other reflectors, however, may be regionally strong expressions of minor events or may be related to diagenetic processes that are not synchronous.

Sedimentation Rates

The oldest sediments cored, at 611 mbsf in Hole 805C, were of latest early Oligocene age (Zone NP23). The distance to acoustic basement below this level may be estimated as approximately 0.15-s two-way traveltime, which corresponds to roughly 190 m of sediment at that depth. If this is all the sediment there is, considerable hiatus formation in the lower Paleogene and Cretaceous would seem to be indicated, assuming that the uncored section represents at least 80 m.y. of time.

Since early Oligocene time, Site 805 has received nannofossil ooze, with rather minor admixtures of siliceous fossils. Sedimentation rates typically varied between 12 m/m.y. (middle and upper Miocene) and almost 40 m/m.y. (upper Pliocene), the overall average being near 20 m/m.y. Two condensed sections may be present, based on nannofossils and foraminifers (see "Biostratigraphy" section, this chapter): one between 10 and 9 Ma (lowermost upper Miocene), and the other centered on 17.5 Ma (uppermost lower Miocene). Both these periods are characterized by strong carbonate dissolution events in the central Pacific (Barron et al., 1985); the younger one is commonly a time of hiatus formation (NH4 of Keller and Barron, 1983).

Comparisons with Sites 289, 803, and 804

The lithology of Site 805 was the same as that of the comparison sites. The carbonate content at Site 805 typically reached values above 90% throughout the section except in the Pleistocene portion and at the upper and lower boundaries of the middle Miocene. In the Pliocene values hover around 90%. The carbonate stratigraphy of Site 803 is quite similar in long-term trends as well as in some of the details. Site 804 also has similar trends, although they are disturbed there by hiatus formation. On the whole, percentages in Site 804 are between 5% and 10% lower, and fluctuate more strongly, than in Site 805.

Mean grain size is typically between 12 and 25 μm at Site 805, with maxima near the Pleistocene/Pliocene boundary and in the uppermost and lowermost upper Miocene. Minima occur in the middle of the lower Pliocene and in the upper half of the upper Miocene. No measurements are available for pre-mid-Miocene sediments. Patterns are quite different for Sites 803 and 804. Site 803 has distinctly higher values in post-Miocene time, despite its greater depth and lower sedimentation rate. Dissolution should decrease sand content there (Johnson et al., 1977), so differences in local winnowing, or in the rate of receiving fines from upslope, may be indicated. In the upper Miocene the situation is reversed: Site 805 has the coarser sediments. This is as expected if dissolution effects dominate. Site 804 has mean grain sizes that are quite comparable with those of Site 805, except for a pronounced coarsening in the section surrounding the hiatus in the lower Pliocene.

Smear slide abundance patterns of the major fossil groups—nannofossils, foraminifers, and radiolarians—are quite similar between Sites 803 and 805. To establish differences, a more quantitative analysis than has been done on board will be necessary. For Site 804, the abundance patterns are quite different, presumably because of carbonate dissolution and hiatus formation at that site. At DSDP Site 289, foraminifers are much more abundant than at Site 805 (Shipboard Scientific Party, 1975b). Several processes must be considered: increased winnowing at Site 289 (2200 m), and the destruction of tests and the delivery of upslope fines at the depth of Site 805 (3200 m). Radiolarian content is low throughout Unit 1 of Site 289.

The ooze-chalk transition was located at 290 mbsf (ca. 11–11.5 Ma) in Site 805. It is deeper and younger here than at Site 803 (217 mbsf, ca. 14–14.5 Ma), but shallower than its location in Site 289 although roughly synchronous with it (350 mbsf, ca. 11.5 Ma). Thus, the comparison of Site 805 with Site 289 supports the hypothesis of Schlanger and Douglas (1974) that age (i.e., conditioning during deposition) is an important parameter in the rate of lithification; the comparison with Site 803 does not. It appears that a distinctly increased overburden may accelerate the process of lithification but not all that much.

Rates of accumulation are about 10%–30% lower in Site 805 than in Site 289, on the whole, in keeping with the greater depth of Site 805. The rates are distinctly higher than in Site 803 by a factor of between 1.2 (upper Miocene) and 1.9 (lower Pliocene and middle and lower Miocene). For Pleistocene sediments, rates are unusually low at all three sites (289, 803, and 805). Also, for this period, the sedimentation rate of Site 805 actually exceeds that of Site 289. This suggests strong winnowing during this period, with downslope transport of fine material presumably mitigating the winnowing effect at Site 805.

REFERENCES

Backman, J., 1979. Pliocene biostratigraphy of DSDP Sites 111 and 116 from the North Atlantic Ocean and the age of the Northern Hemisphere Glaciation. *Stockholm Contrib. Geol.,* 32:115–137.

Barron, J. A., and Keller, G., 1982. Widespread Miocene deep-sea hiatuses: coincidence with periods of global cooling. *Geology,* 10:577–581.

Barron, J. A., Keller, G., and Dunn, D. A., 1985. A multiple microfossil biochronology for the Miocene. *In* Kennett, J. P. (Ed.), *The Miocene Ocean: Paleoceanography and Biogeography.* Mem. Geol. Soc. Am., 163:21–36.

Berger, W. H., 1976. Biogenous deep sea sediments: production, preservation, and interpretation. *In* Riley, J. P., and Chester, R. (Eds.), *Chemical Oceanography* (Vol. 5): New York (Academic Press), 265–328.

Berger, W. H., and Johnson, T. C., 1976. Deep-sea carbonates: dissolution and mass wasting on Ontong Java Plateau. *Science,* 192:785–787.

Berger, W. H., Johnson, T. C., and Hamilton, E. L., 1977. Sedimentation on Ontong-Java Plateau: observations on a classic "carbonate monitor." *In* Anderson, N. R., and Malahoff, A. (Eds.), *The Fate of Fossil Fuel CO_2 in the Oceans:* New York (Plenum Press), 543–567.

Berger, W. H., and Mayer, L. A., 1978. Deep-sea carbonates: acoustic reflectors and lysocline fluctuations. *Geology,* 6:11–15.

Berggren, W. A., Kent, D. V., Flynn, J. J., and Van Couvering, J. A., 1985. Cenozoic geochronology. *Geol. Soc. Am. Bull.,* 96:1407–1418.

Emeis, K.-C., and Kvenvolden, K. A., 1986. Shipboard organic geochemistry on *JOIDES Resolution. ODP Tech. Note,* No. 7.

Espitalié, J., Laporte, J. L., Madec, M., Marquis, F., Leplat, P., Paulet, J., and Boutfeu, A., 1977. Method rapide de caracterisation des roches mère de leur potentiel petrolier et de leur degree d'evolution. *Rev. Inst. Fr. Pet.,* 32:23–42.

Gieskes, J. M., 1981. Deep-sea drilling interstitial water studies: implications for chemical alteration of the oceanic crust, layers I and II. *In* Warme, J. E., Douglas, R. G., and Winterer, E. L. (Eds.), *The Deep Sea Drilling Project: A Decade of Progress.* Spec. Publ., Soc. Econ. Paleontol. Mineral., 32:149–167.

Hay, W. W., 1970. Calcareous nannofossils from cores recovered on DSDP Leg 4. *In* Bader, R. G., Gerard, R. D., et al., *Init. Repts. DSDP,* 4: Washington (U.S. Govt. Printing Office), 455–501.

Hermelin, J.O.R., 1989. Pliocene benthic foraminifera from the Ontong Java Plateau (western equatorial Pacific Ocean): faunal response to changing paleoenvironment. *Spec. Publ., Cushman Found. Foraminiferal Res.,* 26:1–143.

Hussong, D. M., Wipperman, L. K., and Kroenke, L. W., 1979. The crustal structure of the Ontong Java and Manihiki oceanic plateaus. *J. Geophys. Res.,* 84:6003–6010.

Jacobs, J. A., 1984. *Reversals of the Earth's Magnetic Field:* Bristol (Adam Hilger).

Johnson, T. C., Hamilton, E. L., and Berger, W. H., 1977. Physical properties of calcareous ooze: control by dissolution at depth. *Mar. Geol.,* 24:259–277.

Keller, G., and Barron, J. A., 1983. Paleoceanographic implications of Miocene deep-sea hiatuses. *Geol. Soc. Am. Bull.,* 94:590–613.

Kroenke, L., 1972. Geology of the Ontong Java Plateau [Ph.D. dissert.]. Univ. of Hawaii.

Mammerickx, J., and Smith, S. M., 1985. *Bathymetry of the North Central Pacific:* Boulder, CO (Geological Society of America), Map and Chart Ser., No. MC-52.

Mankinen, E. A., Donnelly, J. M., and Grommé, C. S., 1978. Geomagnetic polarity event recorded at 1.1. m.y.r. B.P. on Cobb mountain, Clear Lake volcanic field, California. *Geology,* 6:653–656.

Mayer, L. A., Shipley, T. S, Theyer, F., Wilkens, R. W., and Winterer, E. L., 1985. Seismic modelling and paleoceanography at DSDP Site 574. *In* Mayer, L. A., Theyer, F., Thomas, E., et al., *Init. Repts. DSDP,* 85: Washington (U.S. Govt. Printing Office), 947–970.

Mayer, L. A., Shipley, T. H., and Winterer, E. L., 1986. Equatorial Pacific seismic reflectors as indicators of global oceanographic events. *Science,* 233:761–764.

McDuff, R. E., 1981. Major cation gradients in DSDP interstitial waters: the role of diffusive exchange between seawater and upper ocean crust. *Geochim. Cosmochim. Acta,* 45:1705–1713.

McDuff, R. E., and Gieskes, J. M., 1976. Calcium and magnesium profiles in DSDP interstitial waters: diffusion or reaction? *Earth Planet. Sci. Lett.,* 33:1–10.

Peterson, L. C., and Backman, J., 1990. Late Cenozoic carbonate accumulation and the history of the carbonate compensation depth in the western equatorial Indian Ocean. *In* Backman, J., Duncan, R. A., Peterson, L. C., et al., *Proc. ODP, Sci. Results,* 115: College Station, TX (Ocean Drilling Program), 467–507.

Resig, J. M., 1989. Stratigraphic distribution of late Neogene species of the planktonic foraminifer *Streptochilus* in the Indo-Pacific. *Micropaleontology,* 35:49–62.

Sanfilippo, A., Westberg-Smith, M. J., and Riedel, W. R., 1985. Cenozoic radiolaria. *In* Bolli, H. M., Saunders, J. B., and Perch-Nielsen, K. (Eds.), *Plankton Stratigraphy:* Cambridge (Cambridge Univ. Press), 631–712.

Schlanger, S. O., and Douglas, R. G., 1974. The pelagic ooze-chalk-limestone transition and its implication for marine stratigraphy. *In* Hsü, K. J., and Jenkyns, H. C. (Eds.), *Pelagic Sediments: On Land and Under the Sea.* Spec. Publ., Int. Assoc. Sedimentol., 1:117–148.

Shackleton, N. J., Backman, J., Zimmerman, H., Kent, D. V., Hall, M. A., Roberts, D. G., Schnitker, D., Baldauf, J., Desprairies, A., Homrighausen, R., Huddlestun, P., Keene, J. B., Kaltenback, A. J., Krumsiek, K.A.O., Morton, A. C., Murray, J. W., and Westberg-Smith, J., 1984. Oxygen isotope calibration of the onset of ice-rafting in DSDP Site 552A: history of glaciation in the North Atlantic region. *Nature,* 307:620–623.

Shackleton, N. J., and Opdyke, N. D., 1976. Oxygen-isotope and paleomagnetic stratigraphy of Pacific Core V28-239: late Pliocene to latest Pleistocene. *In* Cline, R. M., and Hays, J. D. (Eds.), *Investigations of Late Quaternary Paleoceanography and Paleoclimatology.* Mem. Geol. Soc. Am., 145:449–464.

Shipboard Scientific Party, 1971. Site 64. *In* Winterer, E. L., Riedel, W. R., et al., *Init. Repts. DSDP,* 7: Washington (U.S. Govt. Printing Office), 473–606.

Shipboard Scientific Party, 1975a. Site 288. *In* Andrews, J. E., Packham, G., et al., *Init. Repts. DSDP,* 30: Washington (U.S. Govt. Printing Office), 175–229.

Shipboard Scientific Party, 1975b. Site 289. *In* Andrews, J. E., Packham, G., et al., *Init. Repts. DSDP,* 30: Washington (U.S. Govt. Printing Office), 231–398.

Shipboard Scientific Party, 1986a. Site 586. *In* Moberly, R., Schlanger, S. O., et al., *Init. Repts. DSDP,* 89: Washington (U.S. Govt. Printing Office): 213–235.

Shipboard Scientific Party, 1986b. Site 586: western equatorial Pacific. *In* Kennett, J. P., von der Borch, C. C., et al., *Init. Repts DSDP,* 90: Washington (U.S. Govt. Printing Office), 19–114.

Wise, S. W., Jr., 1973. Calcareous nannofossils from cores recovered during Leg 18, Deep Sea Drilling Project: biostratigraphy and observations of diagenesis. *In* Kulm, L. D., von Huene, R., et al., *Init. Repts. DSDP,* 18: Washington (U.S. Govt. Printing Office), 569–615.

Wu, G., and Berger, W. H., 1989. Planktonic foraminifera: differential dissolution and the Quaternary stable isotope record in the west-equatorial Pacific. *Paleoceanography,* 4:181–198.

Ms 130A-107

NOTE: All core description forms ("barrel sheets") and core photographs have been printed on coated paper and bound as Section 5, near the back of the book, beginning on page 559.

Hole 805C: Resistivity-Sonic-Gamma Ray Log Summary

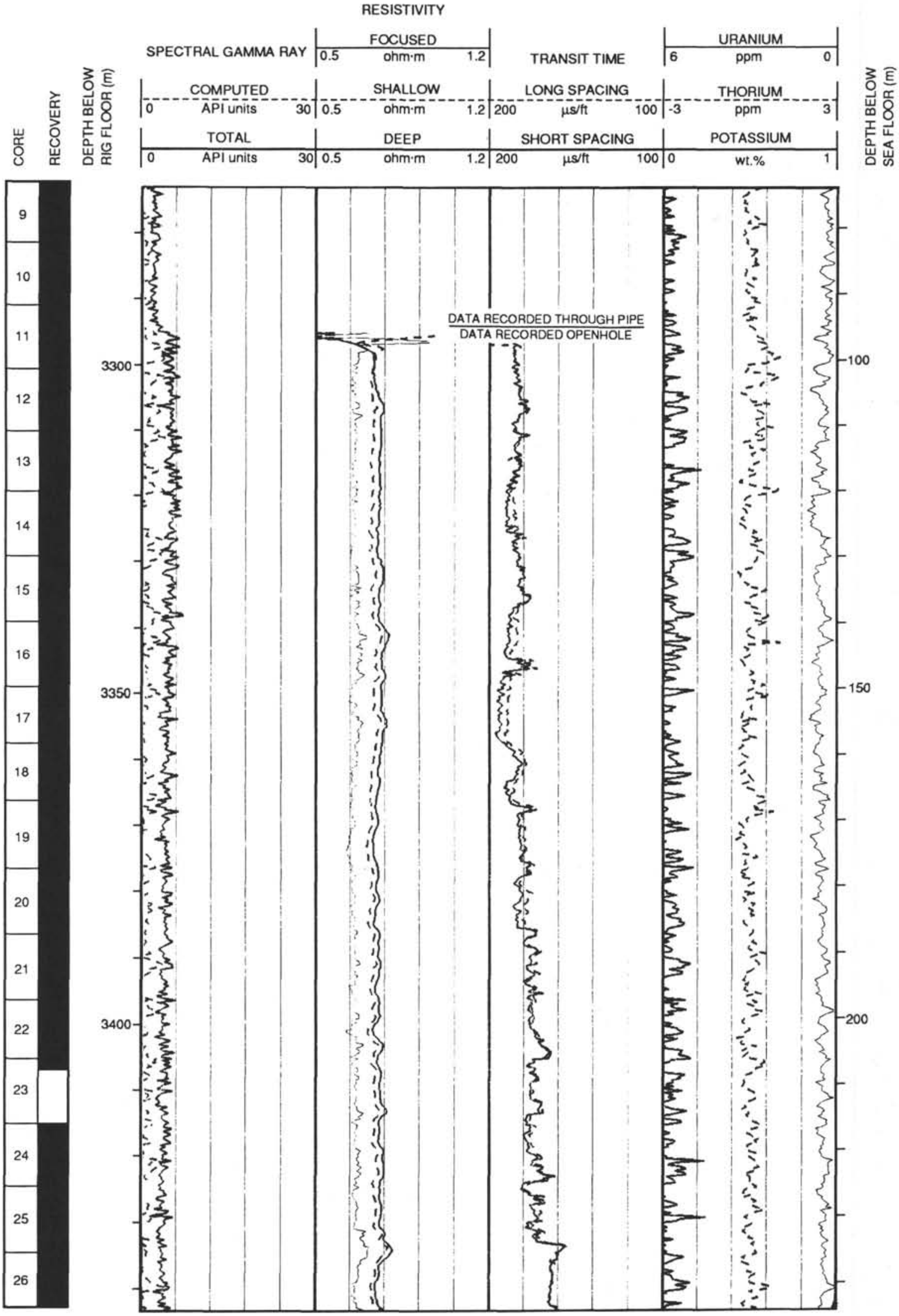

Hole 805C: Resistivity-Sonic-Gamma Ray Log Summary (continued)

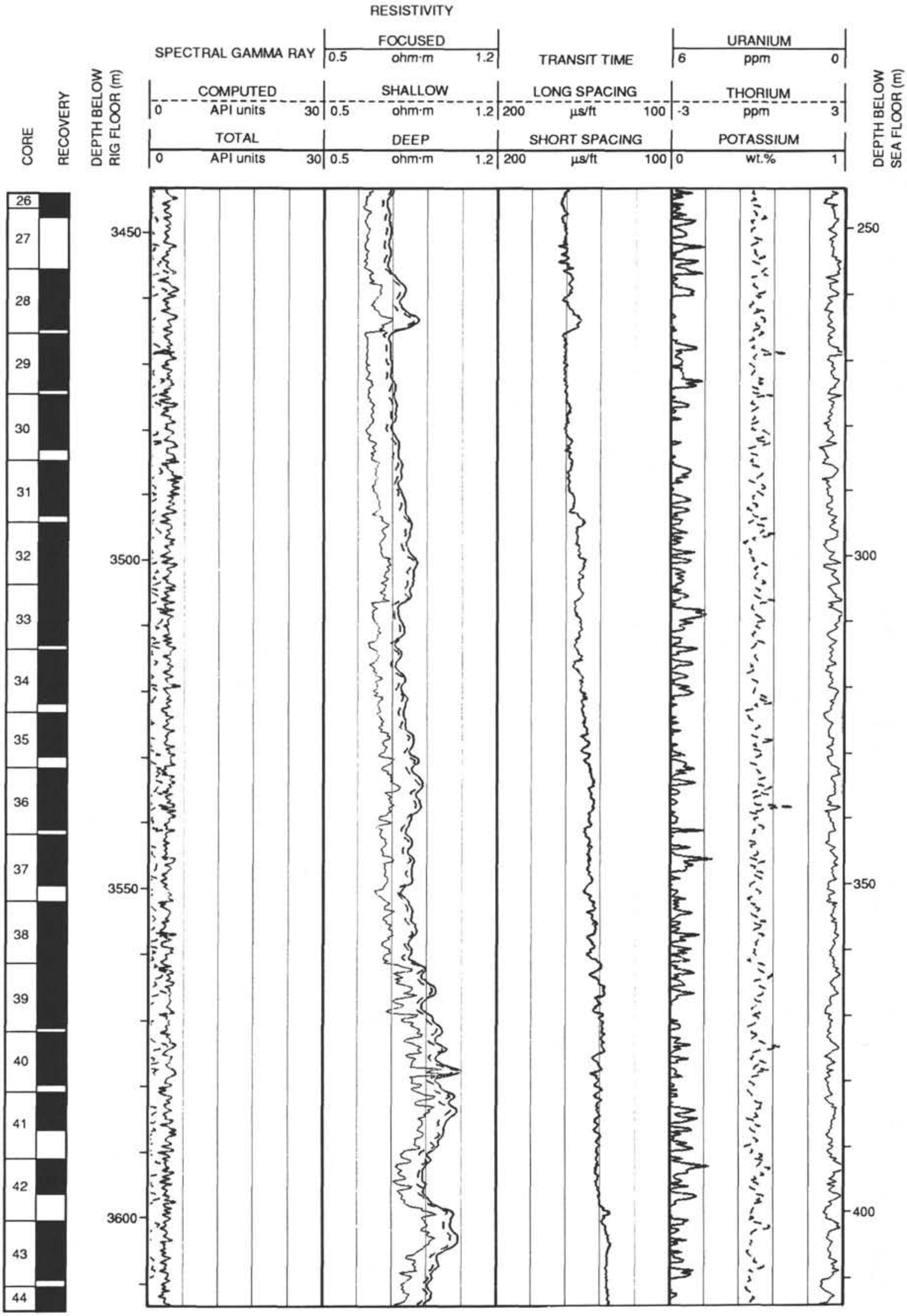

Hole 805C: Resistivity-Sonic-Gamma Ray Log Summary (continued)

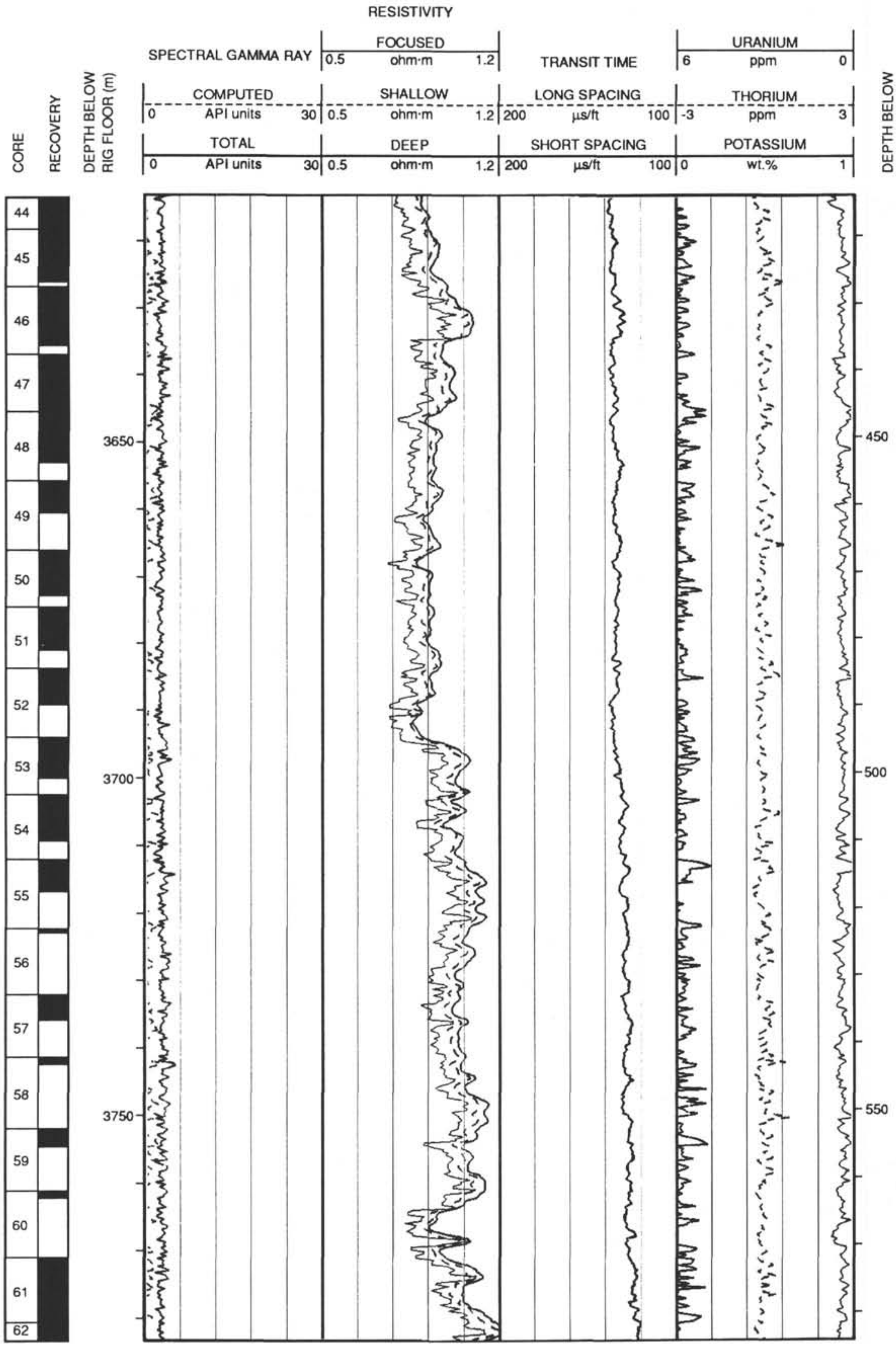

Hole 805C: Resistivity-Sonic-Gamma Ray Log Summary (continued)

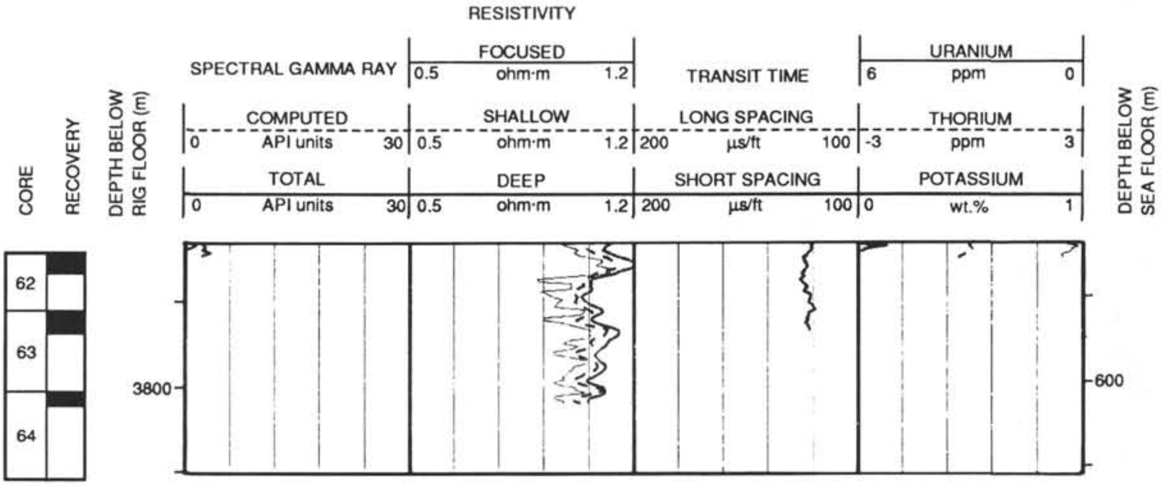

Hole 805C: Density-Gamma Ray Log Summary

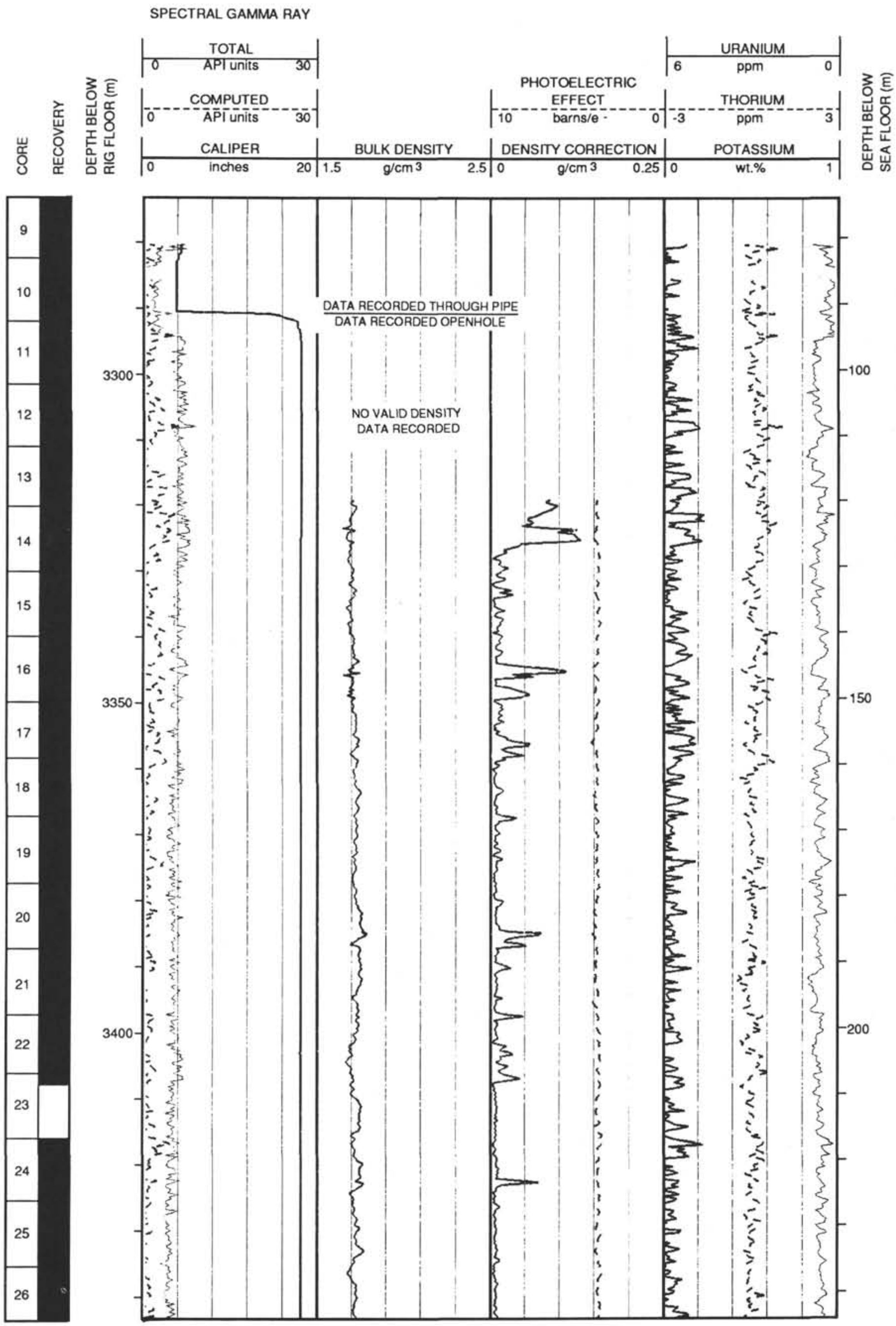

Hole 805C: Density-Gamma Ray Log Summary (continued)

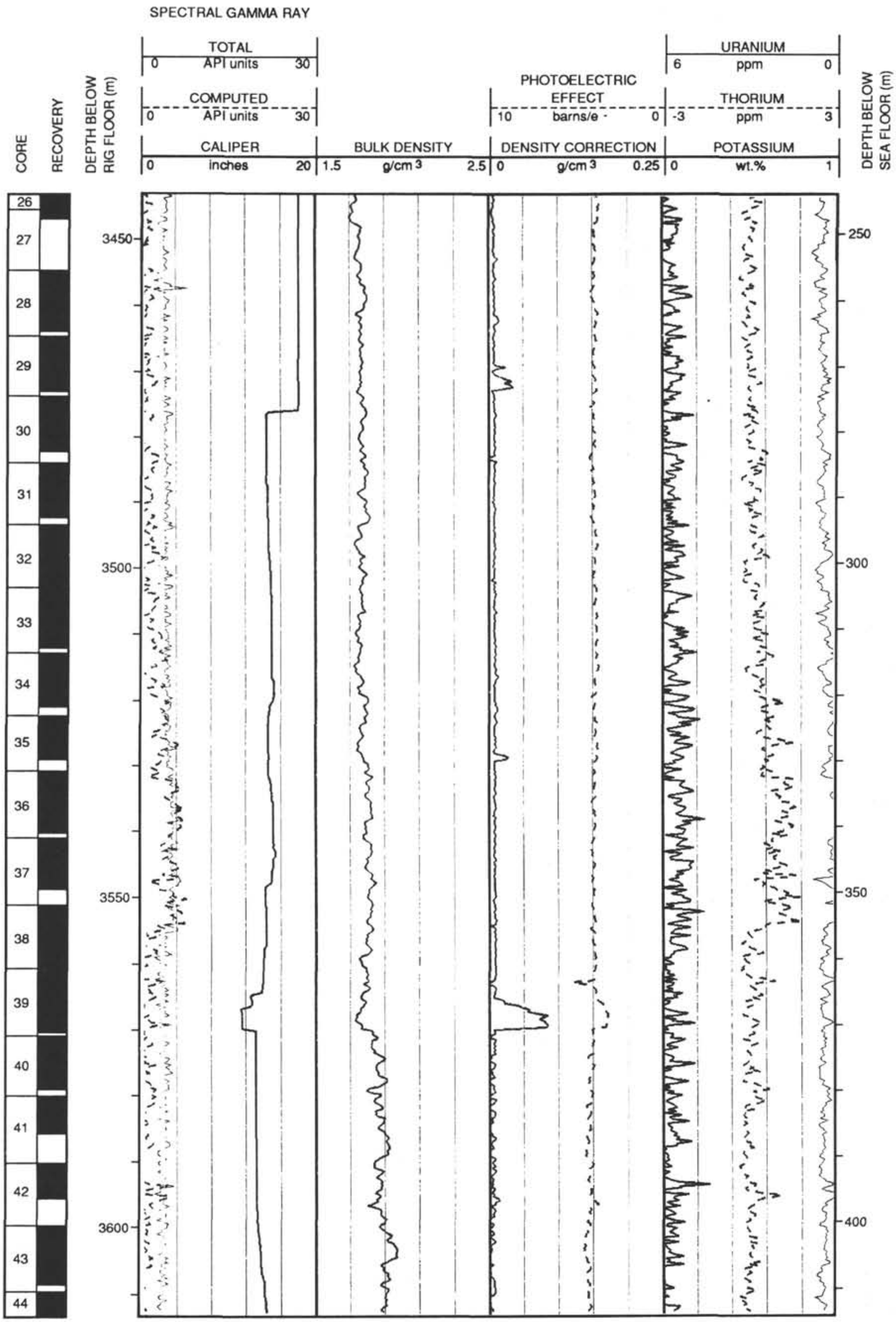

Hole 805C: Density-Gamma Ray Log Summary (continued)

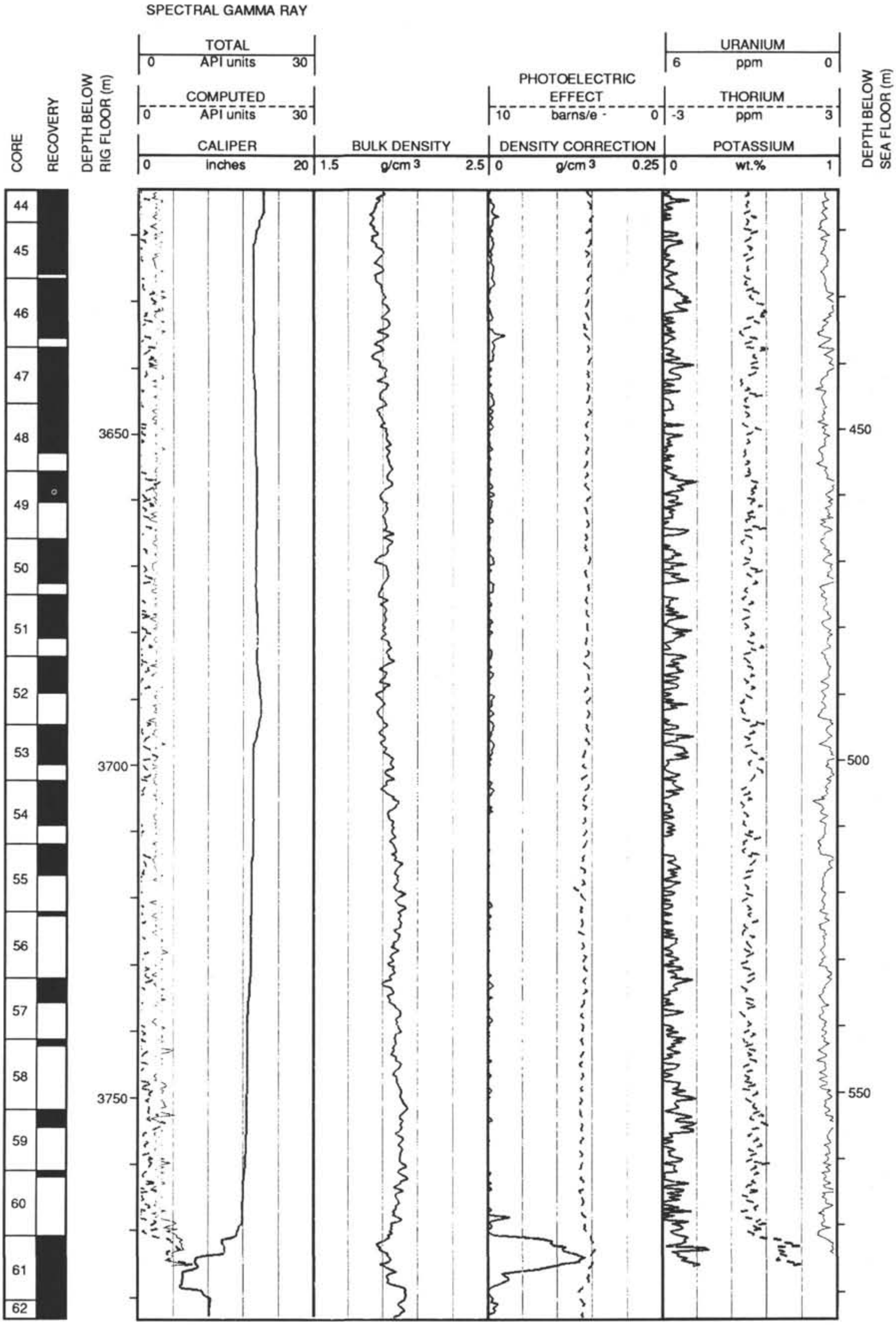

Hole 805C: Density-Gamma Ray Log Summary (continued)

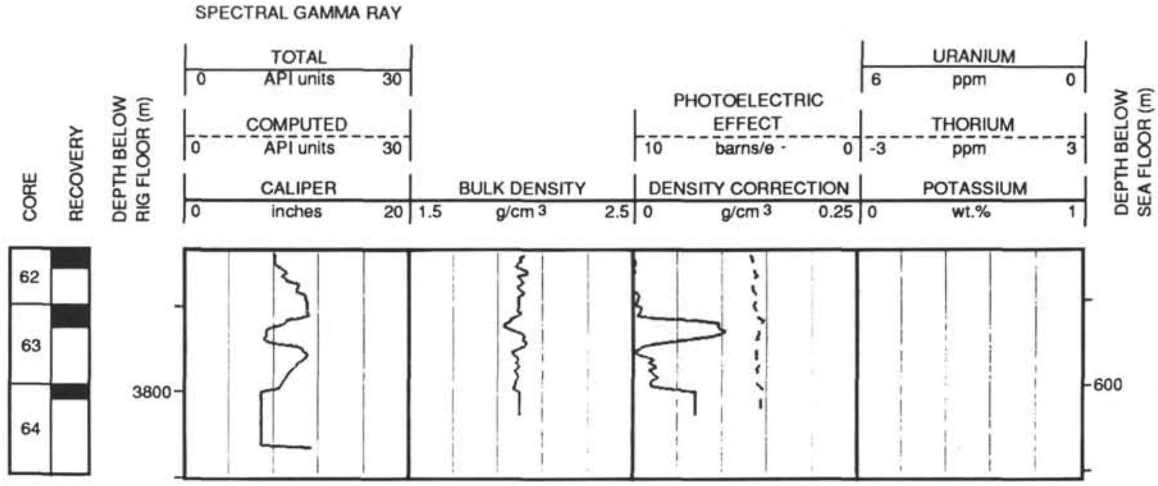

Hole 805C: Geochemical Log Summary

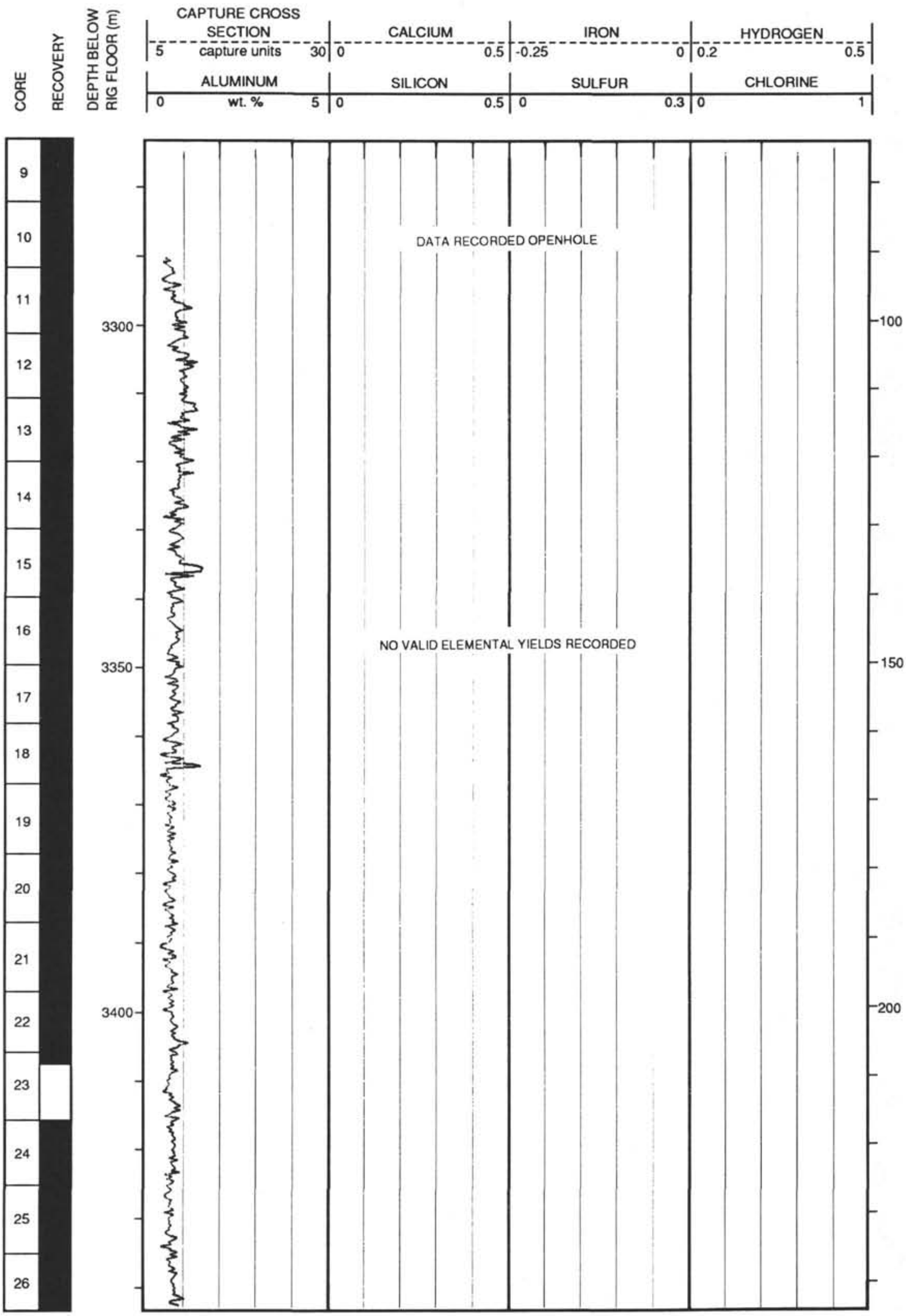

Hole 805C: Geochemical Log Summary (continued)

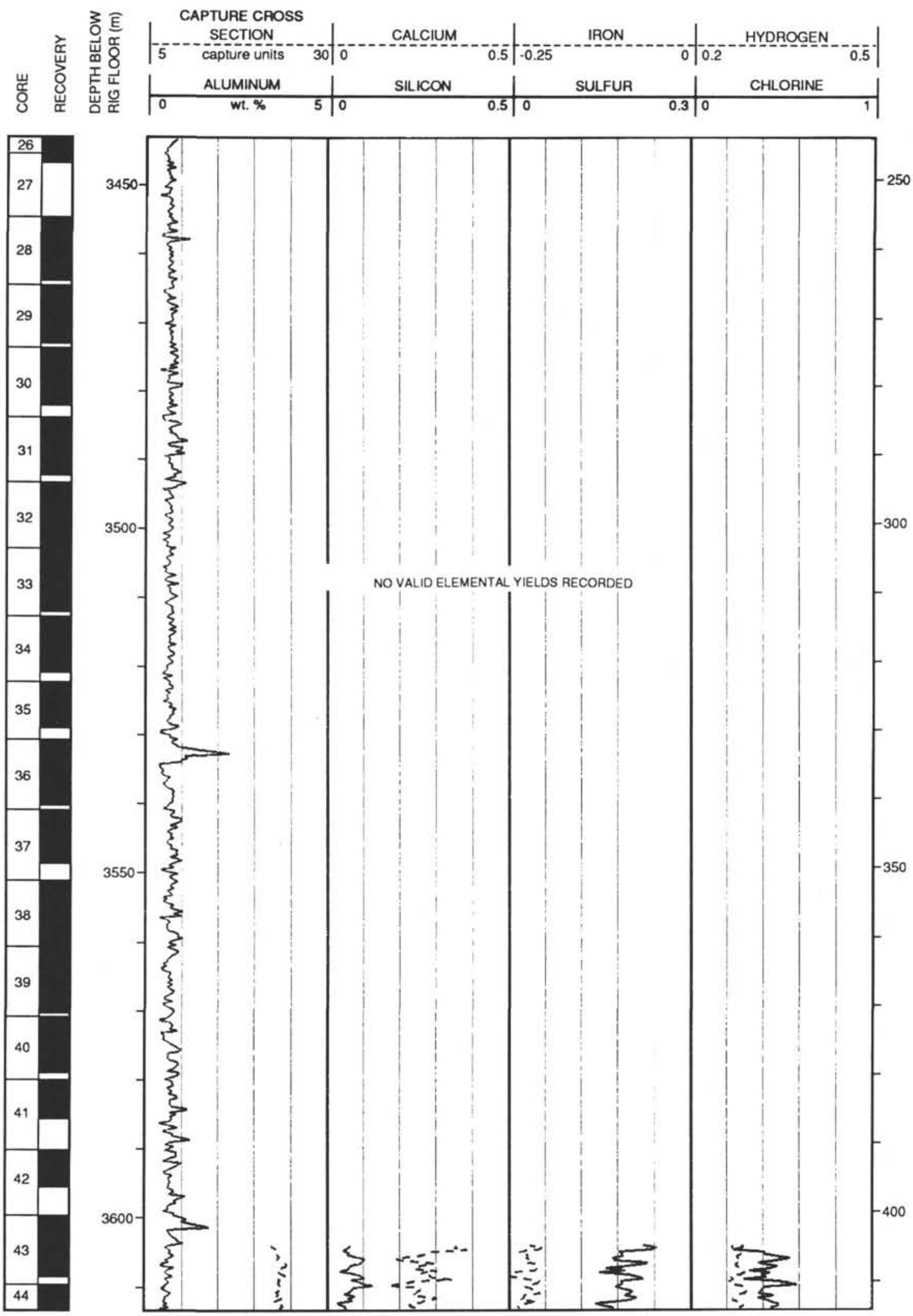

Hole 805C: Geochemical Log Summary (continued)

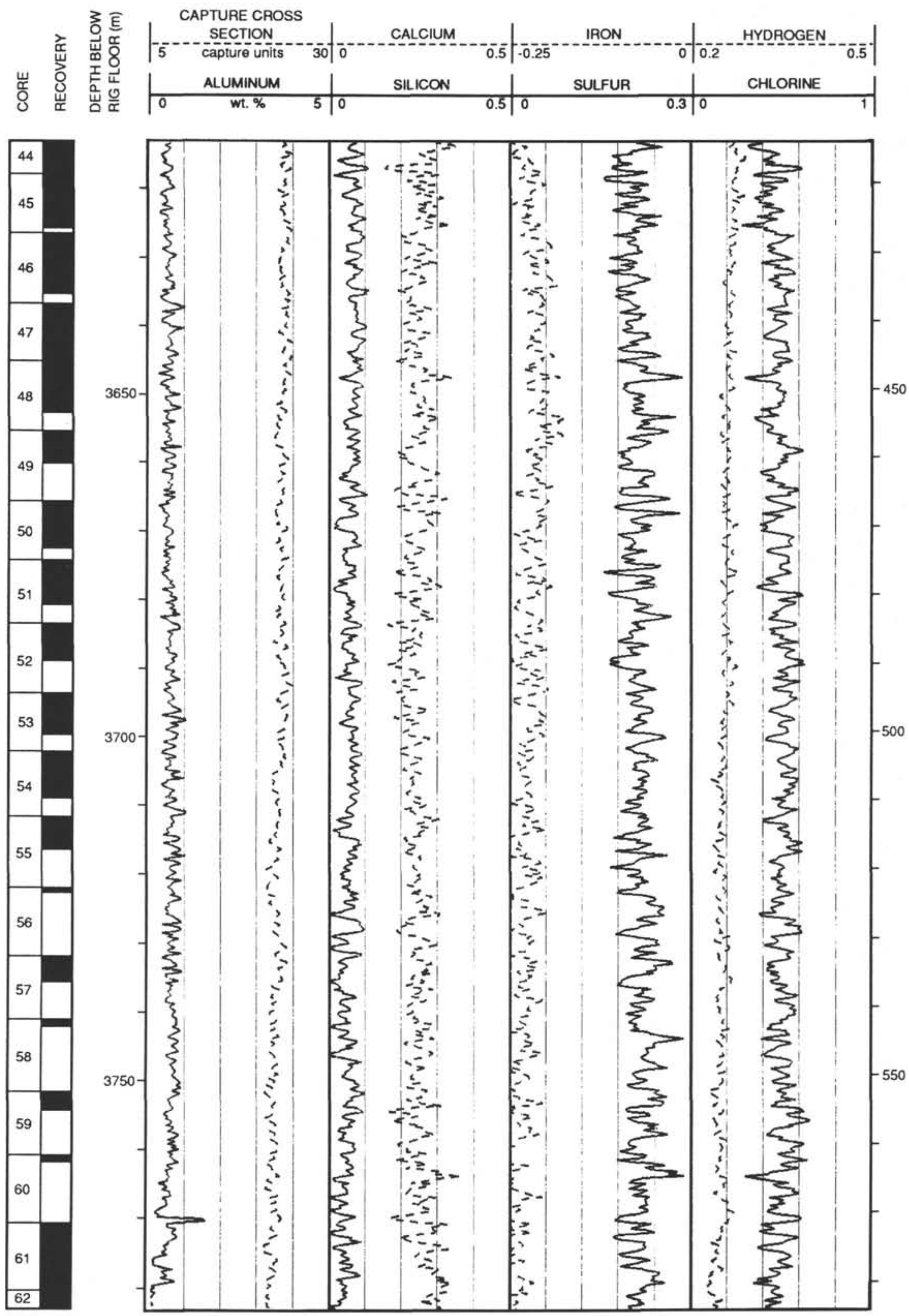

Hole 805C: Geochemical Log Summary (continued)